



# Dendritic Interior Constructed by Glycerol Units for Host-Guest Complex

Lee, Haejoo

---

(Degree)

博士 (工学)

(Date of Degree)

2012-03-25

(Date of Publication)

2013-04-03

(Resource Type)

doctoral thesis

(Report Number)

甲5480

(URL)

<https://hdl.handle.net/20.500.14094/D1005480>

※ 当コンテンツは神戸大学の学術成果です。無断複製・不正使用等を禁じます。著作権法で認められている範囲内で、適切にご利用ください。



Doctoral Dissertation

Dendritic Interior Constructed by Glycerol Units for  
Host-Guest Complex

Graduate School of Engineering

Kobe University

January 2012

HAEJOO LEE

Doctoral Dissertation

# Dendritic Interior Constructed by Glycerol Units for Host-Guest Complex

ホスト-ゲスト錯体に向けたポリグリセロールデンドリマー分子内部に関する基礎的研究

Graduate School of Engineering

Kobe University

January 2012

HAEJOO LEE

## Table of contents

## Chapter 1 General Introduction

## ***“Host-Guest chemistry of Dendritic Molecules”***

<b>1. 1 Introduction; Supramolecular system</b>	<b>1</b>
<b>1. 2 Host-Guest Chemistry</b>	<b>2</b>
1. 2. 1 Intermolecular forces	3
1. 2. 1. 1 Van der Walls interaction: Dispersion interaction	4
1. 2. 1. 2 Hydrophobic interactions	5
1. 2. 1. 3 Hydrogen bonding	6
<b>1. 3 Dendrimers</b>	
1. 3. 1 Dendritic molecules	7
1. 3. 1. 1 Comparison of dendritic architecture properties with traditional polymer	8
1.3.1.2 Hyperbranched polymers and dendrimers	12
1.3.1.3 Various types of dendrimers	15
1. 3. 2 Conformational Characteristics	22
1. 3. 3 Dendritic interior for molecular encapsulation	26
<b>1. 4 Dendritic Host-Guest Chemistry</b>	<b>28</b>
1. 4. 1 Nonspecific internal binding	28
1. 4. 2 Directed internal binding	29
1. 4. 2. 1 Using hydrogen bonding	29
1. 4. 2. 2 Apolar binding	30
<b>1. 5 Perspectives and objective of this study</b>	<b>32</b>
<b>1. 6 Survey of this dissertation</b>	<b>34</b>
<b>References</b>	<b>35</b>



## **Chapter 2**

### ***“Preparation of Polyglycerol Dendrimers (PGD-G1 and G2) and their Host-Guest Interaction with Fluorescent Probe”***

<b>2. 1 Introduction</b>	<b>43</b>
<b>2. 2 Experimental</b>	
2. 2. 1 Material	44
2. 2. 2 Synthesis and purification of PGD-G1, G2, G3, G4 and G5	44
2. 2. 3 Fluorescent measurements of AHSA in the presence of various concentrations of PGDs	46
2. 2. 4 <sup>1</sup> H-NMR titration of AHSA toward PGDs	46
2. 2. 5 ITC titration between AHSA and PGDs	47
<b>2. 3 Results and discussion</b>	
2. 3. 1 Fluorescent measurement of AHSA in the presence of various concentrations of PGDs	48
2. 3. 2 <sup>1</sup> H-NMR titration of AHSA in the presence of various concentrations of PGDs	52
2. 3. 2. 1 <sup>1</sup> H-NMR titration between PGD-G2 and AHSA	52
2. 3. 2. 2 <sup>1</sup> H-NMR titration between PGD-G2 and AHSA	54
2. 3. 3 ITC titration of AHSA in the presence of various concentrations of PGDs	57
<b>2. 4 Conclusion</b>	<b>60</b>
<b>References</b>	<b>61</b>

## **Chapter 3**

### ***“Dendritic Host-Guest Interaction of Polyglycerol Dendrimers of Generation 3 (PGD-G3) and 4 (PGD-G4) with Fluorescent Probe”***

<b>3. 1 Introduction</b>	<b>62</b>
<b>3. 2 Experimental</b>	
3. 2. 1 Material	62
3. 2. 2 Synthesis and purification of PGD-G3 and G4 (Fig. 3. 1)	63
3. 2. 3 Fluorescent measurements of AHSA in the presence of various concentration of PGDs	65
3. 2. 4 Fluorescent measurements of AHSA in various solvents	65
3. 2. 5 <sup>1</sup> H-NMR titration of AHSA toward PGDs	65
3. 2. 6 Isothermal titration calorimetry (ITC) experiments between AHSA and PGDs	66
3. 2. 7 DLS of PGDs	66
<b>3. 3 Results and discussion</b>	
3. 3. 1 Fluorescent measurements of AHSA in the presence of various concentration of PGDs	67
3. 3. 2 ITC titration of AHSA in the presence of various concentrations of PGD-G3 and PGD-G4	71
3. 3. 3 DLS study of PGDs in the presence of AHSA	73
3. 3. 4 <sup>1</sup> H-NMR titration of AHSA in presence of various concentration of PGDs	77
<b>3. 3 Conclusion</b>	<b>80</b>
<b>References</b>	<b>81</b>

## **Chapter 4**

### ***“NMR study of Host-Guest Interaction between Polyglycerol Dendrimers and an Anti-Cancer Drug”***

<b>4. 1 Introduction</b>	<b>82</b>
<b>4. 2 Experimental</b>	
4. 2. 1 Material	84
4. 2. 2 Fluorescent measurement of 5-Fu in the presence of various concentrations of PGDs	84
4. 2. 3 $^1\text{H}$ , $^{19}\text{F}$ -NMR titration of 5-Fu toward PGDs	84
<b>4. 3 Results and discussion</b>	
4. 3. 1 $^1\text{H}$ , $^{19}\text{F}$ -NMR titration of 5Fu in the presence of various concentrations of PGDs	86
4. 3. 2 Fluorescent measurement of 5-Fu in the presence of various concentrations of PGDs	90
<b>4. 3 Conclusion</b>	<b>93</b>
<b>References</b>	<b>94</b>

## **Chapter 5**

### ***“Exploratory Study of Guest Molecules toward Polyglycerol Dendrimers by Isothermal Titration Calorimetry”***

<b>5. 1 Introduction</b>	95
<b>5. 2 Experimental</b>	
5. 2. 1 Material	96
5. 2. 2 Preparation of amino(2-(2-hydroxyethoxy)ethylamino)methaniminium chloride (AEMC)	96
5. 2. 3 ITC study of amino acids and guanidium salt against PGD-G3	97
5. 2. 4 $^1\text{H}$ -NMR and 2D $^1\text{H}$ - $^1\text{H}$ NOESY NMR of L-arginine or L-lysine against PGD-G3	98
<b>5. 3 Results and discussion</b>	
5. 3. 1 ITC study of amino acids and AEMC against PGD-G3	99
5. 3. 2 $^1\text{H}$ -NMR and 2D $^1\text{H}$ - $^1\text{H}$ NOESY NMR of L-arginine or L-lysine against PGD-G3	105
<b>5.4 Conclusion</b>	111
<b>References</b>	112
 <b>Chapter 6 General Conclusion</b>	 113

## **Chapter 1**

# **Host-Guest Chemistry of Dendritic Molecules**

# Chapter 1

## Host-Guest Chemistry of Dendritic Molecules

### 1.1 Introduction; Supramolecular System

From the discovery of intermolecular force by Johannes Diderik Van Der Waals in 1873, supramolecular system was established by Donald J. Cram, Jean-Marie Lehn, and Charles J. Pederson who awarded the Nobel Prize for chemistry in 1987 in the field of selective “host-guest” complexes, in which a host molecule recognizes and selectively binds a certain guest. Supramolecular systems are defined as chemistry beyond the molecule which means the chemistry of intermolecular bond, implying the structures and functions of the entities formed by association of two or more chemical species<sup>1)</sup>. These include attractive and repulsive intermolecular forces, such as van der Waals forces (including dipole-dipole), hydrophobic interactions, electrostatic interactions, hydrogen bonding, and  $\pi$ - $\pi$  stacking. The supramolecular science is highly interdisciplinary field of science including the chemical, physical and biological features of chemical species. These intermolecular forces are the glue which holds molecules together and therefore they play crucial roles in building up supramolecular structure. In order to emphasize the importance of these intermolecular interactions, the definitions of these forces are discussed below.

## 1.2 Host-Guest Chemistry

- Molecular Recognition;

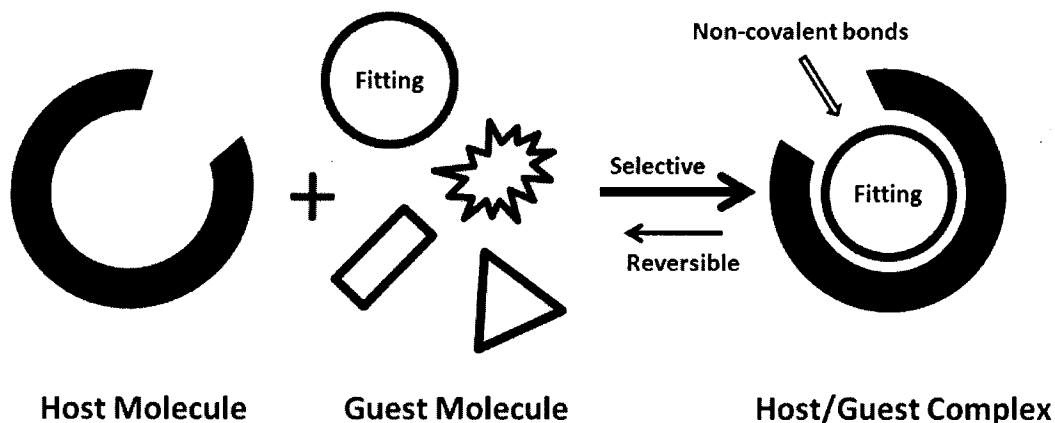
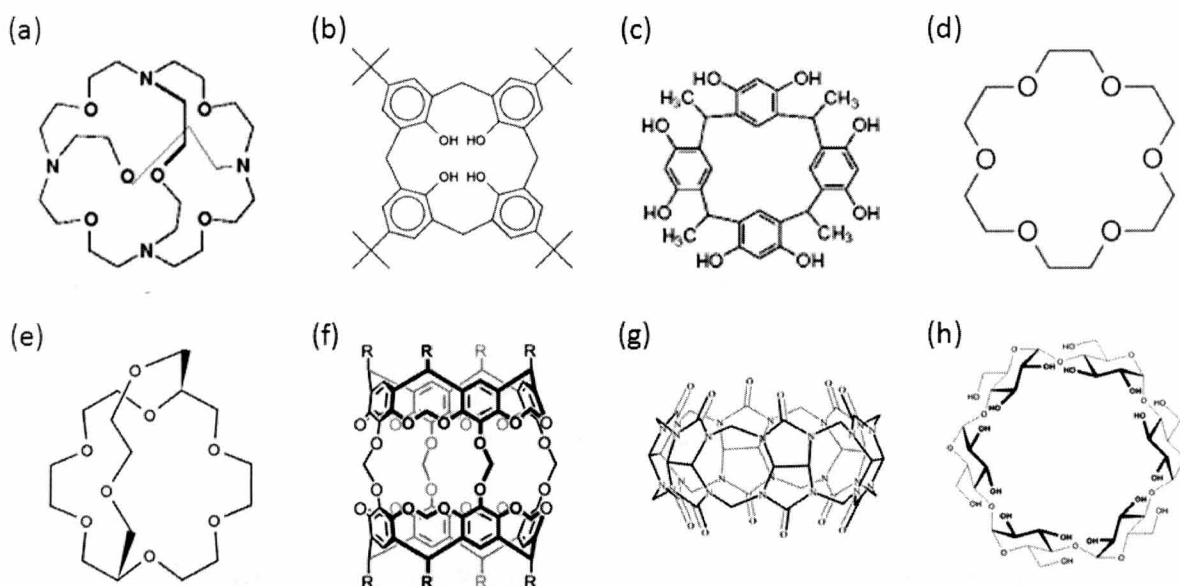


Fig. 1. 1 Host-Guest system

In a general definition of “Host-Guest Chemistry”, we generally consider a molecule (morphologically big one, host) binding another molecule (as a guest) to produce the so-called “host-guest” complex. According to D.J. Cram, the hosts are defined as synthetic molecules containing convergent binding sites, and guests as molecules or ions containing divergent binding sites. Depending on the compatibility of the two (or more) interacting species, the host-guest complex can be considered as non-specific or specific and highly specific complexes which can be considered as recognition complexes. Most common host is understood as a concave organic molecule, which can be preorganized for the guest and which utilizes multivalent and cooperative interactions. Spherands<sup>2)</sup>, calixarenes<sup>3)</sup>, resorcarenes<sup>4)</sup>, crown ethers<sup>5)</sup>, cryptands<sup>6)</sup>, carcerands<sup>7)</sup>, and cavitands<sup>8)</sup> are representative molecules which have confirmed their ability to form host-guest complexes (**Fig. 1.2**).

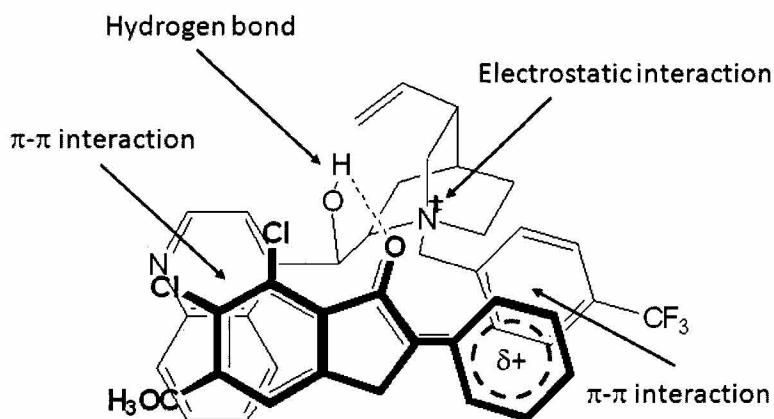


**Fig. 1. 2** Representative supramolecules (a) Spherand, (b) calixarene, (c) resorcarene, (d) crown ether, (e) cryptand, (f) carcerand, (g) Cucurbituril, (h) cyclodextrin

### 1.2.1 Intermolecular forces

Intermolecular interactions are defined as interaction between one molecule and a neighbouring molecule. The forces of interaction which holds an individual molecule together are known as intramolecular interactions. An example of the importance of these intermolecular interactions is illustrated in **Fig. 1.3**. Cinchona alkaloids as asymmetric catalysts was provided by Wynberg<sup>9)</sup>, who reported, among numerous other applications, the 1,4-addition of thiols to cyclic enones catalyzed by quinine and quinidine. Three stabilizing interactions were described as being responsible for the high ee observed in this process: (1) electrostatic interactions between the thiol anion and the protonated ammonium salt, (2) the formation of hydrogen bonds between the hydroxyl moiety at position 9 of the alkaloid and the enone carbonyl group and (3) dispersion forces between the quinoline aromatic ring of the catalyst and the thiol anion.

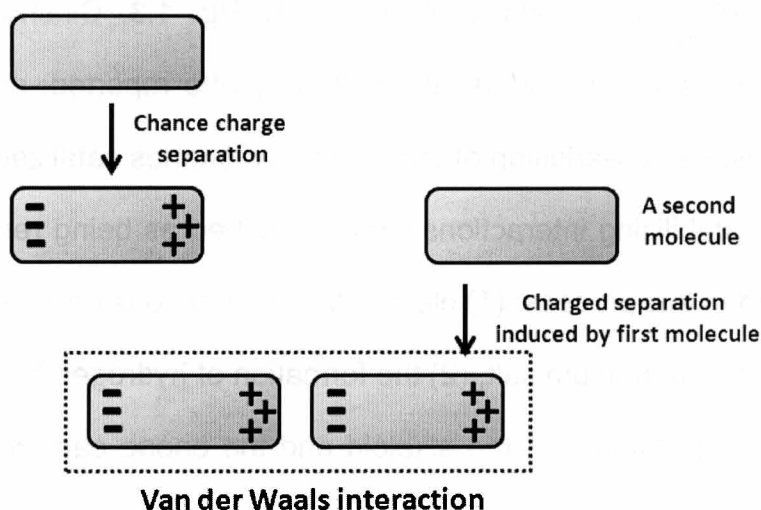




**Fig. 1. 3** Intermolecular interactions <sup>9)</sup>

### 1.2.1.1 Van der Waals interaction: Dispersion interaction <sup>10)</sup>

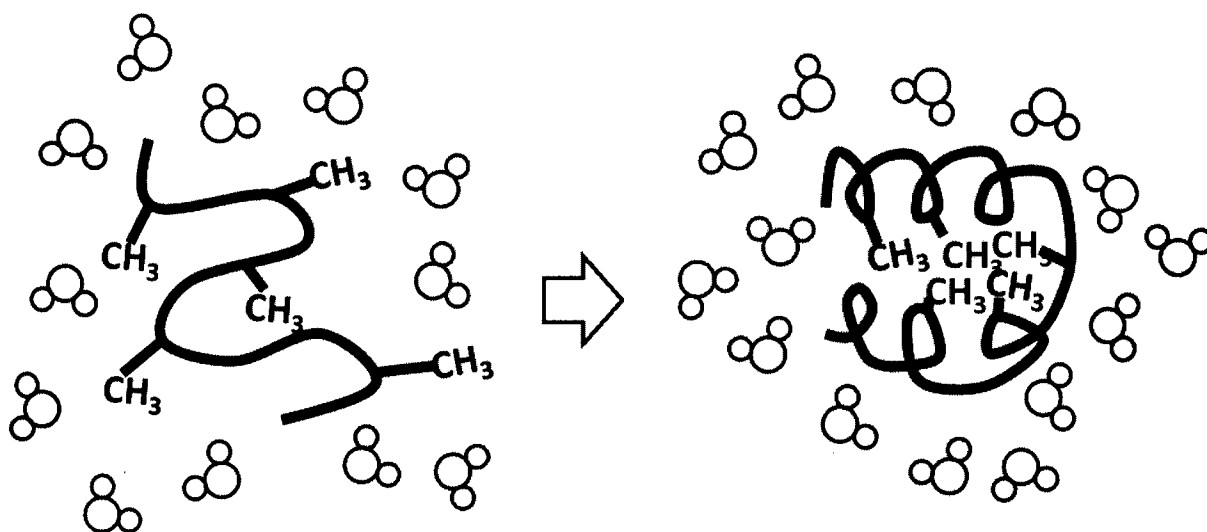
All atoms and molecules attract each other, even in the absence of charged groups, as a result of mutual interactions related to the induced polarization effects. These ubiquitous attractions, known as van der Waals interactions (**Fig. 1. 4**), are weak and close-range, varying as the sixth power of the distance between them,  $d^{-6}$ . They arise from three types of interactions: those between two permanent dipoles, those between a permanent and an induced dipole, and those between two mutually induced dipoles, known as London or dispersion force.



**Fig. 1. 4** Schematic representation of van der Waals interaction

### 1.2.1.2 Hydrophobic interactions <sup>11)</sup>

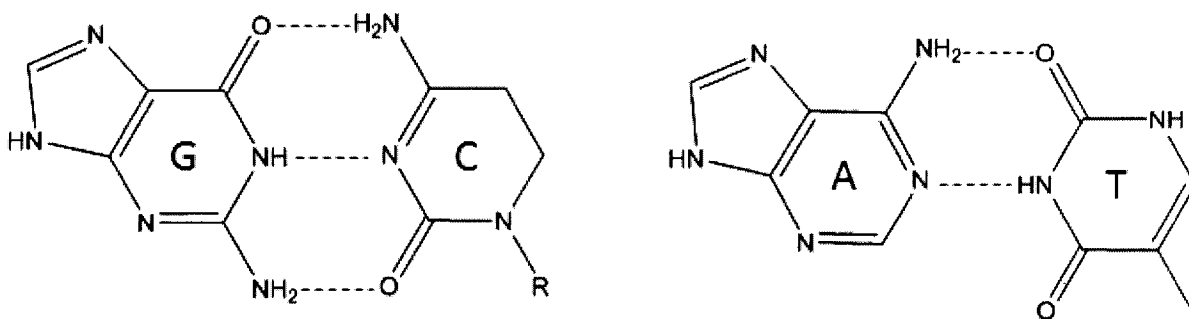
Water is a very poor solvent for non-polar molecules compared with most organic liquids. If the non-polar molecules are added to water, formation of intermolecular hydrogen bonding between water molecules is energetically much more favorable than between water and the non-polar molecules (**Fig. 1. 5**). In those conditions, the non-polar molecules hardly participate in the hydrogen bonding, resulting in association or aggregation of the non-polar molecules in liquid water. Aqueous solutions of such molecules have many anomalous physical properties. If the interaction between non-polar molecules and water is energetically favorable, non-polar molecules should be dissolved in water. The association of the non-polar molecules under aqueous environments is known as “hydrophobic interactions”. The interaction between non-polar side group of a molecule and the other non-polar side groups cause to aggregate to minimize surface area exposed to water, allowing these molecules to associate with each other in aqueous environment.



**Fig. 1. 5** A schematic description of a conformational change of a biopolymer. One methyl group is transferred from an essentially aqueous environment to the interior of the polymer. This phenomenon is that the free energy of transferring methane from water into a non-polar solvent is a good measure of the free energy change for the transfer of a  $-\text{CH}_3$  group from the random-coil conformation to the interior of the polymer in the native configuration <sup>12)</sup>.

### 1.2.1.3 Hydrogen bonding<sup>13)</sup>

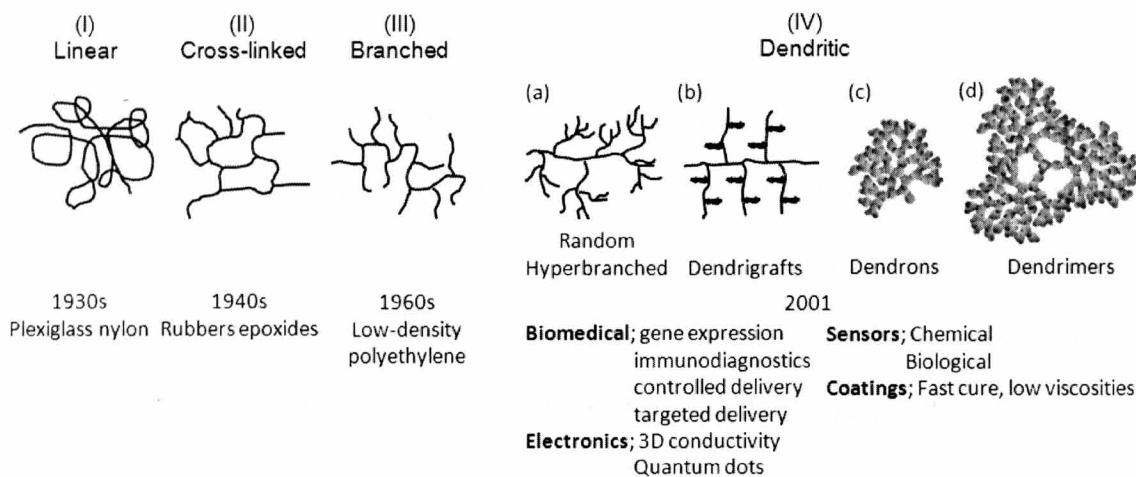
A hydrogen bond occurs when two electronegative atoms compete for the same hydrogen atom. The hydrogen atom is formally bonded covalently to one of the atoms as a donor, and is also interacts favorably with the other as an acceptor. In strong and short hydrogen bonds, the hydrogen atom is symmetrically placed between the two electronegative atoms, but usually it is covalently bonded to one of the atoms, with a normal covalent bond length. The main component of the hydrogen bond is an electrostatic interaction between the dipole of the covalent bond to the hydrogen atom, in which the hydrogen atom has a slightly positive and negative charge on the other electronegative atom. One of examples of hydrogen bonding is base pair of nucleic acids (**Fig. 1. 6**). Adenine (A) forms two hydrogen bonds only with thymine (T). Guanine (G) forms three hydrogen bonds only with cytosine (C). In each case, the hydrogen bonding is formed between the positive hydrogen end of a polar N-H bond and a pair of electrons on either a nitrogen or a carbonyl oxygen.



**Fig. 1. 6** Formation hydrogen bonds between guanine and cytosine, adenine and thymine

# 1.3 Dendrimers

## 1.3.1 Dendritic molecules



**Fig. 1. 7** Representation of the four major classes of macromolecular architecture<sup>14)</sup>

About 60 years after introducing the “macromolecular hypothesis” by Staudinger, the field of polymer science has been summarized as consisting of three major architectural class, (i) linear topologies, (ii) crosslinked architectures, and (iii) branched architectures (**Fig. 1.7**). Twenty years ago, the fourth new class of polymer architecture, so called dendritic architecture, was suggested by D. A. Tomalia. They showed unprecedented new physicochemical properties compared with classical architectural polymers, and attracted the attention of researchers in disciplines as diverse as chemistry, biology, physics, and engineering. Dendritic polymers consist of three subsets based on degree of structural control, namely; (a) random hyperbranched polymers (statistical polymers), (b) dendrigrraft polymers (semi-controlled polymers), (c) dendrons (highly controlled structure), and (d) dendrimers (highly controlled structure). All dendritic polymers are open covalent assemblies of branch cells. Each subclass and the level of structure control are

defined by the propagation methodology used to produce these assemblies.

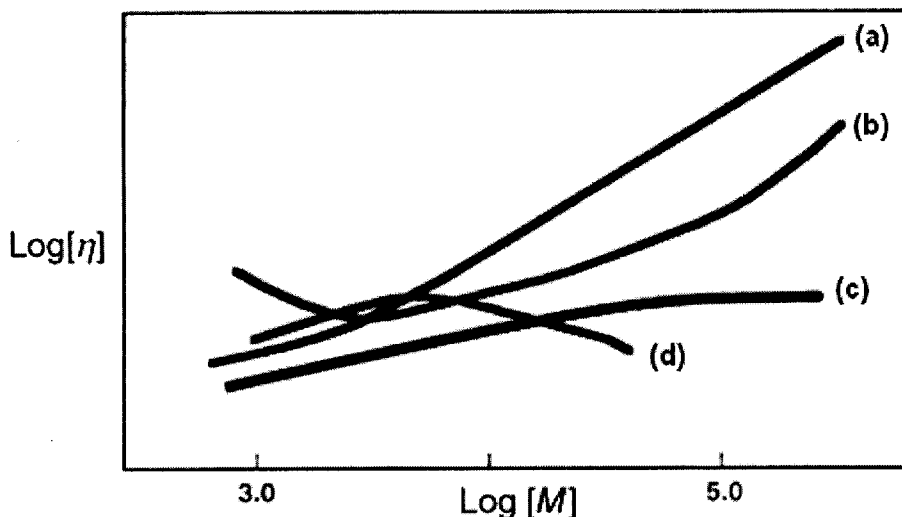
The name of dendrimer is derived from Greek words Dendron and meros meaning “tree” and “part”, respectively. Dendrimers that are perfectly branched tree-like structure were firstly reported by Tomalia, et al. over 15 year ago<sup>15)</sup>. Comparing with incomplete or irregular hyperbranched polymer which can be prepared easily using “one-pot” techniques, dendrimer can precisely control molecular weight, size, water solubility and their toxicity validate them as excellent candidates in chemical and biological area. Dendrimers differ from classical monomers and random coil polymers by their extraordinary symmetry, high branching and maximized terminal functionality density.

Influence of dendritic architecture on physical or chemical properties is totally different from linear polymer. This means that dramatic changes in physical and chemical properties are observed by simply concerting a linear topology of common composition to a crosslinked architecture.

#### **1.3.1.1 Comparison of dendritic molecules and traditional polymers**

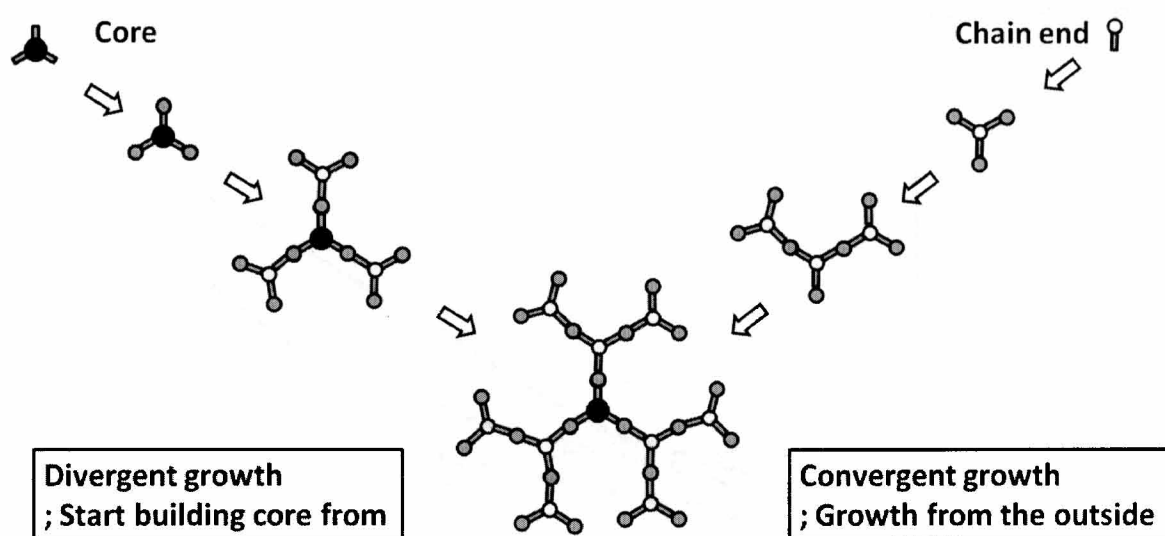
The most significant difference in physical property of dendrimer is viscosity. In contrast to linear polymer that obeys the Mark-Howwink-Sakurada equation<sup>16)</sup>, the intrinsic viscosity of dendrimer does not increase with molecular mass. Comparing the viscosity parameter for linear topologies, as well as random hyperbranched polymer, dendrimer and dendritic graft are firstly reported by Fréchet in 1996<sup>17)</sup>. From this report, all three dendrite topologies behave differently as compared with the linear polymer (**Fig. 1. 8**). In **Fig. 1. 8**, the relationship between Log  $[\eta]$  and  $[M]$  of the hyperbranched polymers shows similar with that of the linear ones. However, the dendrigrafts exhibit intermediary behavior whereas dendrimers show a completely

different relationship as a function of molecular weight.




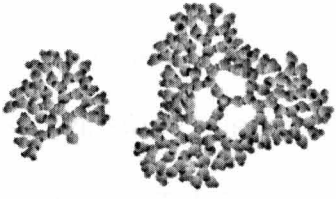
**Fig. 1. 8** Comparison of intrinsic viscosities ( $\log(\eta)$ ) versus molecular weight ( $\log M$ ) for (a) linear, (b) hyperbranched, (c) dendrimer and (d) dendrigraft topologies.<sup>18)</sup>

Another important difference of dendritic compounds is monodispersity. Dendritic compounds also show a completely different relationship as a function of molecular weight. As I said, linear or hyperbranched polymers are mostly prepared using “one-pot” synthesis techniques. By the “one-pot” synthesis technique, linear or hyperbranched polymers are randomly synthesized and polydispersed system with different topologies and molecular size. In contrast, dendrimer synthesis consisting of multi step involving divergent or convergent is hierarchical assembly strategies that required the construction components as shown in **Fig. 1. 9**. According to the considerate synthesizing method, the monodispersed nature of dendrimer has been extensively reported by mass spectroscopy<sup>18)</sup>, size exclusion chromatography<sup>19)</sup>, gel electrophoresis<sup>20)</sup> and electron microscopy (TEM)<sup>21)</sup>. Other unique properties of dendrimers comparing with traditional polymer are summarized in **Table 1.1**.



**Fig. 1. 9** Two major synthetic method of dendrimer; divergent and convergent methods which have each different direction which the dendrimer molecules are being built (where G is generation number). Divergent methods are radial synthetic method from the central core to the outer dendrimer surface. Convergent methods have opposite direction which is formation of single Dendron in order to obtain a multidendron dendrimer one additional synthetic step is necessary.

Table 1. 1

Linear	Dendritic
	
Flexible coil	Dendron    Dendrimer
<ol style="list-style-type: none"> <li>1. Random coil configurations</li> <li>2. Semicrystalline/crystalline materials <ul style="list-style-type: none"> <li>• <i>higher glass temperatures</i></li> </ul> </li> <li>3. Lower solubility <ul style="list-style-type: none"> <li>• <i>Decreases with Mw.</i></li> </ul> </li> <li>4. Intrinsic viscosity follows logarithmic <ul style="list-style-type: none"> <li>• <i>Increases with Mw.</i></li> </ul> </li> <li>5. Entanglement directed rheological properties <ul style="list-style-type: none"> <li>• <i>Shear sensitivity</i></li> </ul> </li> <li>6. Mobility by repetition <ul style="list-style-type: none"> <li>• <i>Segmental and molecular mobility</i></li> </ul> </li> <li>7. Anisotropic electronic conductivity</li> </ol>	<ol style="list-style-type: none"> <li>1. Predictable shape changes as a function of <i>Mw.</i> and core <ul style="list-style-type: none"> <li>• <i>Robust spheroids; breathing deformability</i></li> </ul> </li> <li>2. Non-crystalline, amorphous materials <ul style="list-style-type: none"> <li>• <i>Lower glass temperatures</i></li> </ul> </li> <li>3. Increased solubility <ul style="list-style-type: none"> <li>• <i>Increases with Mw.</i></li> </ul> </li> <li>4. Exhibits viscosity maximum and minimum plateau with <i>Mw.</i> <ul style="list-style-type: none"> <li>• <i>Low viscosity</i></li> </ul> </li> <li>5. Newtonian-type rheology <ul style="list-style-type: none"> <li>• <i>No shear sensitivity, considerably lower viscosity</i></li> </ul> </li> <li>6. Mobility involving whole dendrimer as the kinetic flow unit <ul style="list-style-type: none"> <li>• <i>Virtually no repetition</i></li> </ul> </li> </ol>



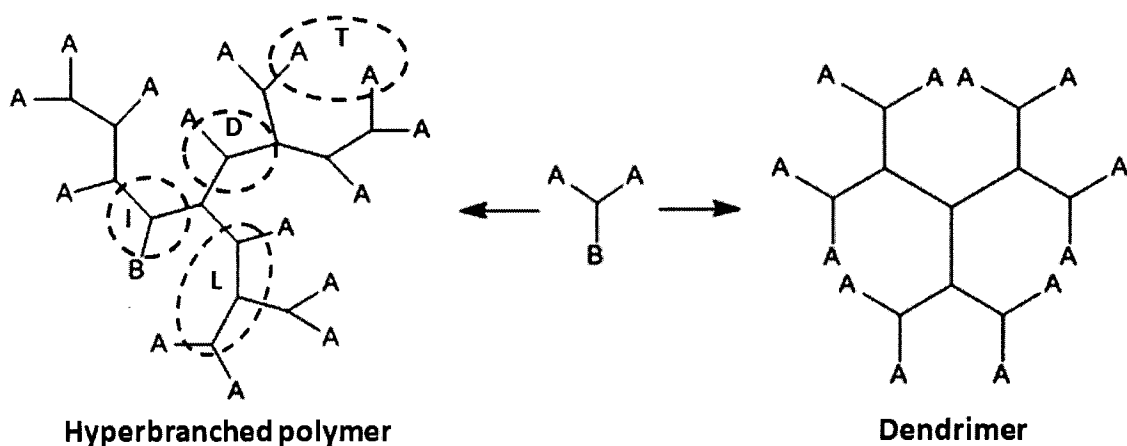
### 1.3.1.2 Hyperbranched polymers and dendrimers<sup>22)</sup>

Hyperbranched polymers and dendrimers have been extensively studied as representative irregular and regular dendritic polymers, respectively. Hyperbranched polymers contain perfectly and imperfectly branched parts. The preparation of hyperbranched polymers can be simplified by comparing with that of dendrimers that do not require protection / deprotection step. The most common synthetic route is one-pot procedure where  $A_xB$  monomers are condensed in the presence of a catalyst. However, due to broad distribution of molecular weight and undesired side reactions, hyperbranched polymers are considered as ill-defined materials. Compared with hyperbranched polymers, dendrimers are well-defined materials which exhibit controlled molecular structure, shape, size and functional groups, due to their step-wise synthetic method. The more detailed characteristics are summarized in **Table 1.2**.

The concept of degree of branching (DB) was introduced by Fréchet and coworkers to correlate between the units of hyperbranched polymer. The DB is defined as the structure of hyperbranched polymers as follows: .

$$DB = \frac{(No.of dendritic units)+(No.of terminal units)}{Total No.of units} = \frac{D+T}{D+T+L} \quad (\text{e.q. 1.1})$$

where,  $D$  is total number of dendritic units,  $T$  the total number of terminal units, and  $L$  the total number of linear units. Focusing on DB, the dissimilarity between dendrimer and hyperbranched polymer was shown in, **Fig. 1.10**.



**Fig. 1. 10** Schematic structure of hyperbranched polymer and dendrimer prepared from  $A_2B$ -type monomer. There are initial (I), linear (L), dendritic (D), and terminal (T) repeating units in a hyperbranched polymer.

In a dendrimer, there are only terminal and branched units. According to Frécht and Hawker<sup>23)</sup>, DB of dendrimer is 1. For a hyperbranched polymer with large molecular weight, the number of terminal units ( $T$ ) is very close to that of dendritic units ( $D$ ). Therefore, **e.q. 1.1** can be simplified as **e.q. 1.2**.

$$DB = \frac{1}{1+L/2D} \quad (\text{e.q. 1.2})$$

R. Haag and coworkers have investigated the DB of hyperbranched polymers prepared by using glycidol as latent branching  $A_2B$  monomer and allyl phenyl glycidyl ether as representative linear comonomer. The DB was 9% - 58% calculated from  $^1\text{H-NMR}$  spectra<sup>22)</sup>.

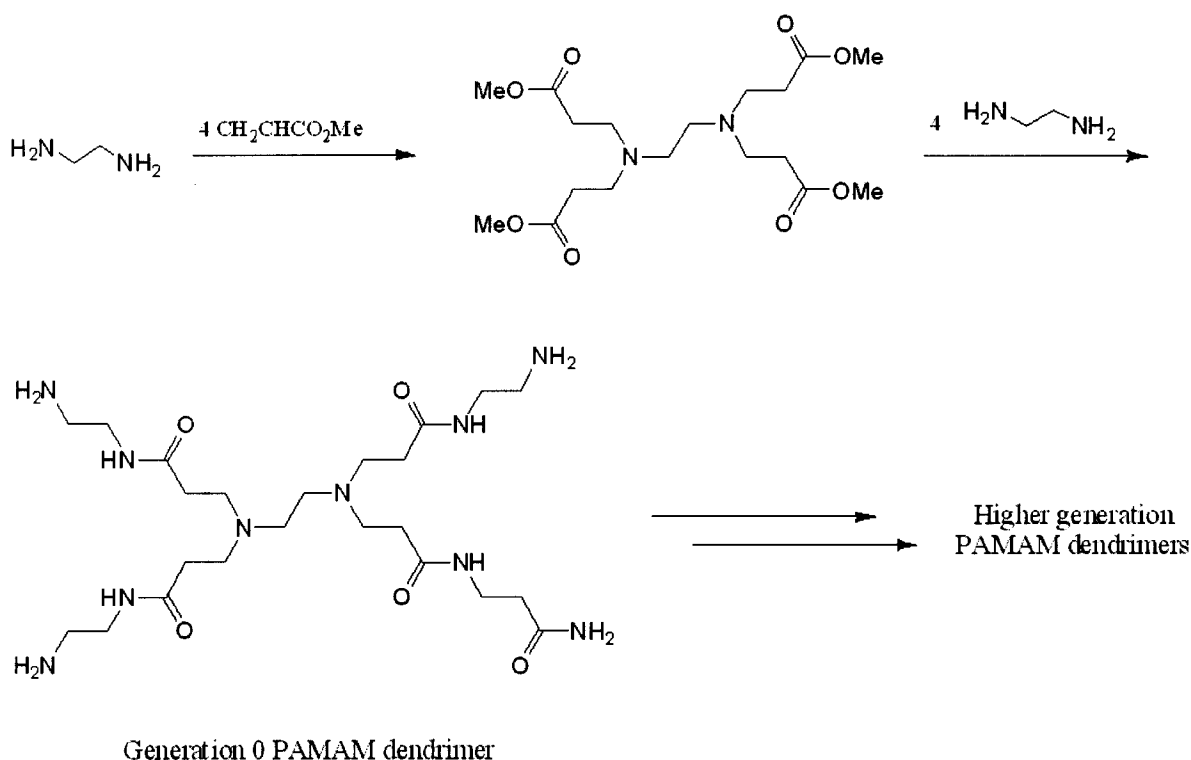
**Table 1. 2**

	Hyperbranched	Dendrimer
Topology	3D, ellipsoidal	3D, globular
Synthesis	One-step, cost-effective	Multistep, laborious
Purification	Precipitation	Chromatography
Molecular weight	Mixed molecular weight	Same molecular weight
Polydispersity Index	> 3.0	1.0
Degree of branching	0.4 – 0.6	1.0
Entanglement	Weak	Very weak or no
Viscosity	Low	Very low
Solubility	High	Very high
Functional group	At linear and terminal units	At terminal units
Reactivity	High	Very high

### 1.3.1.3 Various types of dendrimers

#### (A) Polyaminoamine (PAMAM) dendrimer

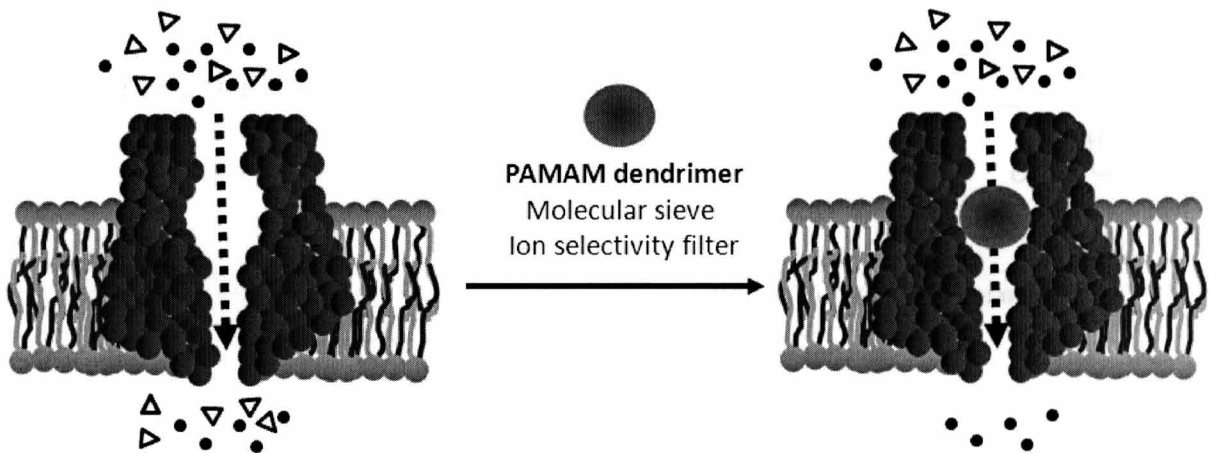
PAMAM dendrimer was firstly reported by D. A. Tomalia in 1985. In this report, starburst polymer, was synthesized by a divergent method involving two step process; Micheal addition of amine initiator core with methyl acrylate and amidation of the esters with ethylenediamine (EDA) (**Fig. 1. 11**).



**Fig. 1. 11** Synthesis of PAMAM dendrimer

After reporting this report, physicochemical properties of PAMAM dendrimer have been studied, and applied in the fields of physical, chemical and biomedical area. For example, William's group has clarified the conformational change of PAMAM depending on pH change<sup>24</sup>). In those studies, they profiled the pH-induced conformational change from a "dense core" (high pH) to a "dense shell" (low pH) and suggested the possibility of PAMAM as a drug delivery vehicle, where encapsulation and release of guest molecules can be controlled by using pH as the trigger.

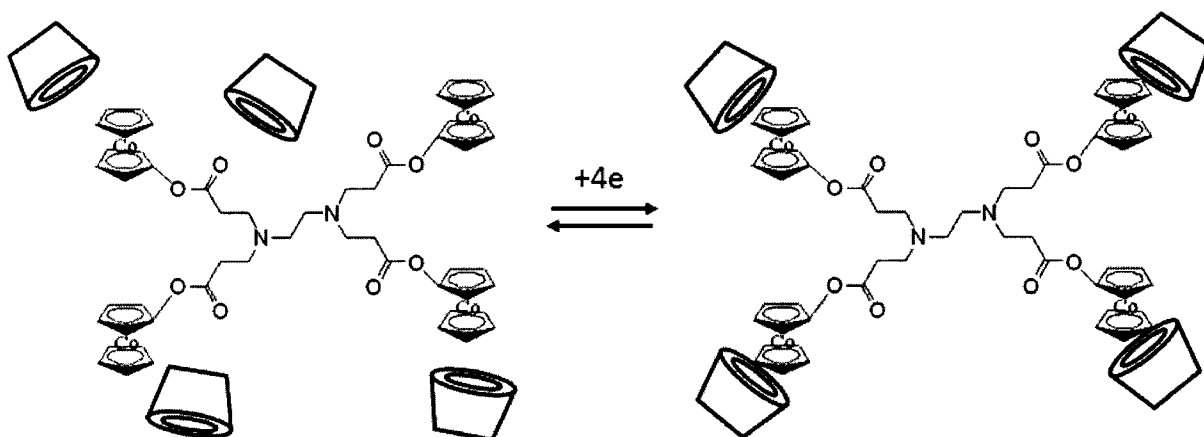
Howorka's group has tried to control nanoscale protein pores placing PAMAM dendrimers into a pore lumen for ion-selectivity filters of molecular sieves (**Fig. 1. 12**)<sup>25)</sup>. In this study, G3-PAMAM dendrimer in the channel lumen reduced the ionic current by 45%, indicating that the hyperbranched and positively charged polymer blocked the passage of ions through the pore. Use of PAMAM dendrimers has advantages over other spherical materials such as quantum dots of similar size or functionality including that;(a) dendrimers have residual degree of structural flexibility which can help overcome small steric permeation barriers, and (b) controlling and tuning the flow of matter through the engineered pore while solid impermeable spheres would likely lead to much more drastic and less tunable changes in the permeation properties.



**Fig. 1. 12** Nanoscale protein pore placing PAMAM dendrimer into a pore lumen

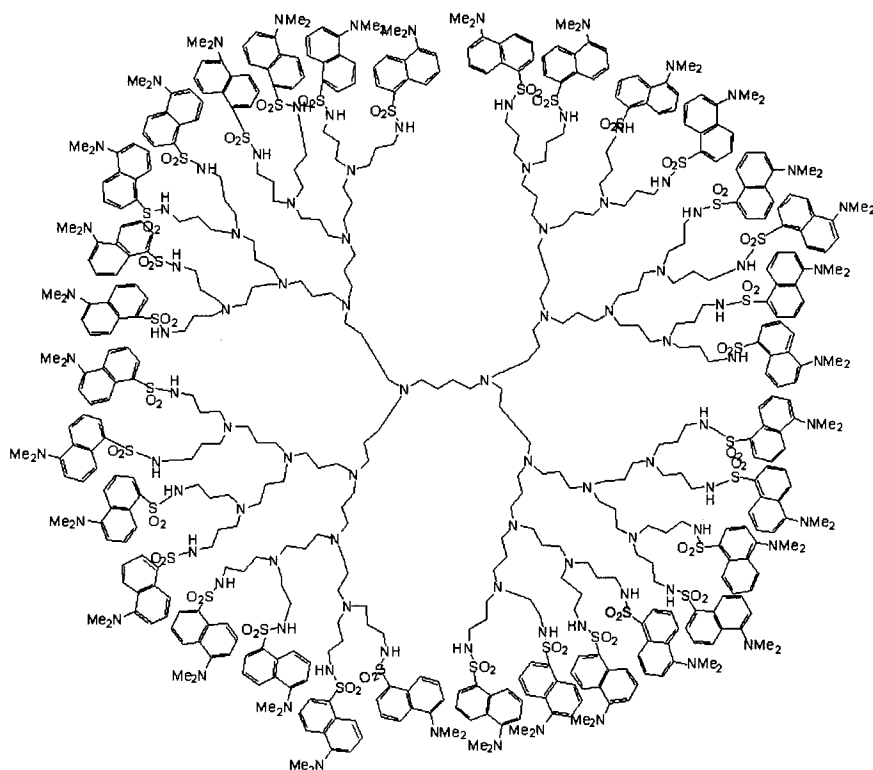
### (B) Poly(propylene imine) (PPI) dendrimer

PPI dendrimer was firstly synthesized by Meijer group in 1993<sup>26)</sup>. Until now, there are several kinds of improved synthetic method of PPI dendrimers. The firstly reported PPI dendrimers were synthesized by two step process consisting of Michael addition (primary amines to acrylonitrile) and heterogeneous hydrogenation with a Raney cobalt catalyst. Using their terminal amino groups, PPI dendrimers can readily be *per*-functionalized. For example, Kaifer's group prepared and characterized PPI dendrimers functionalized with peripheral cobaltocenium subunit<sup>27)</sup>. Such a fourth-generation dendrimer proved to be suitable guest system for  $\beta$ -cyclodextrin as a host compound (**Fig. 1. 13**).



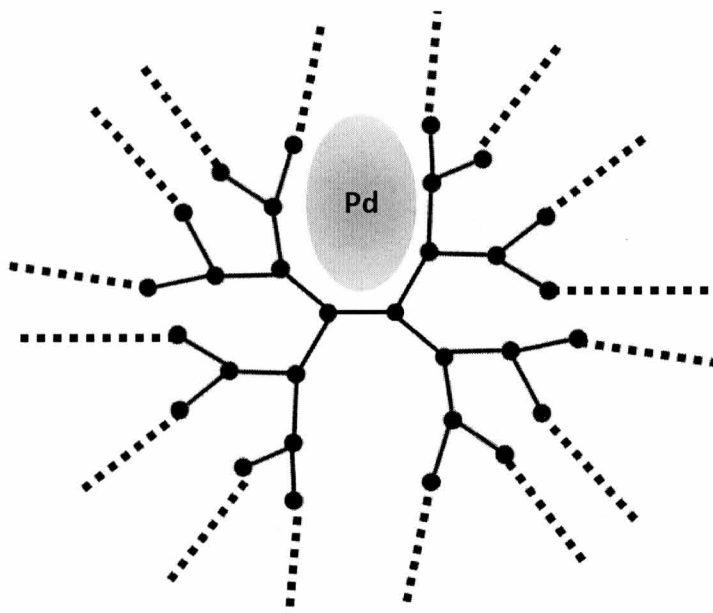
**Fig. 1. 13** Electrochemical activation of  $\beta$ -CD binding to dendrimer

Balzani's group succeeded in obtaining the PPI dendrimers functionalized in periphery with dansyl unit with increasing the generation of dendrimer, but not in strict dependence upon the number of fluorophores (**Fig. 1. 14**)<sup>28)</sup>. The quenching of the fluorescence of the dansyl units was induced by complexation of the metal ions.



**Fig. 1. 14** Chemical structure of dansylated PPI dendrimer, G4

Kaneda's group has tried the preparation of palladium complexes within PPI dendrimer modified with decanoyl chloride and 3,4,5-triethoxybenzoyl chloride, respectively, to give the alkylated and akylated dendrimer<sup>29</sup>). Palladium particles were encapsulated through ionic interaction (**Fig. 1. 15**). The nano-scaled environment created by the densed amino group located in the PPI dendrimer can provide high catalytic activity and stability for the palladium complexes.

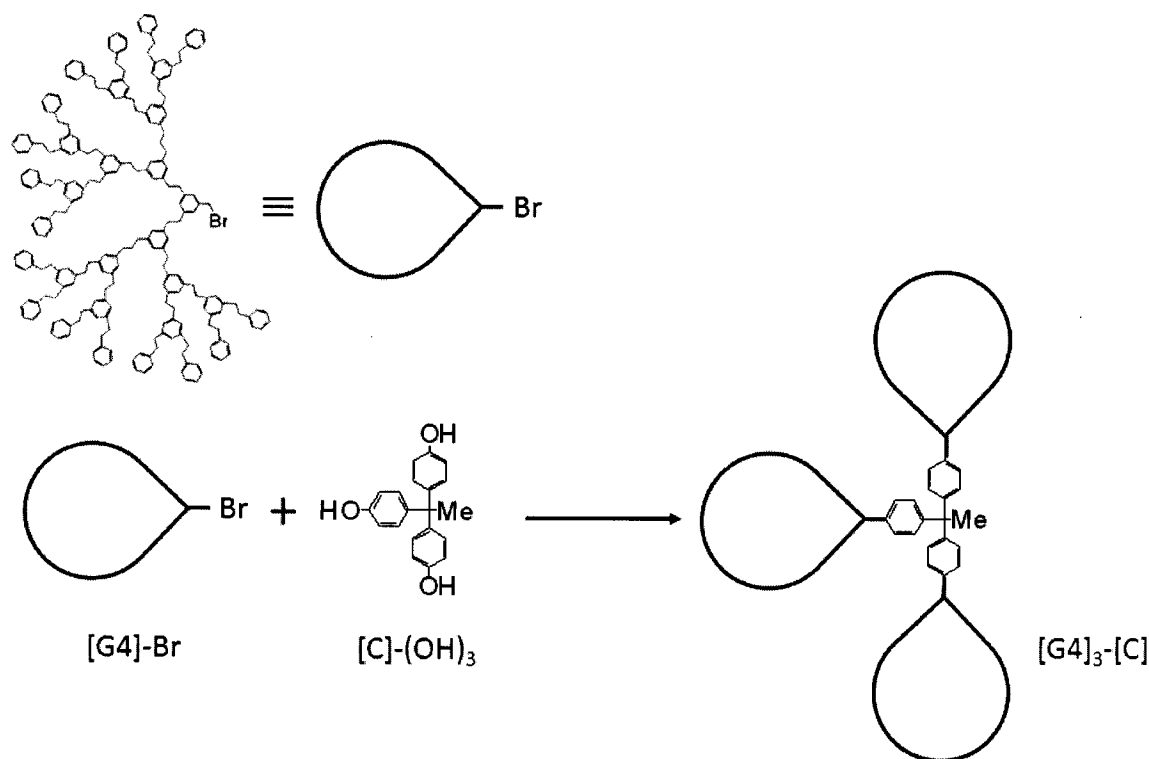


**Fig. 1. 15** Proposed structure of dendrimer-encapsulated Pd complex

### **(C) Carbon/oxygen-based Fréchet type dendrimer**

Fréchet's group introduced new approach to convergent synthetic method of dendrimer, which possesses a number of significant features, such as controlled molecular architecture (**Fig. 1. 16**)<sup>30)</sup>. Convergent method allows the synthesis of almost monodisperse dendritic molecules with highly controlled molecular architecture. Taking this advantage of convergent method, Gitsov<sup>31)</sup> and Leuduc<sup>32)</sup> have prepared Fréchet type-dendrimers using anionic or living free radical polymerization. This type of dendrimer is used as multifunctional platform of diverse dendritic molecules. For example, di- or tri-block ABA copolymer hybrids<sup>33)</sup>, side-chain functionalized or dendronized copolymer hybrid<sup>34)</sup> and amphiphilic hybrids<sup>35)</sup> were prepared for multifunctional dendrimers.

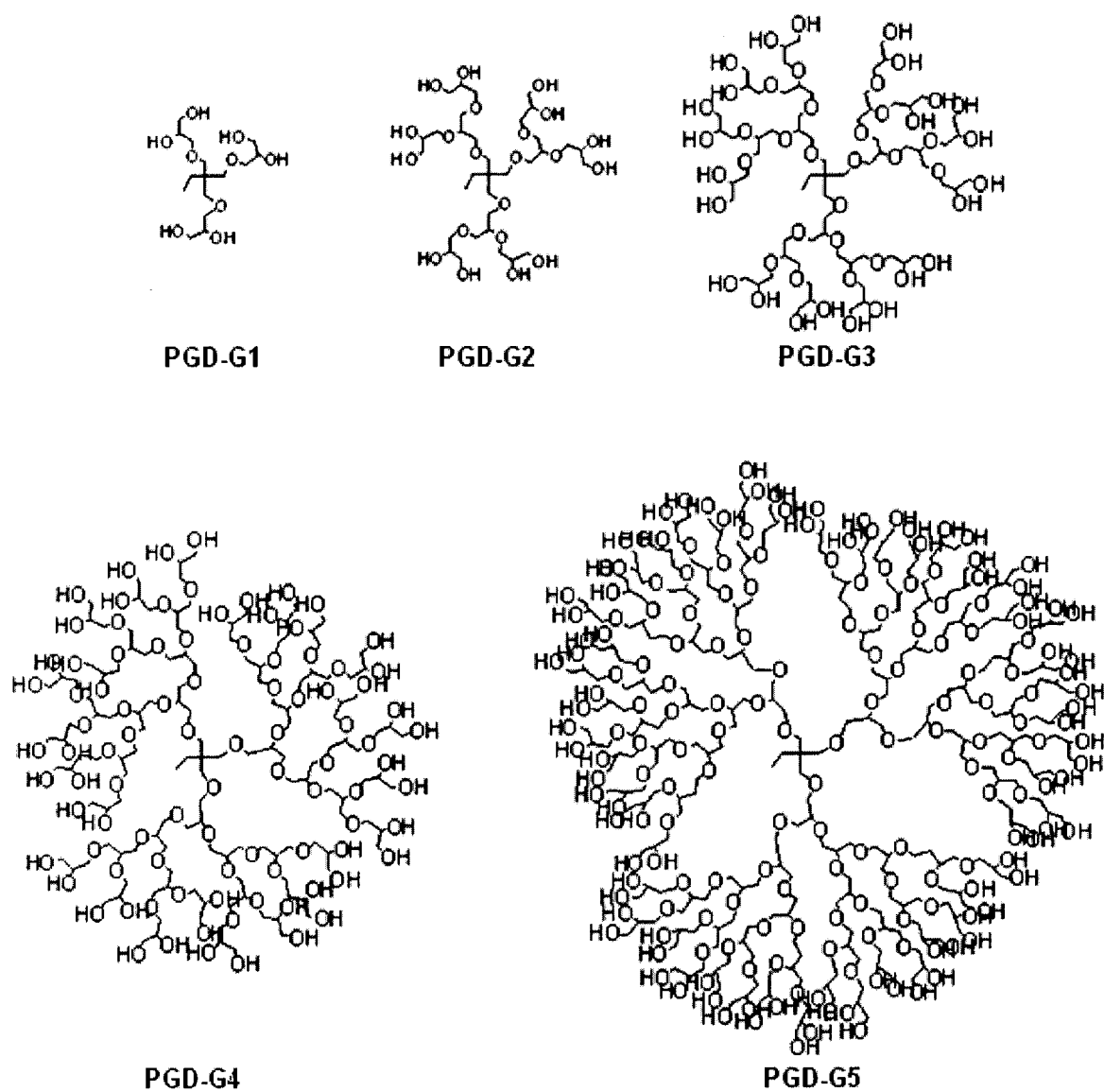




**Fig. 1. 16** Convergent synthetic method of Fréchet type-dendrimer

#### (D) Polyglycerol dendrimer

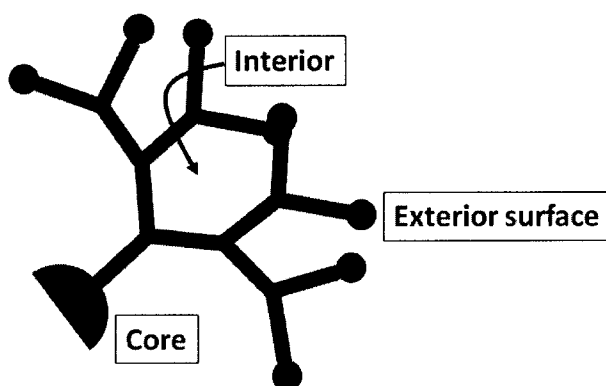
Polyglycerol dendrimers (PGDs) (**Fig. 1. 17**), which were firstly reported by R. Haag in 2000, have considered as bio-inert materials and low toxicity materials due to their elementary compositions of carbon, oxygen and hydrogen atom. Low toxicity of PGDs is attributed to their lack of any nitrogen atoms as seen in PPI and PAMAM dendrimer, the cationic nature of which is believed to cause cytotoxicity<sup>36)</sup>. Since the solubility of a poorly water-soluble drug in 50 wt% PGD aqueous solution was significantly higher than that in PEG aqueous solution, dendritic architecture of PGDs can increase solubility of the poorly water-soluble drug<sup>37)</sup>. Another characteristic of PGDs is that intramolecularly cross-linked PGDs synthesized by polyallylation and catalytic cross-linking displayed crown-type binding of picrate ions in organic phases<sup>38)</sup>.



**Fig. 1. 17** Chameical structuere of polyglycerol dendrimers of generation 1 (PGD-G1), generation 2 (PGD-G2), generation 3 (PGD-G3), generation 4 (PGD-G4) and generation 5 (PGD-G5)

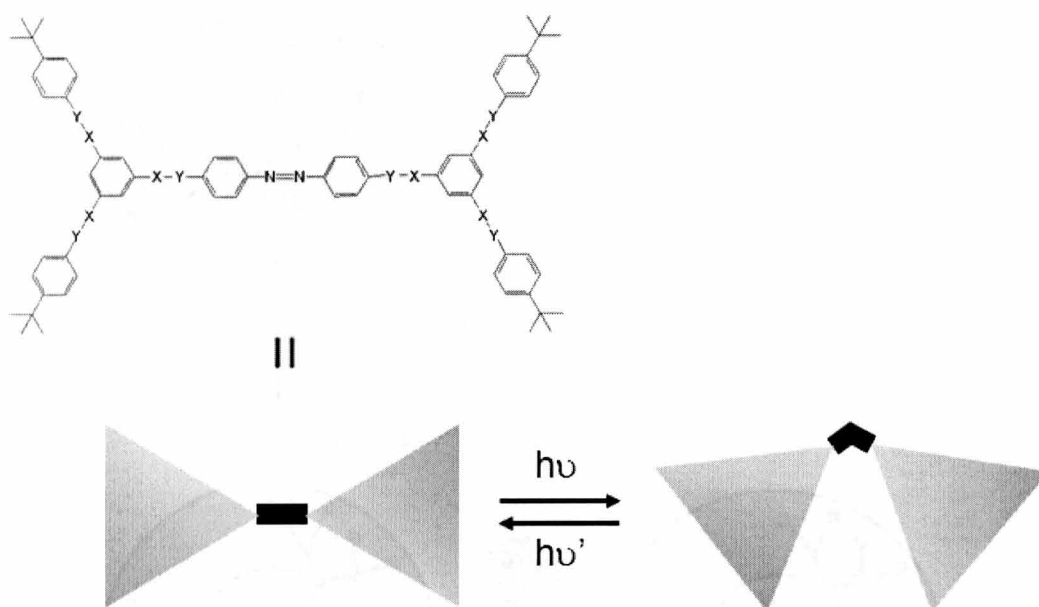
### 1.3.2 Conformational Characteristics

In previous section, I classified and characterized the macromolecular architectures. Main reason why the dendrimer and dendron are classified fourth class is their highly controlled architecture. Dendrimers possess three distinguished architectural components; core, interior and surface functionality (**Fig. 1. 18**). Each part of dendritic architecture exhibits specific functions described below. The core decides the dendritic shape, directionality and multiplicity which are expressed via the covalent connectivity to the outer shells. The surface group has the possibility of chemical modification to provide functionality of dendrimer. Also, the surface group is passive or reactive gate controlling entry or release of guest molecules from the interior part. Finally, the interior part constructs void space that is enclosed by the terminal groups with increasing the generation of the dendrimer. This space is found in not only dendritic architecture but also the other polymers. The interior space has the nature of guest-host properties that are possible with a particular dendrimer family and generation. The conformational characteristics contribute to modulation of their properties and their potential applications in interdisciplinary field. The several applications applying the property of dendritic conformation are summarized in the following section.



**Fig. 1. 18** Dendritic conformation

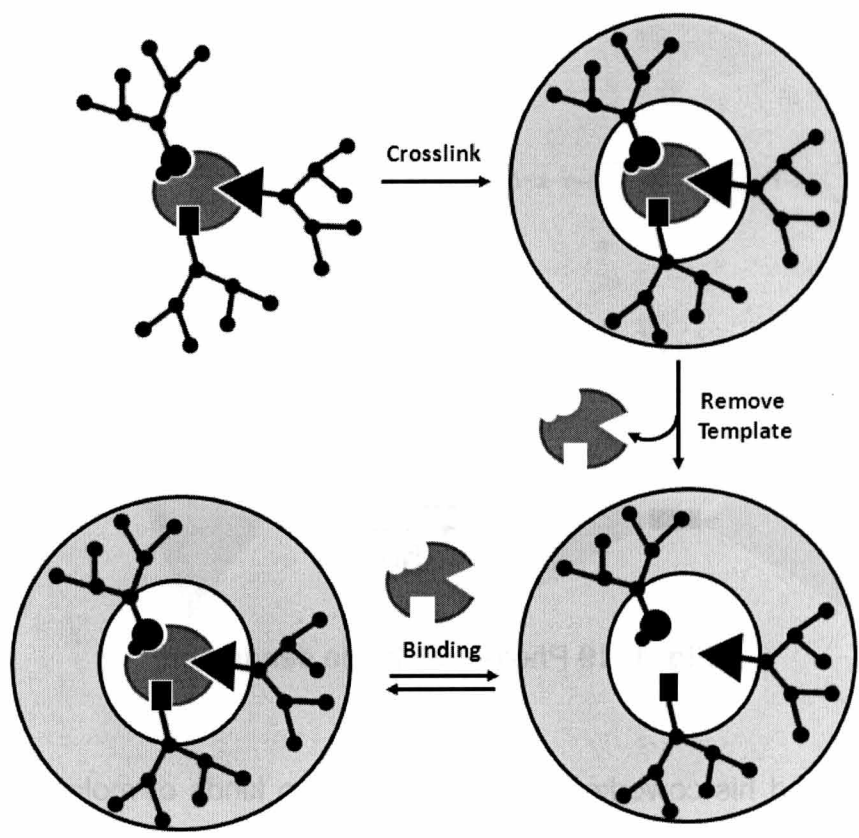
The core part that is located at the central position of the dendrimer is hardly come close to the surrounding bulk solvent. The nano-environment, where interior parts are located between the core and the bulk solvent, was functionalized by designing the nano-environment using stimuli-responsive moieties. McGrath and his coworkers have prepared two analogous types (flexible or rigid) of dendrimer with a single azobenzene moiety at the core (**Fig. 1. 19**)<sup>39</sup>. Due to the photonic properties of azobenzene located on core moiety, The E isomer is switched to the Z form by irradiating with UV light at 313 nm and can be converted back to the E form by irradiation of light at 254 nm or by heating. The E  $\rightarrow$  Z photoisomerization quantum yield decreased due to the localization of 2p orbital on benzene ring. The dendrimers can play a role of photo-switchable hosts for eosin Y.



**Fig. 1. 19** Photo-switchable dendrimers

Zimmerman and his coworkers have reported two kinds of molecularly imprinted polymer (MIP) after removing the template molecule used as a core moiety (**Fig. 1. 20**)<sup>40</sup>. The MIP was prepared by crosslinking dendrimer shell, the core part of which is capable of binding porphyrin at center. Two kinds of templates (5, 10, 15,

20-tetrakis(4-hydroxyphenyl)porphyrin and 5, 10, 15, 20-tetrakis(3,5-dihydroxyphenyl)porphyrin) were esterified with fourth- and third-generation Fréchet-type dendrons containing homoallyl end groups, respectively. After removal of the porphyrin cores by hydrolysis, the dendrimers were investigated for selective binding of porphyrins by spectrophotometric method. And rigorous test of imprinting which performed in the cross-reactivities of two dendrimers derived from different templates are compared. The highly cross-linked hosts showed rapid, elective, high affinity, two-point binding of straight-chain diamine guests. This test reveals a guest-dependent kinetic binding effect masquerading as evidence of highly selective two-point imprinting process.



**Fig. 1. 20** Schematic representation of the dendritic MIP

Compared with linear polymer, dendrimers have extensive surface in their molecular weight. This makes it very attractive toward applications for stimuli-responsive materials or catalysts with large reacting area. Taking these distinguishing properties into account many researchers have tried to functionalize dendrimers through chemical modification of dendritic surface. Thayumanvan and his coworkers have characterized self-assembly of an amphiphilic dendrimer in which every repeat unit within the macromolecule contains hydrophilic and hydrophobic functionalities on opposite faces of dendritic bone on surface<sup>41)</sup>. Substrate that was modified with amphiphilic dendrimer showed the effective modification of surface. In their research, hydrophobic surface could not be converted to hydrophilic surface by these dendrimers, due to surface affinity against surface energy competition of alkyl group. However, they suggest the possibility of modification of substrates using dendritic molecule.

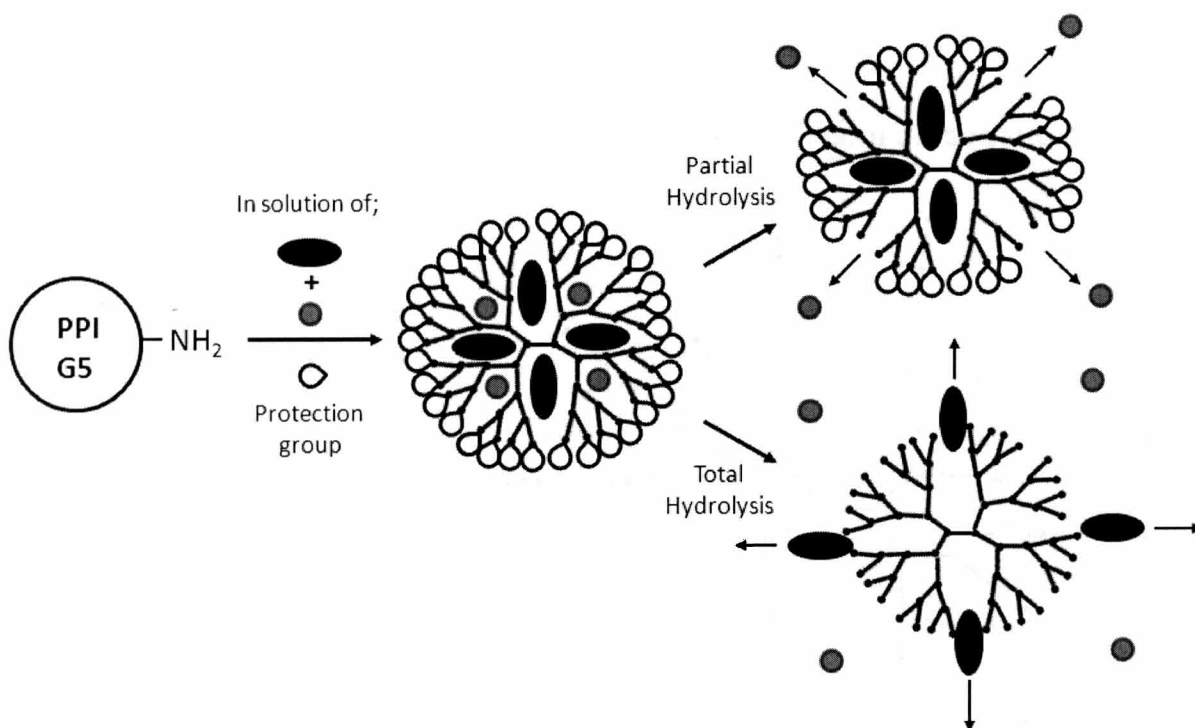
Since polymers proved their therapeutic use, dendrimers have also studied as a therapeutic material, due to their well-defined and nanoscaled polymeric scaffold bearing monodispersity and the controlled surface functionalities. Nanometer-sized dendrimers (range of 1-100 nm) may interact effectively and specifically with cellular membrane, cell organelles and proteins, as all these cellular components are themselves nanometer in size range<sup>42)</sup>. However, toxicity associated with terminal-NH<sub>2</sub> groups and multi cationic charge limits their candidatures for biomedical applications<sup>43)</sup>. Therefore, many researchers tried to reduce the toxicity through dendritic surface modification such as PEGylation<sup>44)</sup>, acetylation<sup>45)</sup> and conjunction with carbohydrates<sup>46)</sup> or amino acids<sup>47)</sup>.

Finally, the interior of dendrimers is protected from the outside bulk solvent by the dendrimer surface. The dendritic area is most attractive nature compared with classic

polymers.

### 1.3.3 Dendritic interior for molecular encapsulation

The three-dimensional motif of dendrimer imparts with interior space, unlike linear polymer which possesses random coil structure with high conformational degree. The idea of molecular encapsulation within dendritic interior, *i.e.* topological trapping, has been suggested for the first time by Maciejewski in 1982<sup>48)</sup>. Compared to the relatively open structures, dendrimers which are proper generations, *i.e.* PAMAM generations 4 or 5, tend to adopt an extended conformation with a spherical surface containing pockets of space in the interior capable of forming guest-host complex. After the report of topological trapping by shell molecules, the first host-guest complex within dendritic interior was reported by Meijer group, in 1994 (**Fig. 1. 21**)<sup>49)</sup>. In their report, they referred to this new construction as the 'dendritic box'. Fifth generation of amine-functionalized poly(propylene imine) (PPI) dendrimer with (*t*-Boc)-protected induced dendritic encapsulation of L-phenylalanine or the other amino acids<sup>50)</sup> due to densely formed hydrogen-bonded surface shells and the tertiary amines. The maximum number of encapsulated guest molecules per dendritic interior was directly related to the shape and the size of the guest molecules, as well as to the number, shape and size of the available interior. Most remarkable point was the controlled "On and Off system of dendritic box". Partial hydrolysis of the hydrogen-bonded shell liberated only small guest molecules.



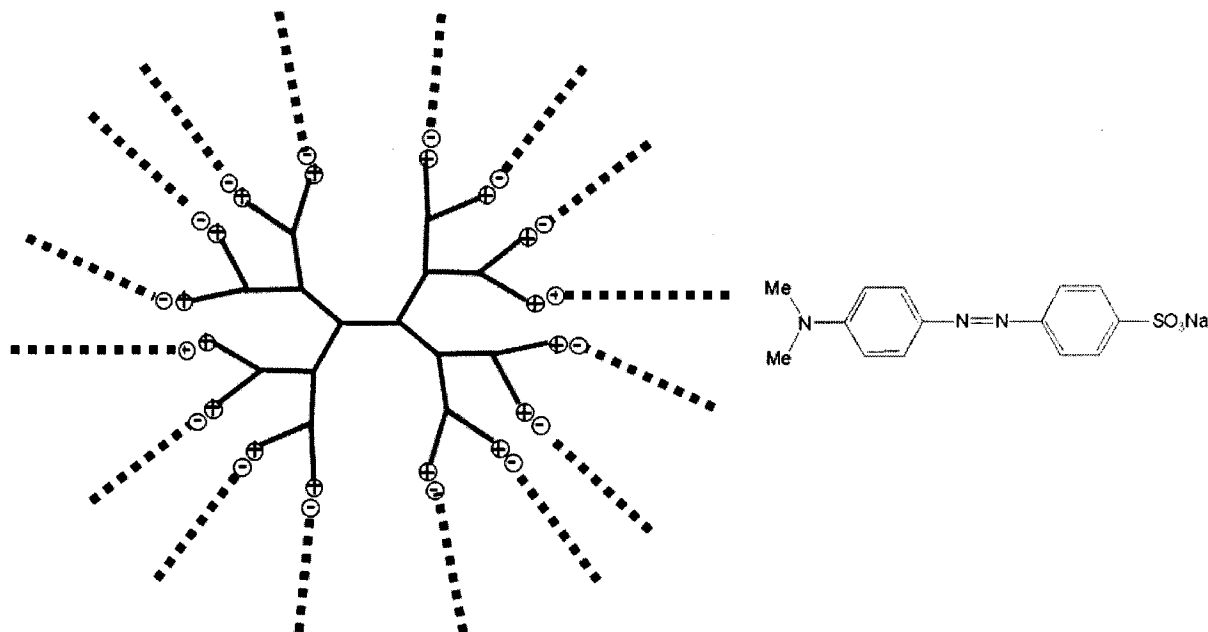
**Fig. 1. 21** Topological encapsulation of guest molecules within dendritic box

According to “dendritic box theory of Meijier”, the presence of internal interior within dendrimers is strongly related to their conformational behavior and to the number of terminal groups. Through several studies, these factors not only involve the nature of the dendrimer and terminal groups but also the surrounding solvent and  $\text{pH}^{51}$ ).



## 1.4 Dendritic host-guest chemistry

### 1. 4. 1 Nonspecific internal binding



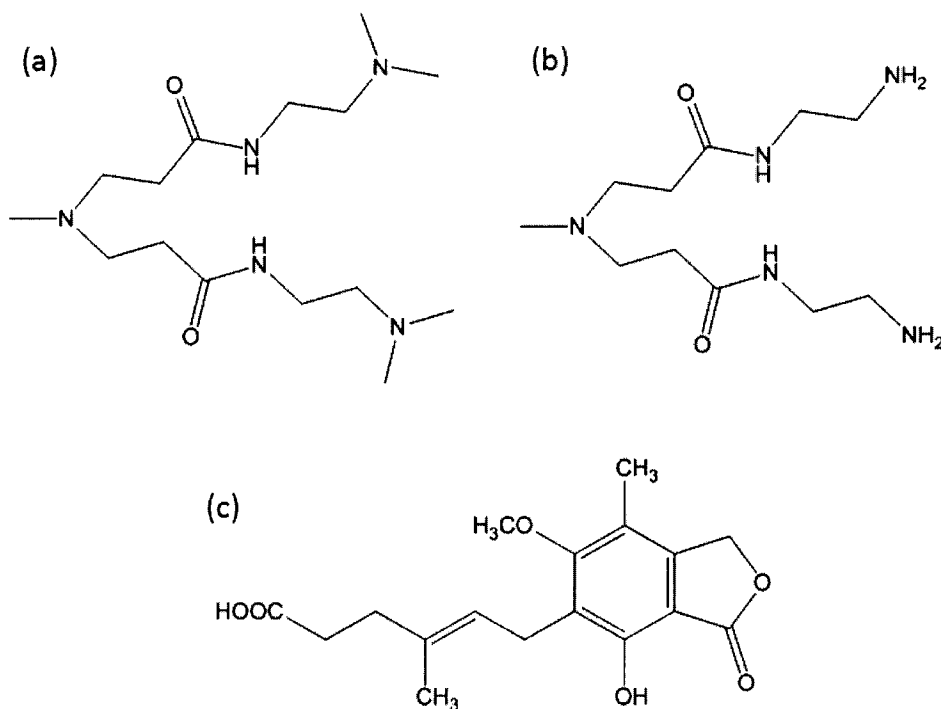
**Fig. 1. 22** Formation of the host-guest complexation between PAMAM dendrimer bearing ionic assembled shell with dodecanoic acid (left) and methyl orange (right).

Crooks groups reported host-guest complexation of inverted micelle-like structures that are formed by ionic complexation between fatty acids (decanoic acid) and an amine-terminated PAMAM dendrimer of fourth-generation (G4-PAMAM) and a hydrophilic guest molecule (**Fig. 1. 22**). In this report, they suggested its potential as a extraction system toward hydrophilic guest molecules into nonpolar solvents from aqueous phase<sup>52)</sup>. Methyl orange, a hydrophilic dye, is used as the guest molecule capable of binding to amine groups in micelle-like structures. Metal particles (Cu) also could be prepared by sorption of metal ions into the interior of dendrimers. Taking this advantage of dendrimer into account, they tested dendrimer-encapsulated Pd particles in toluene solution for catalytic activity by examining their effectiveness toward hydrogenation<sup>53)</sup>.

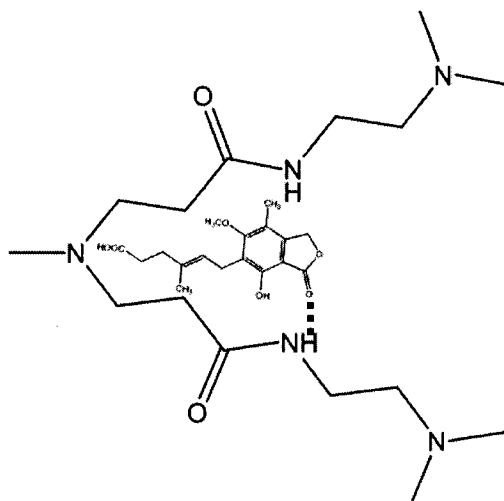
## 1. 4. 2 Directed internal binding

### 1. 4. 2. 1 Using hydrogen bonding

W. Xu's groups investigated the host-guest chemistry of PAMAM dendrimer-drug complexes by NMR techniques, including  $^1\text{H}$ -NMR and 2D-NOESY. One of their reports suggest the interaction between PAMAM dendrimer and mycophenolic acid (MPA) (**Fig. 1. 23, Fig. 1. 24**)<sup>54</sup>. The  $^1\text{H}$ -NMR spectroscopy techniques showed that the MPA molecules are bound in the interior of dendrimer pockets by hydrogen-bond interactions and hydrophobic interactions. The 2D NOESY analysis predicted the localization of MPA molecules in the pockets of dendrimers.



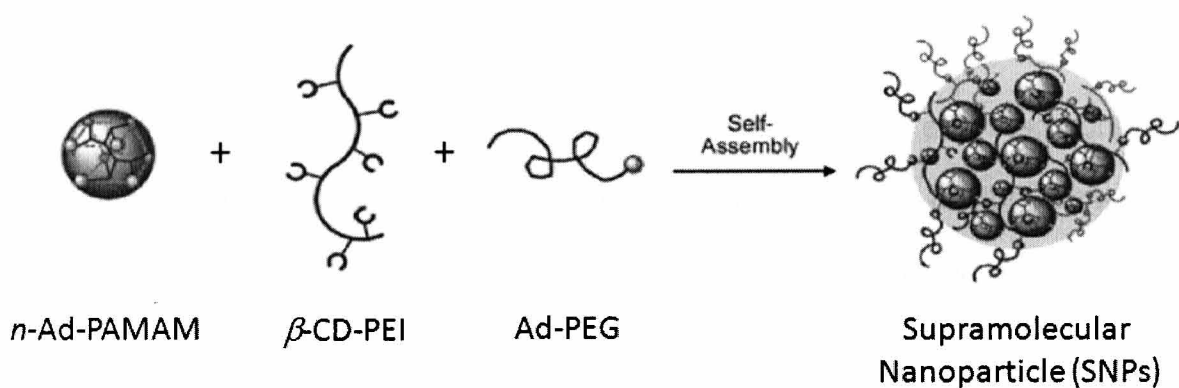
**Fig. 1. 23** Chemical structure in the (a) G5 PAMAM dendrimer interior repetitive units, (b) G5 PAMAM dendrimer outermost layer, and (c) MPA molecule.



**Fig. 1. 24** Host-guest complexes; Encapsulation of MPA molecules in the interior of dendrimers by hydrophobic interactions / hydrogen-bond interaction

#### 1. 4. 2. 2 Apolar binding

H. R. Tseng's group reports a convenient, flexible and modular synthetic approach to the preparation of size-controlled (30-45 nm) supramolecular nanoparticle (SNPs) (**Fig. 1. 25**)<sup>55</sup>. Cyclodextrin/Adamantan (CD/Ad) complex was employed to achieve self-assembly of SNPs from three different molecular building blocks. To analyze how the mixing ratios between Ad-PAMAM and CD-PEI affect the size of the resulting SNPs, they utilized dynamic light scattering (DLS) measurements to analyze the freshly prepared SNPs.



**Fig. 1. 25** A convenient, flexible, and modular synthetic approach for preparation of size-controlled supramolecular nanoparticles (SNPs). A molecular recognition system based on adamantane (Ad) and  $\beta$ -cyclodextrin (CD) was employed to assemble three molecular building blocks. 1) *n*-Ad-PAMAM ( $n=4^*$  or 8), 2) CD-PEI, and 3) Ad-PEG.

## 1.5 Objective of this study

Dendrimers are well-defined dense branched architecture that is obtained via step-wise addition of repeated layers of branched segments to a multifunctional core. These unique architectures have been observed in nature, such as neuron which carries impulses to cell body.

The significant difference between dendrimers and classical polymers is interior space which can entrap guest molecules. Dendritic systems reveal highly dense endgroups, increasing with each new generation of branched segments. The dense endgroups and the branched structure construct the interior space that is distinguished from external environment of bulk solvent. Since 1994 at the first report “dendritic box” by Meijer, the interior space has been demonstrated as encapsulating space for guest molecules, suggesting that they act as nano-sized macromolecular carriers. For example, PAMAM dendrimer and its derivatives could encapsulate drugs via electrostatic interaction or/and hydrophobic interaction. Since PAMAM dendrimers contain peripheral primary amine and internal tertiary amine groups, those groups can be protonated below their  $pK_a$  in aqueous conditions, which becomes driving force to form complexes with oppositely charged guest molecules. However, the amine-based dendrimers express toxicity due to their high number of cationic charge, leading to the limited biomedical application.

Polyglycerol dendrimers (PGDs) consist of glycerol units, and their application is expected in the field of bio-functional materials due to their good biocompatibility. To apply the PGDs for practical use, the dense surface hydroxyl groups have been modified for protein resistance. However, interior spaces of PGDs are still veiled for the development of PGDs. Therefore, I hypothesized that PGDs can act as host molecules with non-toxic properties if the physicochemical properties of interior space

are clarified.

This dissertation describes the study of dendritic host-guest systems by using PGDs as a host and several guest molecules. In order to understand the properties of host-guest complex of PGDs, fluorescent and thermodynamic analyses for the host-guest complex was carried out by means of fluorescence spectroscopy, NMR titration and isothermal titration calorimetry (ITC). In this dissertation, 4-amino-3-hydroxynaphthalene-1-sulphonic acid (AHSA), 5-fluorouracil (5-Fu) and amino acids were used as the guest molecules. AHSA will give some information of the complication within the interior parts of PGDs in terms of hydrophobic environments and intermolecular interactions. For the practical application of host-guest system using PGDs, I selected 5-Fu as a model drug. In combination with mosodispersed nature of PGDs, stoichiometric analysis may be achieved and applicable for pharmaceutical use. As an exploratory study of further guest molecules toward PGDs, amino acids were subjected for complexation with PGDs, which are tried to perform using ITC to get stoichiometric information.

Through the investigation of the interior space for the host-guest systems, the scientific evidences will provide new opportunity of PGDs as a host molecule for encapsulation of biologically active agents toward pharmaceutical applications.

## 1.6 Survey of this dissertation

This dissertation is classified by the guest molecules. In chapter 2, synthesis and purification of PGDs of generation 1 and 2 (PGD-G1 and –G2) were described, and the analyses of molecular interaction between PGD-G1 or G2 and AHSA were described. Here, the binding constant and stoichiometry were evaluated by ITC. In chapter 3, synthesis and purification of PGDs of generation 3 and 4 (PGD-G3 and –G4) were described, and molecular interaction between PGD-G3 or G4 and AHSA were investigated. Here, the binding constant and stoichiometry were evaluated by ITC. In order to determine the average diameter of PGD-G3 or G4 in presence or absence of AHSA in aqueous solution, DLS was employed. In chapter 4, the interaction between PGDs and 5-Fu were discussed by  $^1\text{H}$ -,  $^{19}\text{F}$ -NMR and fluorescent measurements. In chapter 5, exploratory study of amino acids as alternative guest molecules was investigated to evaluate the interaction between side chains of amino acids and interior of PGDs.

## References

1. J.M. Lehn, *Science*, **1993**, 260, 1762  
J.M. Lehn, *Angew. Chem.*, **1988**, 27(1), 89  
J.M. Lehn, *Pro. Indian. Acad. Sci (Chem. Sci.)*, **1994**, 106, 915  
J.M. Lehn, *Proc. Natl. Acad. Sci. USA*, **2002**, 99, 4763  
J.M. Lehn, *Science*, **2002**, 295, 2400  
J.M. Lehn, *Nobel lecture*, **1987**  
D.J. Cram, *Nobel lecture*, **1987**
2. D. J. Cram, *J. Am. Chem. Soc.*, **1982**, 104, 6828  
D. J. Cram, *J. Am. Chem. Soc.*, **1985**, 107, 3645  
D. J. Cram, *J. Am. Chem. Soc.*, **1990**, 112, 5837  
R. C. Helgeson, *J. Am. Chem. Soc.*, **1993**, 115, 11506
3. S. Kaneko, *J. Phys. Chem.*, **2011**, 115, 10846  
S. Kunsagi-Mate, *Anal. Chem. Acta*, **2001**, 428, 301  
Y. Kawabata, *Sensors and Actuators B*, **1995**, 29, 135  
M. Kubo, *Tetrahedron Lett.*, **2006**, 47, 1927  
S. L. Gac, *Tetrahedron*, **2007**, 63, 10721
4. S. Nummelin, D. Falabu, A. Shivanyuk, K. Rissanen, *Org. Lett.*, **2002**, 4(18), 3019  
D. Namor A. F., Chaaban J. K., Piro, O. E., Castellano E. E., *J. Phys. Chem. B*, **2006**, 110, 2442  
D. Namor A. F., Al Rawi N., Piro, O. E., Castellano E. E.; Gil, E., *J. Phys. Chem. B*, **2011**, 115, 6922  
M. Mäkinen, P. Vainiotalo, K. Rissanen, *J. Am. Soc. Mass Spectrom.* **2002**, 13, 851  
M. Mäkinen, P. Jalkanen, P. Vainiotalo, *Tetrahedron*, **2002**, 58, 8591
5. C. J. Pedersen, *Nobel Lecture*, **1987**  
D. Alivertis, V. Theodorou, G. Paraskevopoulos, K. Skobridis, *Tetrahedron Lett.*, **2007**, 48, 4091  
M. Lee, Z. Niu, D. V. Schoonover, C. Slebodnick, H. W. Gibson, *Tetrahedron*, **2010**, 66, 7077  
H. Okamoto, M. Owari, M. Kimura, and K. Satake, *Tetrahedron Lett.* **2001**, 42, 7453



- S. Maleknia, J. Brodbelt, J., *J. Am. Chem. Soc.*, **1993**, 115, 2837  
 P. E. Stott, J. S. Bradshaw, W. W. Parish, *J. Am. Chem. Soc.*, **1980**, 102, 4810  
 S. Maleknia, J. J. Brodbelt, *J. Am. Chem. Soc.*, **1992**, 114, 4295
6. F. Huang, C. Slebodnick, A. L. Rheingold, K. A. Switek, H. W. Gibson, *Tetrahedron Lett.* **2005**, 46, 6765  
 F. Huang, A. L. Rheingold, C. Slebodnick, A. Ohs, K. A. Switek., H. W. Gibson, *Tetrahedron*, **2005**, 61, 10242  
 F. Huang, C. Slebodnick, E. J. Mahan, H. W. Gibson, *Tetrahedron*, **2007**, 63, 2875  
 E. Garrier, S. Le Gac, I. Jabin, *Tetrahedron*, **2005**, 16, 3767  
 N.K. Dalley, K. E. Krakowiak, *Tetrahedron*, **1994**, 50(9), 2721  
 B. Owenson, R. D. MacElroy, A. Pohorille, *J. Am. Chem. Soc.*, **1988**, 110, 6992  
 F. Eggers, T. Funck, H. Richmann, H. Schneider, E. M. Eyring, S. Petrucci, *J. Phys. Chem.*, **1987**, 91, 1961  
 D. M. Smith, C.W. Park, J. A. Ibers, *Inorg. Chem.*, **1996**, 35, 6682
7. K. Paek, H. Ihm, S. Yun, H. C. Lee, *Tetrahedron Lett.*, **1999**, 40, 8905  
 H. Konishi, T. Mita, O. Morikawa, K. Kobayashi, *Tetrahedron Lett.*, **2007**, 48, 7489
8. B. Zhang, R. Breslow, *J. Am. Chem. Soc.*, **1996**, 118, 8495  
 N. Balabai, B. Linton, A. Napper, S. Priyadarshy, A. P. Sukharevsky, and D. H. Waldeck, *J. Phys. Chem. B.*, **1998**, 102, 9617  
 Y. Takashima, M. Osaki, A. Harada, *J. Am. Chem. Soc.*, **2004**, 126, 13588  
 G. Nelles, M. Weisser, R. Back, P. Wohlfart, G. Wenz, S. Mittler-Neher, *J. Am. Chem. Soc.*, **1996**, 118, 5039  
 K. A. Udachin, L. D. Wilson, J. A. Ripmeester., *J. Am. Chem. Soc.*, **2000**, 122, 12375  
 Y.M. Jeon, J. Kim, D. Whang, K. Kim, *J. Am. Chem. Soc.*, **1996**, 118, 9790  
 V. P. Fedin, V. Gramlich, M. Wörle, T. Weber, *Inorg. Chem.* **2001**, 40, 1074  
 V. P. Fedin, A. V. Virovets, M. N. Sokolov, *Inorg. Chem.*, **2000**, 39, 2227  
 J. Kim, I.S. Jung, S. Y. Kim, E. Lee, J.K. Kang, S. Sakamoto, K. Yamaguchi, K. Kim, *J. Am. Chem. Soc.*, **2000**, 122, 540  
 W.L. Mock, N.Y. Shih, *J. Org. Chem.* **1983**, 48 (20), 3618  
 J. W. Lee, S. Samal, N. Selvapalam, H. J. Kim, K. Kim, *Acc. Chem. Res.*, **2003**, 36, 621  
 W. A. Freeman, W. L. Mock, N. Y. Shih, *J. Am. Chem. Soc.*, **1981**, 103, 7367-
9. H. Hiemstra, H. Wynberg, *J. Am. Chem. Soc.* **1981**, 103, 417

10. J. N. Isreaelachvili, *Quart. Rev. Biophys*, **1973**, 6, 341  
D. Chandler, J. D. Weeks, H. C. Andersen, *Science*, **1983**, 220, 787  
A. D. Buckingham, P. W. Fowler, J. M. Hutson, *Chem. Rev.*, **1988**, 88, 963
11. W. Kauzmann, *Adv. Protein Chem.*, **1959**, 14, 1  
R. L. Baldwin, *Proc. Natl. Acad. Sci. USA*, **1986**, 83, 8069  
P. L. Privalov, S. J. Gill, *Adv. Protein Chem.*, **1988**, 39, 191  
N. Muller, *Acc. Chem. Res.*, **1990**, 23, 23
12. W. Kauzmann, *Adv. Protein Chem.* **1959**, 14, 1  
C. Tanford, *J. Mol. Biol.* **1972**, 67, 59
13. G. C. Pimentel, A. L. McClellan, *Ann. Rev. Phys. Chem.* **1971**, 22, 347  
H. Umeyama, K. Morokuma, *J. Am. Chem. Soc.*, **1997**, 99, 1316  
A. C. Legon, D. I. Millen, *Acc. Chem. Res.*, **1987**, 20, 39046
14. J. M. J. Frechet and D. A. Tomalia, dendrimers and other dendritic polymers, John Wiley & Sons, Ltd., 2001,
15. D. A Tomalia, J.R. Dewald, M.J. Hall, S.J. Martin, P.B. Smith, *SPSJ Int. Polm. Conference*, Kyoto, Japan, **1984**, 65  
D. A. Tomalia, H. Baker, J. Dewald, M. Hall, G. Kallos, S. Martin, J. Roeck, J. Ryder, P. Smith, *Polym. J.* **1985**, 17, 117
16. H. L. Wagner, *J. Phys. Chem. Ref. Data*, **1985**, 14(4), 1101  
H. Sue, Y. Nakamoto, S. Ishida, *Polymer Bulletin*, **1989**, 21, 97  
D. Lath, K. Csomorová, G. Kolláriková, M. Stankovská, L. oltés, *Chem. Pap.*, **2005**, 59(5), 291  
S. Ishida, T. Kitagawa, Y. Nakamoto, K. Kaneko, *Polymer Bulletin*, **1983**, 10, 533
17. J. M. J. Frechet, Hawker, I. Gitsov, J. W Leon, *J. Pure Appl. Chem. A33*, **1996**, 10, 1399
18. W. A. Tao, B. Wollscheid, R. O'Brien, J. K. Eng, X. J. Li, B. Bodenmiller, J. D. Watts, L. Hood, R. Aebersold, *Nature Methods*, **2005**, 2(8), 591  
M. He et al, *Rapid Commun. Mass Spectrom.* **2004**, 18, 690

- W. James, R. P. Nogue, G. K. C. Wai, *Polymer Bulletin*, **1995**, 35, 449
- J. C. Hummelen, J. L. J. v. Dongen, E. W. Meijer, *Chem. Eur. J.*, **1997**, 3(9), 1489
19. Y. Mengerink, M. Mure, E. de Brabander, Sj. van der Wal, *J. chromatogr. A*, **1996**, 730, 75  
 P. L. Dubin, S. Edwards, J. I. Kaplan, M. S. Mehta, D. Tornalia, D.; J. Xia,, *Anal. Chem.* **1992**, 64, 2344  
 D. Tyssen, S. A. Henderson, A. Johnson, J. Sterjovski, K. Moore, *Mol. Pharm.*, **2006**, 3(5) 614  
 L. Tao, J. Geng, Y. Xu, V. Ladmiral, G. Mantovani, D. M. Haddleton, *Chem. Commun.*, **2007**, 3441
  20. A. Sharma, D. Mohanty, A. Desai, R. Ali, *Electrophoresis*, **2003**, 24, 2733  
 R.K. DeLong, Y. Hoon, S.K. Alahari, M. Fisher, S.M. Short, S.H. Kang, R. Kole, V. Janout, S.L. Regan, *Pharmaceutical research*, **1999**, 16(12), 1799  
 X. Shi, A. K. Patri, W. Lesniak, M. T. Islam, C. Zhang, J. R. Baker, L. Balogh, *Electrophoresis*, **2005**, 26, 2960  
 X. Shi X, I. J. Majoros, A. K. Patri, X. Bi, M. T. Islam, *Mol. Pharm.*, **2005**, 2(4), 278
  21. C. L. Jackson, H. D. Chanzy, F. P. Booy, B. J. Drake, D. A. Tomalia, B. J. Bauer, E. J. Amis, *Macromolecules*, **1998**, 31(18), 6259  
 R. M. Murphy, H. Slayter, P. Schurtenberger, R. A. Chamberlin, C. K. Colton, M. Yarmush, L., *Biophys. J.*, **1998**, 54, 45  
 A. Kulczynska, T. Frost, L. D. Margerum, *Macromolecules*, **2006**, 39, 7372  
 D. A. Tomalia, A. M. Naylor, W. A. Goddard III, *Angew. Chem.*, **1990**, 29(2) 138
  22. H. Frey et al, *Hyperbranched Polymers*, Wiley, 1 ed, **2011**, 1-26, 301  
 A. Hult, M. Johansson, E. Malmströ, *Adv. Polym. Sci.*, **1999**, 143, 1  
 H. Türk, R. Haag, H. Frey, *Macromol.*, **2000**, 33, 7682  
 C. J. Hawker, R. Lee, J. M. J. Frechet et al., *J. Am. Chem. Soc.*, **1991**, 113-4583
  23. J. M. J. Frechet, C. J. Hawker, *React. Funct. Polym.*, **1995**, 26, 127
  24. Y. Liu, V.S. Bryantsev, M. S. Diallo, W. A. Goddard., *J. Am. Chem. Soc.*, **2009**, 131, 2798  
 A. Sunder, H. Turk, R. Haag, H. Frey, *Macromolecules* **2000**, 33, 7682

25. H. Martin, H. Kinns, N. Mitchell, Y. Astier, H. Bayley, S. Howorka, *J. Am. Chem. Soc.*, **2007**, 129, 9640
26. E. M. M. de Brabander-van der Berg, E. Meijer, *Angew. Chem. Int. Ed. Engl.*, **1993**, 32(9), 1308  
E. M. M. De Brabander-van den Berg, E. W. Meijer, *Angew. Chem.*, **1993**, 105, 1370
27. B. Gonzalez, C.M. Casado, B. Alonso, I. Cuadrado, M. Moran, Y. Wang, A. E Kaifer,, *Chem. Commun.*, **1998**, 2569
28. V. Balzani, *J. Am. Chem. Soc.*, **2000**, 122(42), 10398
29. M. Ooe, M. Murata, T. Mizugaki, K. Ebitani, K. Kaneda, *J. Am. Chem. Soc.*, **2004**, 126, 1604
30. C. J. Hawker, J. M. J. Fréchet, J. Ciwm, *Chem. Commun.*, **1990**, 1010  
C. J. Hawker, J. M. J. Fréchet, *J. Am. Chem. Soc.*, **1990**, 112, 7638
31. I. Gitsov, P. T. Ivanova, J. M. J. Fréchet, *Macromol. Rapid. Commun.*, **1994**, 15, 387
32. M. R. Leduc, C.J. Hawker, J. Dao, J.M.J. Fréchet, *J. Am. Chem. Soc.*, **1996**, 118, 11111  
M. R. Leduc, W. Hayes, J. M. J. Fréchet, *J. Polymer Sci.* **1998**, 36(a) 1
33. I. Gitsov, J. M. J. Fréchet, *Macromolecules*, **1994**, 27, 7309  
T. Emrick, W. Hayes and J. M. J. Fréchet, *Polym. Sci. A*, **1999**, 37, 3748
34. C. J. Hawker, J.M.J.Fréchet, *Polymer*, **1992**, 33, 1507  
G. Draheim, H. Ritter, *Macromol. Chem. Phys.*, **1995**, 196, 2211  
V. Percec, M. Kawasumi, *J. Am. Chem. Soc.*, **1996**, 118, 9855  
V. Percec, C.-H. Ahn, G. Ungar, D. J. P. Yeardley, M. Moeller and S. S. Sheiko, *Nature*, **1998**, 391, 161
35. M. Liu, K. Kono, J. M. J. Fréchet, *Controlled Release*, **2000**, 65, 121  
G. R. Newkome, C. N. Moorefield, G. R. Baker, M. J. Saunders, S. H. Grossman, C. Alkane, *J. Org. Chem.*, **1993**, 58, 3123  
D. J. Abdallah, R. G. Weiss, *Adv. Mat.*, **2000**, 12, 1237

- I. Gitsov, K. L. Wooley, J. M. J. Frechet, *Angew. Chem.. Int. Ed. Engl.*, **1992**, 31, 1200
36. L. X. Liao, F. Stellacci, D. V. McGrath, *J. Am. Chem. Soc.*, **2004**, 126, 2181
37. N. Malik, R. Wiwattanapatapee, R. Klopsch, K. Lorenz, H. Frey, J. W. Weener, E. W. Meijer, W. Paulus, R. Duncan, *Journal of Controlled Release* **2000**, 65, 133.
38. T. Ooya, J. Lee, K. Park, *J. Control. Release* **2003**, 93, 121
39. S. C. Zimmerman, J. R. Quinn, E. Burakowska, R. Haag, *Angew, Chem. Int. Ed.* **2007**, 46, 8164
40. S. C. Zimmerman, M. S. Wendland, N. A. Rakow, I. Zharov, K. S. Suslick, *J. Am. Chem. Soc.*, **2003**, 125, 13504  
E. Mertz, S.C. Zimmerman, *J. Am. Chem. Soc.*, **2003**, 125, 3424
41. Y. Chen, A. V. Ambade, D. R. Vutukuri, S. Thayumanavan, *J. Am. Chem.. Soc.*, **2006**, 128(46), 14760
42. S. H. Choi, S. H. Lee, T. G. Park, *Biomacromolecules*, **2006**, 7(6), 1864  
S. H. Lee, S. H. Choi, S. H. Kim, T. G. Park, *J. Control Release*, **2008**, 125, 25
43. W. Meijer, R. Paulus, J. Duncan, *J. Controlled Release*, **2000**, 65, 133  
D. S. Wilbur, D. K. Hamlin, P. M. Pathare, S. A. Weerawarna, *Bioconjugate Chem.*, **1997**, 8, 572
44. K. Fant, E. K. Esbjorner, A. Jenkins, M. C. Grossel, P. Lincoln, B. Norden, *Molecular Pharmaceutics*, **2010**, 7(5), 1734  
N.A. Stasko, C.B. Johnson, M.H. Schoenfisch, T.A. Johnson, E. Holmuhamedov, *Biomacrmolecules*, **2007**, 8, 3853  
H, Lee, R. G. Larson, *Macromolecules*, **2011**, 44, 2291  
S. J. Guillaudeu, M .E. Fox, Y. M. Haidar, E. E. Dy, F. C. Szoka, J. M. J. Frechet, *Bioconjugate Chem.*, **2008**, 19, 461  
H. Maeda, J. Wu, T. Sawa, Y. Matsumura, K. Hori, *Pharmaceutical Research*, **2010**, 27(1), 161

45. H. Lee, J. R. Baker, R. G. Larson, *J. Phys. Chem. C*, **2011**, 115, 5316  
R. S. Dhanikula, P. Hildgen, *Bioconjugate Chem.*, **2006**, 17, 29  
I. J. Majoros, A. Myc, T. P. Thomas, C. B. Mehta, J. R. Baker, *Biomacromolecules*, **2008**, 9, 603  
I. J. Majoros, T. P. Thomas, C. B. Mehta, J. R. Baker, *J. Med. Chem.*, **2005**, 48, 5892  
L. Albertazzi, M. Serresi, A. Albanese, F. Beltram., *Molecular pharmaceuticals*, **2010**, 7(3), 680
46. H. Lee, R. G. Larson, *J. Phys. Chem. B*, **2009**, 113, 13202  
P. Agrawal, U. Gupta, N. K. Jain, *Biomaterials*, **2007**, 28, 3349  
H. Arima, S. Yamashita, Y. Mori, Y. Hayashi, K. Motoyama, K. Hattori, T. Takeuchi, H. Jono, Y. Ando, F. Hirayama, K. Uekama, *J. Controlled Release*, **2010**, 146, 106  
R.D. Kensinger, B.C. Yowler, A.J. Benesi, C.L. Schengrund, *Bioconjugate Chem.* **2004**, 15, 349
47. C. Troiber, E. Wagner et al., *Bioconjugate Chem.*, **2011**, 22, 1737  
A. F. Saleh, A. Arzumanov, R. Abes, D. Owen, B. Lebleu, M. J. Gait et al., *Bioconjugate Chem.*, **2010**, 21, 1902  
T. I. Kim, J. U. Baek, J. K. Yoon, J. S. Choi, K. Kim, J. S. Park, *Bioconjugate Chem.*, **2007**, 18, 309  
M. Fischer, D. Appelhans, S. Schwarz, B. Klajnert, M. Bryszewska, B. Voit, M. Rogers, *Biomacromolecules*, **2010**, 11, 1314  
G. S. Yu, Y. M. Bae, H. Choi, B. Kong, I. S. Choi., J. S. Choi, *Bioconjugate Chem.*, **2011**, 22, 1046  
X. Chen, P. Wu, M. Rousseas, D. Okawa, Z. Gartneer, A. Zettl, and C.R. Bertozzi, *J. Am. Chem. Soc.*, **2009**, 131, 890
48. M. Maciejewski, *J. Macromol. Sci. Chem.*, **1982**, A17(4), 689
49. J. F. G. A. Jansen, E. M. M. de Brabander-van den Berg, E. W. Meije, *Science*, **1994**, 266, 1226
50. J. F. G. A. Jansen, E. W. Meijer, *J. Am. Chem. Soc.*, **1995**, 117, 4417
51. J. W. Weener, J. L. J. van Dongen, E. W. Meijer, *J. Am. Chem. Soc.*, **1999**, 121, 10346

52. V. Chechik, M. Zhao, R. M. Crooks, *J. Am. Chem. Soc.* **1999**, 121, 4910
53. Y. Niu, K. Y. Lee, R. M. Crooks, *J. Am. Chem. Soc.* **2001**, 123, 6840
54. J. Hu, Y. Cheng, Y. Ma, Q. Wu, T. Xu, *J. Phys. Chem. B* **2009**, 113, 64  
L. Zhao, Q. Wu, Y. Cheng, J. Shang, J. Wu, T. Xu, *J. Am. Chem. Soc.* **2010**, 132, 3182
55. H. Wang, S. Wang, H. Su, K. J. Chen, A. Lee, W. Y. Lin, Y. Wang, J. Sun, K. Kamei, J. Czernin, C. G. Radu, H. R. Tseng, *Angew. Chem. Int. Ed.* **2009**, 48, 4344

**Chap 2.**

**Preparation of Polyglycerol Dendrimers (PGD-G1 and G2) and their Host-Guest Interaction with Fluorescent Probe**



## Chapter 2.

# Preparation of Polyglycerol Dendrimers (PGD-G1 and G2) and their Host-Guest Interaction with Fluorescent Probe

### 2.1 Introduction

Recently, PGDs and hyperbranched polyglycerol (HyPG) have been focused on in various biomedical applications due to their positive biocompatibilities and unique physicochemical properties<sup>1)</sup>. Although HyPG shows such the bio-inert properties in aqueous media<sup>2)</sup>, it is reported that shell crosslinked nanocapsules of HyPG can bind not only metal ions<sup>3)</sup>, but also fluorescent dyes accompanied with large aggregation in water<sup>4)</sup>, indicating that the crosslinked shell plays an important role for entrapment of the guest. However, due to its distribution of molecular weight, it is difficult to expect the reproducibility of its functionality.

This chapter deals with (a) the preparation of PGD-G1 and PGD-G2, (b) characterizations of interactions between fluorescent probe and PGD-G1 and G2. In this study, I focused how the generation of PGDs which are relatively low generation of PGDs, affects the localization of a fluorescent molecule in the well-defined dendritic structures, as observed through fluorescence measurement, <sup>1</sup>H-NMR titration, and isothermal titration calorimetry (ITC). From these characterizations, the binding constant and stoichiometry of interactions between fluorescent probe and PGD-G1 and G2 were determined. Based on these results, the interaction between fluorescent probe and PGD-G1 and G2 were discussed.

## 2.2 Experimental

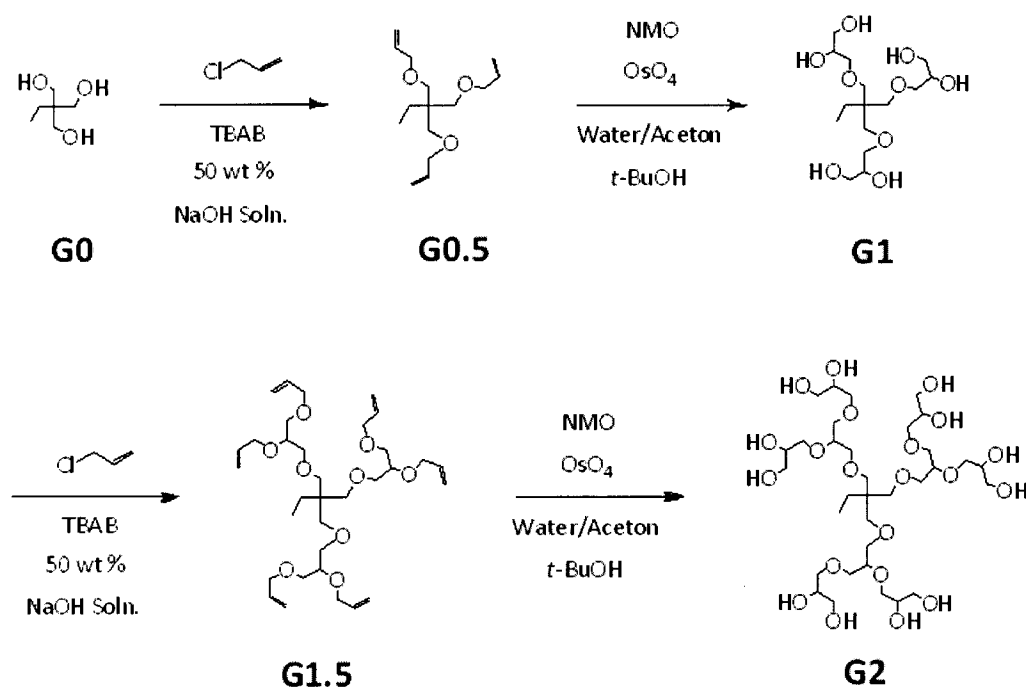
### 2.2.1 Material

Allyl chloride, 4-methylmorpholine *N*-oxide (NMO), and 50 wt% of sodium hydroxide solution were purchased from Sigma-Aldrich Co. (St. Louis, USA) and used without further purification. Tetrabutylammonium bromide (TBAB) and aqueous (4 wt%) osmium tetroxide solution were purchased from Tokyo Chemical Industry Co. (Tokyo, Japan). Sodium hydroxide, 1,1,1-tris(hydroxymethyl)propane (THMP), 4-amino-3-hydroxynaphthalene-1-sulphonic acid (AHSA) and magnesium sulfate were purchased from Wako Pure Chemical Industries (Osaka, Japan) and were used without further purification. *t*-Butyl alcohol (*t*-BuOH), acetone, ethyl acetate, toluene and methanol were reagent grade and purchased from Nacalai Tesque (Kyoto, Japan). Petroleum ether was reagent grade and purchased from Kanto Chemical Co. Inc. (Tokyo, Japan).

### 2.2.2 Synthesis and purification of PGD-G1 and G2

PGDs were synthesized by two-step process based on allylation of alcohols and catalytic dihydroxylation. For preparation of PGD-G1, allylchloride (0.5 mol) was added to a solution of THMP (0.1 mol alcohol equiv.), TBAB (0.01 mol) and 50 % sodium hydroxide solution (0.5 mol) in a three-necked round-bottom flask, over 22 h at 45 °C with stirring using a overhead mechanical stirrer. When the reaction reached completion (monitored by TLC), 100 mL of toluene was added to the flask. The organic phase was separated, dried with MgSO<sub>4</sub>, filtered and concentrated under vacuum. The allylated THMP was purified by a silica gel column chromatography (eluent: petrolether/ethyl acetate). The allylated THMP (0.1 mol equiv.) and

*N*-methylmorpholine-*N*-oxide (0.11 mol) were dissolved in acetone (50 mL), distilled water (50 mL) and *t*-butanol (10 mL), and then 4 wt% OsO<sub>4</sub> solution in water (2 mL) was added to the mixture and stirred for 24 h at 25 °C. When the reaction was over, the volatile compounds were removed *in vacuo*. The obtained crude PGD-G1 (9.5 g) dissolved in methanol (10 mL) was applied to an acidic active alumina column (eluent: methanol/water), and the recovered crude product was then applied to a silica gel chromatography (eluent: ethyl acetate/methanol), giving PGD-G1 as clear and sticky substance. In a similar manner, PGD-G2 was synthesized by using PGD-G1 as a starting material. The obtained PGDs were identified by <sup>1</sup>H-NMR measurements using a 500 MHz FT-NMR apparatus (Bruker Advanced 500 spectrometer) and a MALDI-TOF-MS apparatus (Voyager 2000, AB SCIEX).



**Fig. 2. 1** Synthesis of PGD-G1 and G2

#### PGD-G1 : Yield: 84 %

$^1\text{H-NMR}$  ( $\text{D}_2\text{O}$ , 500 MHz):  $\delta$  = 3.77 (m, 3H,  $\text{HOCHCH}_2\text{-}$ ), 3.55-3.50 (dd, 4H,  $\text{-OCH}_2\text{CH-}$ ), 3.45-3.40 (m, 6H,  $\text{HOCH}_2\text{CH-}$ ), 3.39-3.34 (m, 2H,  $\text{-OCH}_2\text{CHOH}$ ), 3.30 (q, 4H,  $\text{-CCH}_2\text{O-}$ ), 3.22 (s, 2H,  $\text{-CCH}_2\text{O-}$ ), 1.24 (q, 2H,  $\text{-CCH}_2\text{CH}_3$ ), 0.73 (t, 3H,  $\text{-CCH}_2\text{CH}_3$ )

MALDI-TOF-MS (matrix: CHCA)  $m/z$  = 379.16 (PGD-G1 +  $\text{Na}^+$ )

#### PGD-G2 : Yield: 85 %

$^1\text{H-NMR}$  ( $\text{D}_2\text{O}$ , 500 MHz):  $\delta$  = 3.76 (m, 6H,  $\text{HOCHCH}_2\text{O-}$ ), 3.68 (m, 3H,  $\text{-OCHCH}_2\text{O-}$ ), 3.64-3.53 (m, 12H,  $\text{HOCHCH}_2\text{O-}$ ), 3.53-3.48 (m, 12H,  $\text{HOCH}_2\text{CH-}$ ), 3.48-3.38 (m, 12H,  $\text{-OCH}_2\text{CHO-}$ ), 3.29 (q, 4H,  $\text{-CCH}_2\text{O-}$ ), 3.22 (s, 2H,  $\text{-CCH}_2\text{O-}$ ), 1.25 (q, 2H,  $\text{-CCH}_2\text{CH}_3$ ), 0.74 (t, 3H,  $\text{-CCH}_2\text{CH}_3$ )

MALDI-TOF-MS (matrix: CHCA)  $m/z$  = 823.12 (PGD-G2 +  $\text{Na}^+$ )

### **2.2.3 Fluorescent measurements of AHSA in the presence of various concentrations of PGDs**

AHSA (3mg, 13  $\mu\text{mol}$ ) was dissolved in 100 mL of 10 mM acetate buffer (pH 5.0) as a stock solution. PGD-G1 (2, 4, 9, 18, 35, 70  $\mu\text{mol}$ ) was dissolved in 1 mL of 10 mM acetate buffer (pH 5.0). The stock solution of AHSA (30  $\mu\text{M}$ ) was added to each PGD-G2 was incubated for 30 min at 4  $^\circ\text{C}$  in a quartz cell, and emission spectra of the solution were measured (excitation wavelength: 342 nm) by a spectrofluorometer (F-2500, HITACHI, LTD., Japan) at 4  $^\circ\text{C}$  under nitrogen atmosphere. The same experiments were performed using PGD-G2 instead of PGD-G1. Glycerol sample was used as a control sample of PGDs.

### **2.2.4 $^1\text{H-NMR}$ titration of AHSA toward PGDs**

PGD-G1 or G2 was dissolved in 10 mM acetate buffer prepared by  $\text{D}_2\text{O}$ ,  $pD$  of which was adjusted by NaOD and acetic acid- $d_4$  (concentration: 7.37 mM). AHSA dissolved in the buffer was added to the PGD-dissolved solution to be 4.93, 9.87,

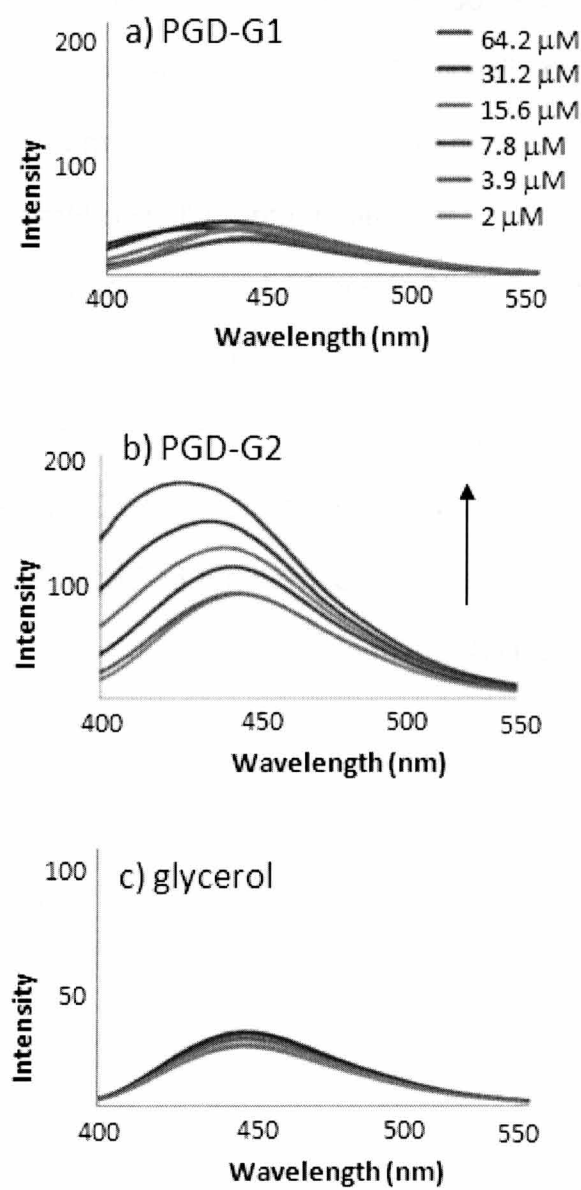
19.7 and 49.3 mM (final concentration of AHSA: 49.3 mM).  $^1\text{H}$ -NMR spectra of each solution were measured using a 500 MHz FT-NMR apparatus (Bruker Advanced 500)

### **2.2.5 ITC (Isothermal Titration Calorimetry) titration between AHSA and PGDs**

ITC titrations were carried out with a VP-ITC microcalorimeter (MicroCal LLC, GE Healthcare). PGDs were dissolved in distilled water (concentration: 0.1 mM). And AHSA salt was also prepared in the same way (concentration: 0.5 mM or 1 mM). The PGD solutions were placed in the calorimeter cell. The titration syringe was loaded with AHSA solution at a 5 ~ 10 times higher concentration than in the cell. The titrations were carried out with 25 injections of 10  $\mu\text{L}$  each with time intervals of 20 second. The solution was stirred at 300 rpm as suggested by the manufacturer. Titrations were carried out at a cell temperature of 25  $^{\circ}\text{C}$  and with a reference power of 10  $\mu\text{cal s}^{-1}$ . ITC data analyses were carried out in Origin 7 SR 2 (OriginLab Corp.) with the provided microcal ITC routines.

2. 3 Results and discussion

2.3.1 Fluorescent measurements of AHSA in the presence of various concentrations of PGDs



**Fig. 2. 2** Fluorescent spectral change for a solution of AHSA on the addition of PGD-G1 and G2

In order to estimate of branched structure of PGDs consisting of 2,3-dihydroxy-propoxymethyl units on the interaction with 4-amino-3-hydroxynaphthalene-1-sulfonic acid (AHSA) as a fluorescent indicator, the change of fluorescent spectra of AHSA as a function of PGD concentrations was firstly examined. Due to various functional groups, relatively small size and simple chemical structure, AHSA was chosen. And AHSA has been previously studied as a fluorescent dye that exhibits changes in fluoresce intensity in response to external polarity<sup>5)</sup>. If difference in the generation of PGDs between glycerol and G2 affects the polarity change, one can imagine that hypsochromic or bathochromic shifts might be observed.

A fluorescence spectrum of AHSA itself was observed at wavelength between 358 and 550 nm, with a maximum intensity at 450 nm. Comparing with glycerol, the intensity of AHSA in presence of PGD-G2 was increased with increasing the concentration of PGD-G2. And hypsochromic shift was observed, whereas such an increase was not observed in the presence of any concentration of glycerol (**Fig. 2. 2 a), c)**).

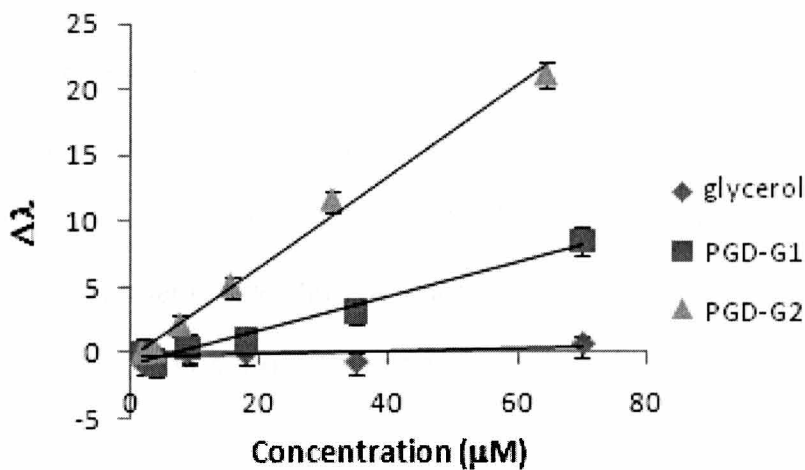
The increased fluorescence intensity means that the expanded 2,3-dihydroxy-propoxymethyl units of PGDs provide an hydrophobic region capable of binding with AHSA as well as the other solvatochromic fluorescent molecules such as 1-anilinonaphthalene-8-sulfonate<sup>5)</sup>. In addition to the fluorescence intensity change, the hypsochromic shift value ( $\Delta\lambda$ ) was calculated by subtraction between the wavelengths at the maximum intensity of AHSA in the absence and presence of PGDs (**Eq. 2-1**).

$$\Delta\lambda = \lambda_0 - \lambda_c$$

$\lambda_0$ : wavelength ( $\lambda$ ) at maximum FL intensity of AHSA  
 $\lambda_c$ :  $\lambda_0$  in the presence of PGDs or glycerol at each conc.

**(Eq. 2-1)**

The  $\Delta\lambda$  increased proportionally to the concentration of each of the substrates, where the increment order of substrates was PGD-G2 > PGD-G1 > glycerol (**Fig. 2. 3**). The interaction between PGD-G1 or G2 and AHSA suggests that the increase number of 2,3-dihydroxy-propoxymethyl units in PGDs provided less polar microenvironments than the aqueous environment, which was reflected in the hypsochromic shift.

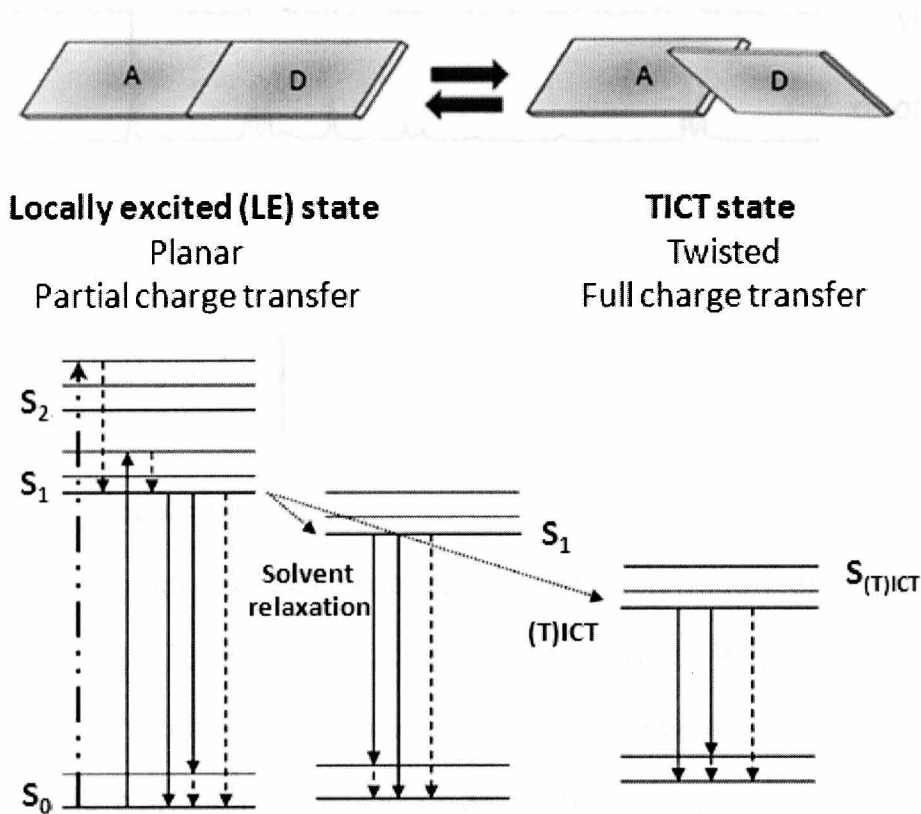


**Fig. 2. 3** Hypsochromic shift of AHSA with increase in the concentration of PGD-G1, G2 and glycerol in the acetate buffer (pH 5.0)

Considerable reason is that the strength of hydrogen bonds between 2-napthol groups of AHSA and hydroxyl groups of PGDs under the different less polar environments. It is reported that some hydroxyarene molecules such as 2-napthol showed hypsochromic shift when a hydrogen bond was accepted to its hydroxylic oxygen atom from protonated solvents<sup>7)</sup>. Since the number of hydroxyl groups of PGD-G1, PGD-G2 and glycerol are 6, 12 and 3, respectively, the increased number



of hydroxylic hydrogen atom in the dendritic structure possibly provides the opportunity of more frequent collisions with the hydroxylic oxygen atoms of AHSA with increasing the generation from 1 to 2, which might be dependent on the formation of less polar internal cavity in the dendritic structure. Another possible explanation is restricted twist motion of C-N bonds of AHSA, which is closely related to excitation/emission energy based on twisted intramolecular charge-transfer (TICT) mechanism (**Fig. 2.4**)<sup>8)</sup>. If the primary amine participates in hydrogen bonding with the hydroxyl groups, typical angles between the ion-pair lobe on nitrogen atom and the carbon 2p $\pi$ -orbital on the naphthalene ring might show high energy, leading to the observed hypsochromic shift.

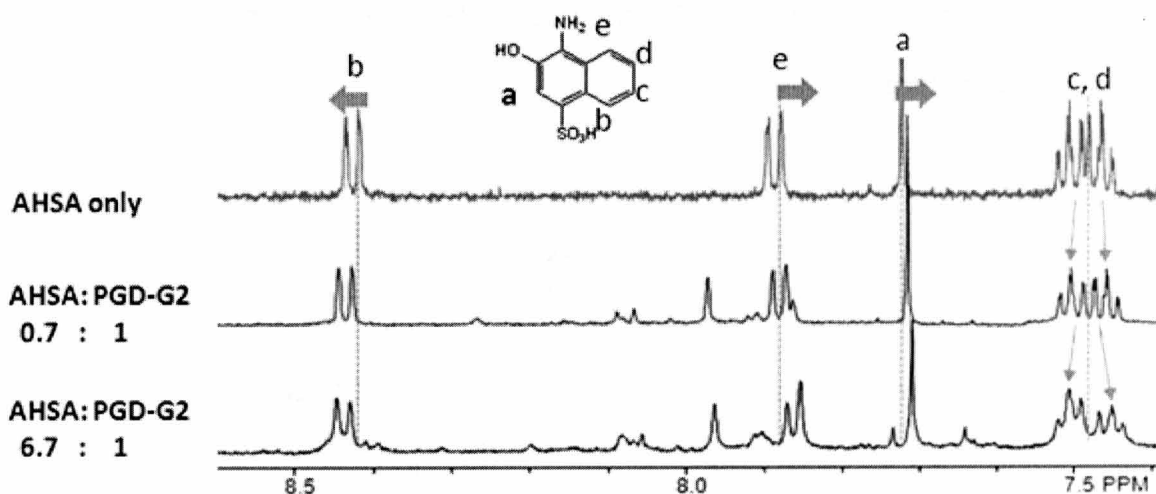


**Fig. 2. 4** Twisted intramolecular charge-transfer (TICT)

### 2.3.2 $^1\text{H}$ -NMR titration of AHSA in the presence of various concentrations of PGDs

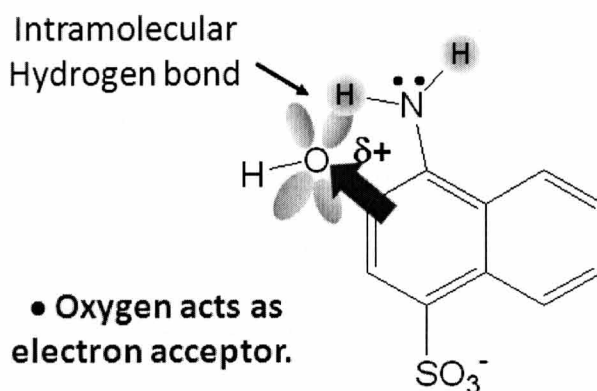
In order to clarify the location and interaction of AHSA in the PGDs via intermolecular interactions,  $^1\text{H}$ -NMR titration of AHSA with PGDs in 10 mM acetate buffer (pD 5.0) was employed.

#### 2.3.2.1 $^1\text{H}$ -NMR titration between PGD-2 and AHSA



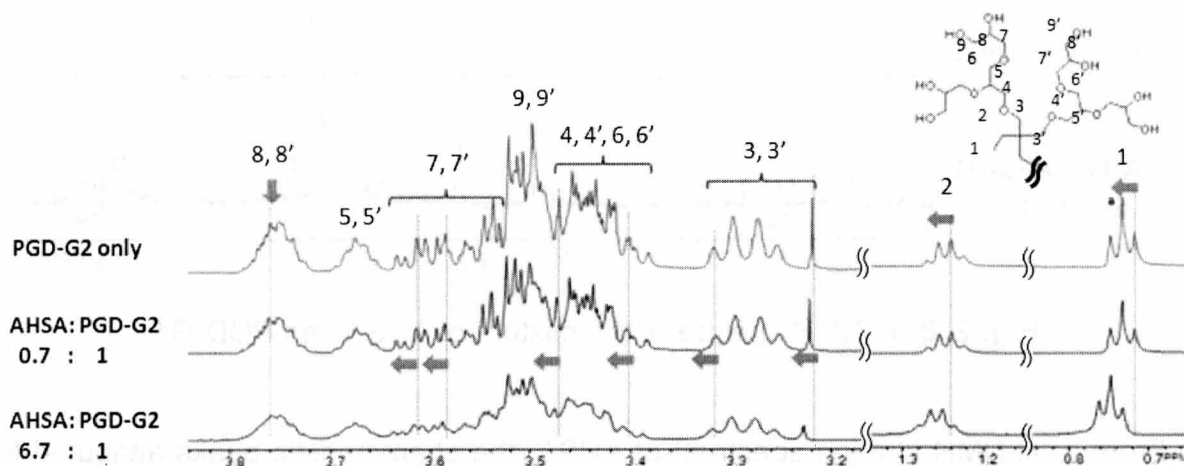
**Fig. 2. 5**  $^1\text{H}$ -NMR spectra of the mixture of AHSA and PGD-G2

When the molar ratio of AHSA to PGD-G2 increased, the doublet peak for  $\text{H}_b$  of naphthalene ring (8.4 ppm) noticeably shifted downfield, and the doublet peak of  $\text{H}_e$  of naphthalene ring (7.9 ppm) and the singlet peak for  $\text{H}_a$  (7.7 ppm) were shifted towards upfield (**Fig. 2.5**). One can account for this observation in that the hydroxyl oxygen atom is positively charged so as to be  $\delta^+$  via attraction of the unshared electron pair of the hydroxyl oxygen atom with the hydroxyl hydrogen atom of PGD-G2 and/or the primary amine of AHSA; hence, the oxygen atom may become an electron acceptor capable of drawing electrons adjacent to the  $\text{H}_a$ -proton in an



**Fig. 2. 6** Image of AHSA in presence of PGD-G2, in acetate buffer (pH 5)

inductive and resonant way (**Fig. 2. 6**). Interestingly, multiplet peaks attributed to  $\text{H}_c$  and  $\text{H}_d$  protons of the naphthalene ring (around 7.5 ppm) were divided into two peak regions. Since the  $\text{H}_c$  and  $\text{H}_d$  protons are considered to be in a non-polar environment, we hypothesized that the  $\text{H}_c$  and  $\text{H}_d$  protons are feasibly located in the hydrophobic environment, resulting in the peak division. Therefore, we next focused on the  $^1\text{H}$  NMR spectra of PGD-G2.

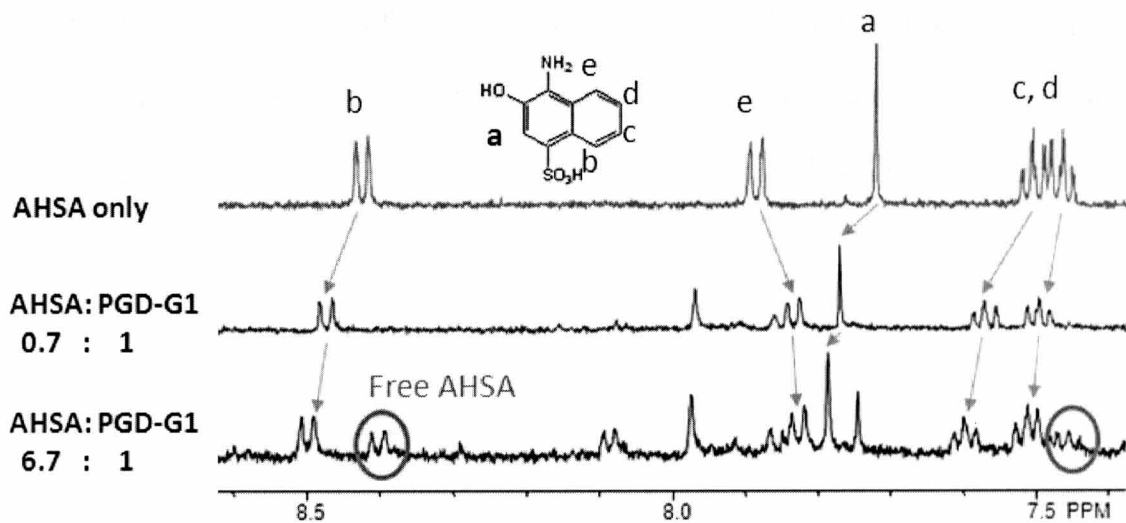


**Fig. 2. 7**  $^1\text{H}$ -NMR spectra of the mixture of AHSA and PGD-G2

When the molar ratio of AHSA to PGD-G2 was increased up to 6.7, the peaks attributed to the protons 1, 2, 3, and 3' of PGD-G2 were found to move downfield

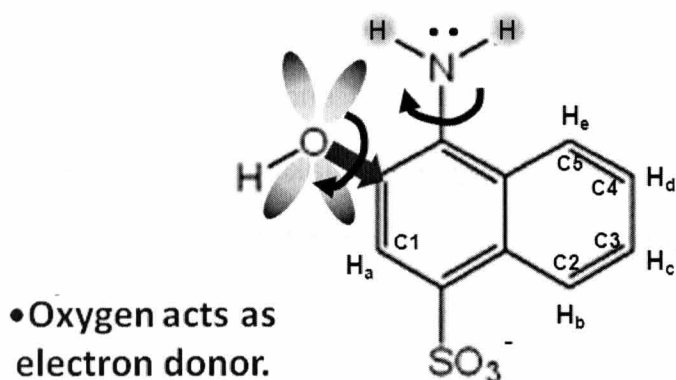
significantly (**Fig. 2. 7**). These results indicate that the AHSA molecule interacted with the core part of PGD-G2. The peaks attributed to 4, 4' 5, 5',6, 6', 7, 7' 8, 8', 9, and 9' of PGD-G2, which are located from interior to outer parts of it, were slightly shifted to downfield and became broader, suggesting that the interior and outer parts of PGD-G2 were also attractively associated with AHSA. Thus, AHSA was likely encapsulated within the PGD-G2 molecule, where the H<sub>c</sub> and H<sub>d</sub> protons of AHSA were interacted with H<sub>1</sub> and H<sub>2</sub> protons that are located at the hydrophobic core parts of PGD-G2.

### 2.3.2.2 <sup>1</sup>H-NMR titration between PGD-G1 and AHSA



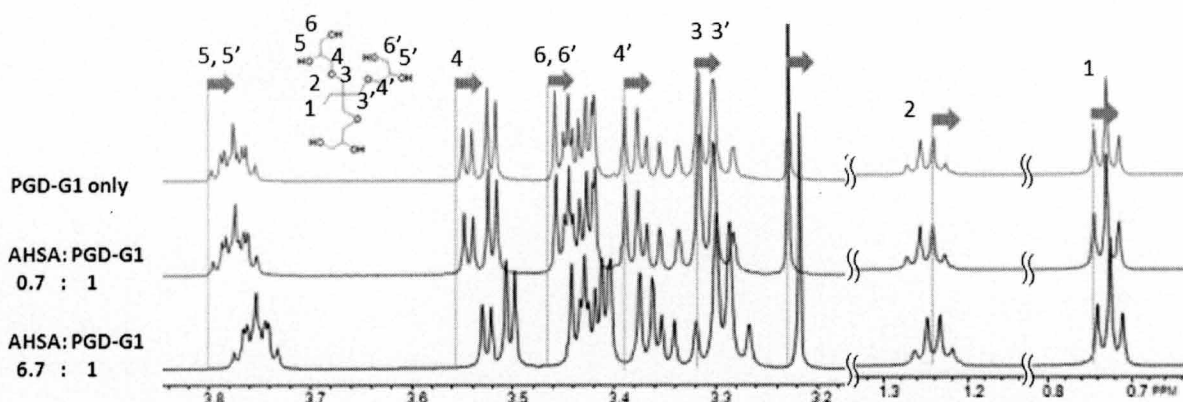
**Fig. 2. 8** <sup>1</sup>H-NMR spectra of the mixture of AHSA and PGD-G1

From a <sup>1</sup>H-NMR titration spectrum of AHSA, the characteristic peaks attributed to AHSA were observed in the range of chemical shifts between 7.0 and 9.0 ppm. With increasing molar ratio of AHSA to PGD-G1, the peaks of AHSA attributed to H<sub>b</sub> (8.4 ppm), H<sub>e</sub> (7.7 ppm) and H<sub>c</sub>, H<sub>d</sub> (7.5 ppm) shifted downfield (**Fig. 2.8**). On the other hand, the doublet peak of H<sub>e</sub> (7.9 ppm) shifted upfield. These results indicate that



**Fig. 2. 9** Image of AHSA in presence of PGD-G1, in acetate buffer (pH 5)

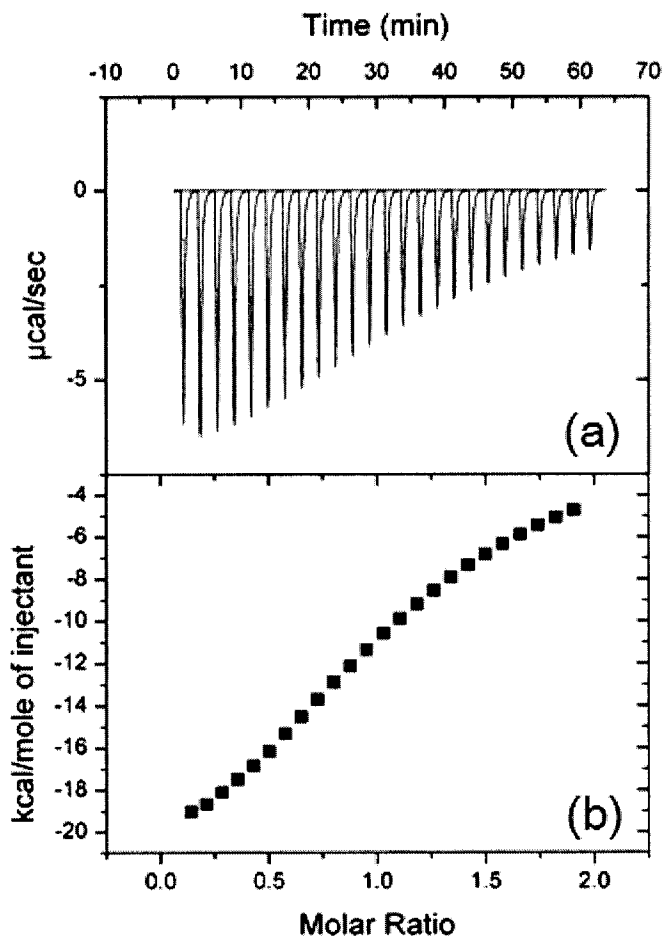
AHSA was actually interacted with PGD-G1. The downfield shift of  $H_a$  (7.7 ppm) denotes enhanced deshielding effect, hence, the hydroxyl oxygen could act as an electron donor (**Fig. 2. 9**), leading to the increased electron density of the C3 position, and, unlike in the PGD-G2, the hydroxyl groups of AHSA do not contribute significant hydrogen bonds. When the molar ratio of AHSA to PGD-G1 was 6.7:1, new peaks were appeared around at 8.4 and 7.5 ppm, indicating the existence of free AHSA molecules under this condition. Since such peaks attributed to the free AHSA molecules were not observed in the case of PGD-G2, the equilibrium shift to AHSA-PGD-G1 complex formation was small as compared with the case of PGD-G2.



**Fig. 2. 10**  $^1\text{H}$ -NMR spectra of the mixture of AHSA and PGD-G1

The peaks attributed to 3, 3', 4, 4', 5, 5', 6 and 6' of PGD-G1 were shifted considerably upfield, while moderate peak shifts of 1 and 2 were observed when the molar ratio of AHSA to PGD-G1 was 6.7 (**Fig. 2.10**). Taking all the above-mentioned results of PGD-G1 into account, it can be surmised that the AHSA molecule preferentially interacted with the outer parts of PGD-G1, where either hydroxyl hydrogen or primary amino hydrogen of AHSA might act as a weak hydrogen donor toward ether oxygen and/or hydroxyl oxygen of PGD-G1.

2.3.3 ITC titration of AHSA in the presence of various concentrations of PGD-G2 and G1

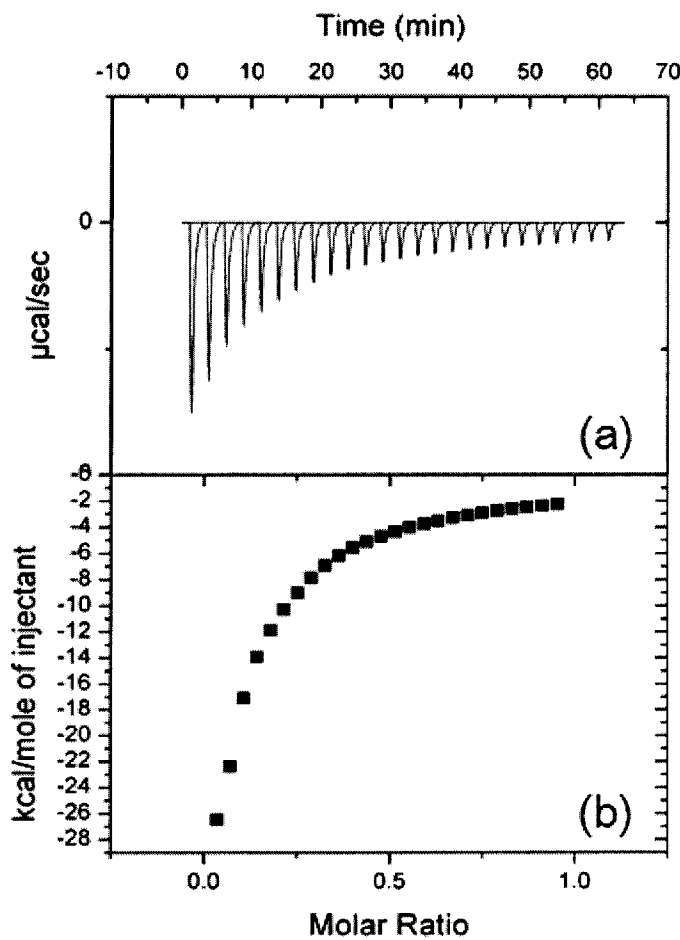


**Fig. 2. 11** ITC titration curves for PGD-G2 and AHSA in water. ITC measurements were performed to establish solution binding constants. In this experiment, a solution of PGD-G2 (0.1 mM) was titrated with a solution of AHSA (Total volume: 1mM).

The results of a typical titration calorimetry measurement, which consisted of adding 10  $\mu$ L aliquots of 1 mM AHSA solution to 0.1 mM PGD-G2 solution in water at 25  $^{\circ}$ C is shown in **Fig 2.11 (a)**. The results exhibit a monotonic decrease in the exothermic heat of binding with each successive injection until saturation is achieved.

A non-linear least-squares fit of the ITC data to the identical site model described by eq 2, is also presented in **Fig. 2. 11 (b)**. As shown by the curve in **Fig. 2. 11(b)**, the incremental heats per mole of added AHSA follows closely the injection number. This result of ITC measurements supported the encapsulation of AHSA into PGD-G2. The  $K_a$  value was calculated to be  $2.6 \times 10^{-4} \text{ (M}^{-1}\text{)}$  with a 1 : 1 stoichiometry of PGD-G2 and AHSA. And the  $\Delta H$  and  $\Delta S$  are  $-2.66 \times 10^{-4} \text{ (M}^{-1}\text{)}$  and  $-67.9 \text{ (M}^{-1}\text{)}$ , respectively.

In a similar manner, calorimetric titration of PGD-G1 solution with AHSA solution was performed under the same conditions.



**Fig. 2. 12** ITC titration curves for PGD-G1 and AHSA in water. ITC measurements were performed to establish solution binding constants. In this experiment, a solution of PGD-G1 (0.1 mM) was titrated with a solution of AHSA (0.5 mM) (Total volume: 1mM).



The results of a typical titration calorimetry measurement, which consisted of adding 10  $\mu\text{L}$  aliquots of 0.5 mM AHSA solution to 0.1 mM PGD-G2 solution in water at 25  $^{\circ}\text{C}$  is shown in **Fig 2.12 (a)**. The raw data (**Fig. 2.12 (a)**) between PGD-G1 and AHSA also exhibit a monotonic decrease in the exothermic heat of binding with each successive injection until saturation is achieved. A non-linear least-squares fit of the ITC data to the identical site model described by eq 1, is also presented in **Fig. 2. 12 (b)**. The  $K_a$  value was calculated to be  $3.4 \times 10^{-4} \text{ (M}^{-1}\text{)}$  with a 1 : 0.02 stoichiometry, suggesting that AHSA actually interacted with PGD-G1, but the number of AHSA molecules that participated in the interaction was much smaller than with PGD-G2. And the  $\Delta H$  and  $\Delta S$  are  $-5.47 \times 10^{-5} \text{ (M}^{-1}\text{)}$  and  $-1.81 \times 10^{-3} \text{ (M}^{-1}\text{)}$ , respectively. Taking all the above-mentioned results of PGD-G1, it can be summarized that 1 mole of AHSA preferentially interacted with 50 moles of PGD-G1, where either hydroxyl hydrogen or primary amino hydrogen of AHSA might act as a weak hydrogen donor toward outer hydroxyl oxygen PGD-G1, showing the same orders of magnitude of the  $K_a$  value with PGD-G2.

## 2.4 Conclusion

Molecular interactions between AHSA and PGD-G1 and G2 were analyzed by fluorescent measurements,  $^1\text{H}$ -NMR titration and ITC. A less polar and hydrophobic environment was formed by PGD of generation 2 (PGD-G2), which enhanced uptake of AHSA into the dendritic interior of PGD-G2 with a 1 : 1 stoichiometry. On the other hand, AHSA was seen to interact with only the outer part in the case of PGD-G1. Therefore, higher generation of PGDs in conjunction with the construction of dendritic interior could be a factor in the enhanced uptake of guest molecules. This concept of molecular uptake using the biocompatible PGDs might have potential application for nanocarriers for drug delivery and nanomaterials for molecular recognition.

## References

1. M. Calderón, M. A. Quadir, S. K. Sharma, R. Haag, *Advanced Materials* **2010**, 22, 190  
D. Wilms, S.-E. Stiriba, H. Frey, *Accounts of Chemical Research* **2010**, 43, 129  
R. K. Kainthan, J. Janzen, E. Levin, D. V. Devine, D. E. Brooks, *Biomacromolecules* **2006**, 7, 703  
J. Khandare, A. Mohr, M. Calderón, P. Welker, K. Licha, R. Haag, *Biomaterials* **2010**, 31, 4268
2. M. Wyszogrodzka and R. Haag, *Langmuir* **2009**, 25, 5703-5712  
M. Wyszogrodzka and R. Haag, *Biomacromolecules* **2009**, 10, 1043-1054  
R. K. Kainthan, Y. Zou, M. Chiao and J. N. Kizhakkedathu, *Langmuir* **2008**, 24, 4907
3. S. C. Zimmerman, J. R. Quinn, E. Burakowska and R. Haag, *Angew. Chem. Int. Ed.*, **2007**, 46, 8164
4. E. Burakowska, J. R. Quinn, S. C. Zimmerman and R. Haag, *J. Am. Chem. Soc.*, **2009**, 131, 10574
5. P. Hauk, C. R. Guzzo, H. R. Ramos, P. L. Ho and C. S. Farah, *J. Mol. Biol.*, **2009**, 390, 722
6. S. Jan, *Biochim. Biophys. Acta (BBA) – Reviews on Biomembranes* **2003**, 1082, 694, 1  
D. Scharbin, M. Szwedzka and N. Bryszewska, *Bioorg. Chem.*, **2007**, 35, 170  
D. Matulis, C. G. Baumann, V. A. Bloomfield and R. E. Lovrien, *Biopolymers*, **1999**, 49, 451
7. K. M. Solntsev, D. Huppert and N. Agmon, *J. phys. Chem.. A*, **1998**, 102, 9599
8. K. Suzuki, H. Tanabe, S. Tobita and H. Shizuka, *J. phys. Chem. A*, **1997**, 101, 4496

## **Chapter 3.**

# **Dendritic Host-Guest Interaction of Polyglycerol Dendrimer of Generation 3 (PGD-G3) and 4 (PGD-G4) with a Fluorescent Probe**

## Chapter 3.

# Dendritic Host-Guest Interaction of Polyglycerol Dendrimer of Generation 3 (PGD-G3) and 4 (PGD-G4) with a Fluorescent Probe

### 3.1 Introduction

In chapter 2, I discussed the interaction between a fluorescent probe (AHSA) and PGD-G1 or G2. From the results, the generation dependency of PGDs toward the interaction with AHSA was observed. This phenomenon suggests that PGDs of generation over 2 affect the intermolecular interactions with AHSA.

This chapter deals with the investigation of the interaction between PGD-G3 or G4 and AHSA. To understand the interactions between PGD-G3 or G4 and AHSA, fluorescence measurement,  $^1\text{H}$ -NMR titration, ITC and DLS were employed as described in chapter 2.

### 3.2 Experimental

#### 3.2.1 Material

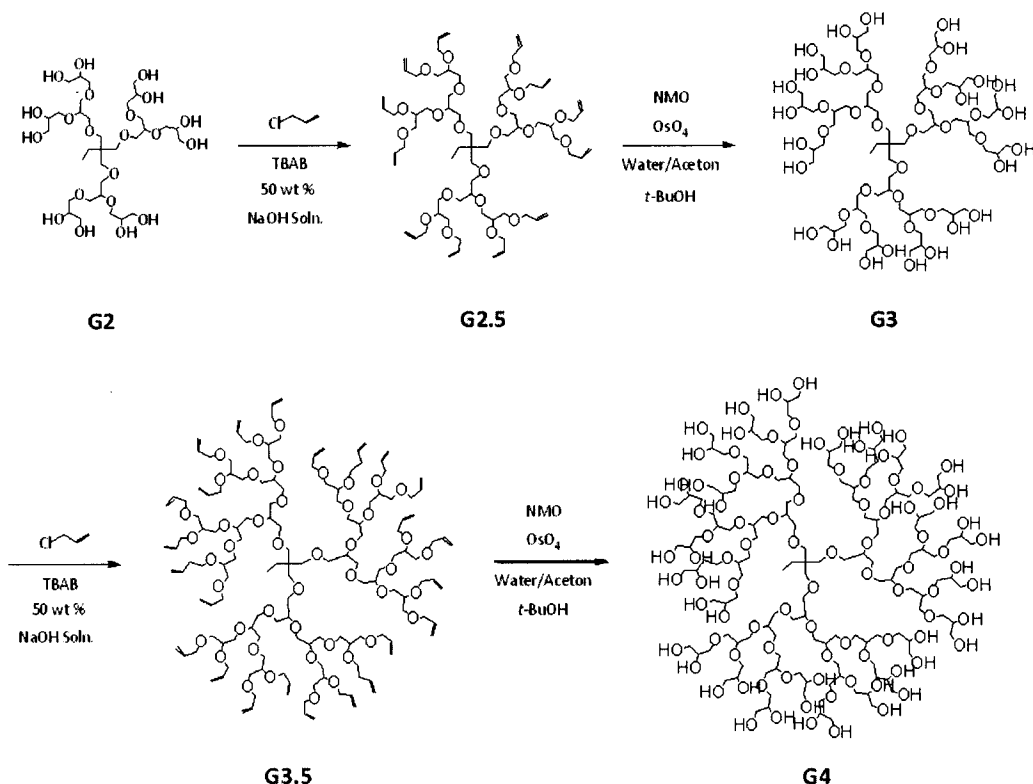
Allyl chloride, 4-methylmorpholine *N*-oxide (NMO), and 50 wt % of sodium hydroxide solution were purchased from Sigma-Aldrich Co. (St. Louis. USA) and used without further purification. Tetrabutylammonium bromide (TBAB) and aqueous (4 wt %) osmium tetroxide solution were purchased from Tokyo Chemical Industry Co. (Tokyo, Japan). 1,1,1-Tris(hydroxymethyl)propane (THMP), 4-amino-3-hydroxynaphthalene-1-sulphonic acid (AHSA), sodium hydroxide and

magnesium sulfate were purchased from Wako Pure Chemical Industries (Osaka, Japan) and were used without further purification. *t*-Butyl alcohol (*t*-BuOH), acetone, ethyl acetate, toluene and methanol were reagent grade and purchased from Nacalai Tesque (Kyoto, Japan). Petroleum ether was reagent grade and purchased from Kanto Chemical Co. Inc. (Tokyo, Japan).

### 3.2.2 Synthesis and purification of PGD-G3 and G4 (Fig. 3.1)

PGD-G3 and G4 were synthesized by two-step process based on allylation of alcohols and catalytic dihydroxylation. For preparation of PGD-G3, allylchloride (1660 mmol) was added to a solution of PGD-G2 (554.2 mmol alcohol equiv.), TBAB (55.4 mmol) and 50 % sodium hydroxide solution (0.5 M) in a three-necked round-bottom flask, over 22 h at 45 °C with stirring using a overhead mechanical stirrer. When the reaction reached completion (monitored by TLC), 100 mL of toluene was added to the flask. The organic phase was separated, dried with MgSO<sub>4</sub>, filtered and concentrated under vacuum. The allylated PGD-G2 was purified by a silica gel column chromatography (eluent: petrolether/ethylacetate). The allylated PGD-G2 (272.6 mmol) and *N*-methylmorpholine-*N*-oxide (299.9 mmol) were dissolved in acetone (270 mL), distilled water (270 mL) and *t*-butanol (55 mL), and then 4 wt% OsO<sub>4</sub> solution in water (4 mL) was added to the mixture and stirred for 24 h at 25 °C. When the reaction was over, the volatile compounds were removed *in vacuo*. The obtained crude PGD-G3 (39.2 g) dissolved in methanol (50 mL) was applied to an acidic active alumina column (eluent: methanol/water), and the recovered crude product was then applied to a silica gel chromatography (eluent: ethyl acetate/methanol) or HPLC, giving PGD-G3 as clear and sticky substance. In a similar manner, PGD-G4 was synthesized by using PGD-G3 as a starting material. The obtained PGDs were

identified by  $^1\text{H}$ -NMR measurements using a 500 MHz FT-NMR apparatus (Bruker Advanced 500 spectrometer) and a MALDI-TOF-MS apparatus (Voyager 2000, AB SCIEX).



**Fig. 3. 1** Synthesis of PGD-G3 and G4

PGD-G3 : Yield: 72 %

$^1\text{H}$ -NMR ( $\text{D}_2\text{O}$ , 500 MHz):  $\delta$  = 4.0 (d, 24H,  $\text{HOCH}_2\text{CHCH}_2\text{-}$ ), 3.8-3.73 (m, 12H,  $\text{HOCHCH}_2\text{O-}$ ), 3.71-3.64 (m, 24H,  $\text{HOCHCH}_2\text{O-}$ ), 3.63-3.56 (m, 9H,  $\text{-OCHCH}_2\text{O-}$ ), 3.56-3.24 (m, 36H,  $\text{-OCH}_2\text{CHCH}_2\text{O-}$ ), 3.08 (t, 6H,  $\text{-CCH}_2\text{OCH}_2\text{CH-}$ ), 2.8 (s, 6H,  $\text{-CCH}_2\text{O-}$ ), 1.27 (q, 2H,  $\text{-CCH}_2\text{CH}_3$ ), 0.77 (t, 3H,  $\text{-CCH}_2\text{CH}_3$ )

MALDI-TOF-MS (matrix: CHCA)  $m/z$  = 1712.83 (PGD-G3 +  $\text{Na}^+$ )

PGD-G4 : Yield: 68 %

$^1\text{H}$ -NMR ( $\text{D}_2\text{O}$ , 500 MHz):  $\delta$  = 3.8-3.73 (m, 48H,  $\text{HOCHCH}_2\text{O-}$ ), 3.71-3.64 (m, 48H,  $\text{HOCHCH}_2\text{O-}$ ), 3.63-3.56 (m, 64H,  $\text{-OCHCH}_2\text{O-}$ ), 3.56-3.24 (m, 48H,  $\text{-OCH}_2\text{CHCH}_2\text{O-}$ ), 3.3-3.2 (q, 36H,  $\text{-OCH}_2\text{CHO-}$ ), 1.28 (q, 2H,  $\text{-CCH}_2\text{CH}_3$ ), 0.78 (t, 3H,  $\text{-CCH}_2\text{CH}_3$ )

MALDI-TOF-MS (matrix: CHCA)  $m/z$  = 3491.85 (PGD-G4 +  $\text{H}_2\text{O}$ )

### **3.2.3 Fluorescent measurements of AHSA in presence of various concentrations of PGDs**

AHSA (3 mg, 13  $\mu$ mol) was dissolved in 100 mL of 10 mM acetate buffer (pH 5.0) as a stock solution. PGD-G3 (1.1, 2.1, 4.2, 8.5, 17, 34  $\mu$ mol) was dissolved in 1 mL of 10 mM acetate buffer (pH 5.0). The stock solution of AHSA (30  $\mu$ L) was added to each PGD-G3 solution, followed by incubation for 30 min at 4 °C in a quartz cell. Emission spectra of the solution were measured (excitation wavelength: 342 nm) using a spectrofluorometer (F-2500, HITACHI, LTD., Japan) at 4 °C under nitrogen atmosphere. The same experiments were performed using PGD-G4. Glycerol sample was used as a control sample of PGDs.

### **3.2.4 Fluorescent measurements of AHSA in various solvents**

AHSA (3 mg, 13  $\mu$ mol) was dissolved in 100 mL of dioxane, poly(ethylene glycerol) (PEG) 400, ethanol and glycerol as a stock solution, respectively. Each stock solution of AHSA (30  $\mu$ L) was added to the corresponding solvents (970  $\mu$ L), and then the mixture (final concentration of AHSA (30  $\mu$ M) was incubated for 30 min at room temperature in a quartz cell. Emission spectra of the solutions were measured (excitation wavelength: 342 nm) using a spectrofluorometer (F-2500, HITACHI, LTD., Japan) at room temperature.

### **3.2.5 $^1\text{H}$ -NMR titration of AHSA toward PGDs**

PGD-G3 or G4 was dissolved in 10 mM acetate buffer prepared by  $\text{D}_2\text{O}$ , pD of which was adjusted by NaOD and acetic acid- $d_4$  (concentration: 7.37 mM). AHSA dissolved in the buffer was added to the PGD-dissolved solution to be 4.93, 9.87, 19.7 and 49.3 mM.  $^1\text{H}$ -NMR spectra of each solution were measured using a 500



mHz FT-NMR apparatus (Bruker Advanced 500)

### **3.2.6 Isothermal titration calorimetry (ITC) experiments between AHSA and PGDs**

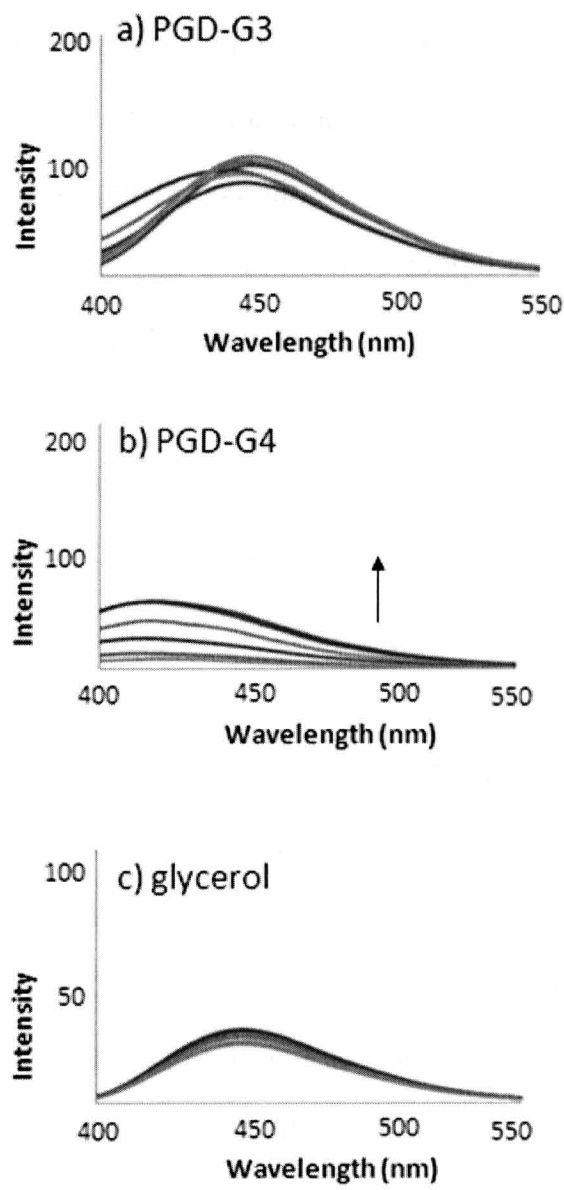
ITC titrations were carried out using a VP-ITC microcalorimeter (MicroCal LLC, GE Healthcare). PGDs were dissolved in distilled water (concentration: 0.1 mM). AHSA was also dissolved in distilled water (concentration: 0.5 or 1 mM). The PGD solutions were placed in the calorimeter cell. The titration syringe was loaded with the AHSA solution at a 5 ~ 10 times higher concentration than in the cell. The titrations were carried out with 25 injections of 10  $\mu$ L each with time intervals of 20 second. The solution was stirred at 300 rpm as suggested by the manufacturer. Titrations were carried out at a cell temperature of 25 °C and with a reference power of 10  $\mu$ cal $s^{-1}$ . ITC data analyses were carried out in Origin 7 SR 2 (OriginLab Corp.) with the provided microcal ITC routines.

### **3.2.7 Dynamic Light Scattering (DLS) of PGDs**

DLS measurements were performed using a Zetasizer Nano-ZS instrument (Malvern Instruments Ltd, Worcestershire, UK). The experimental conditions of PGDs in presence or absence of AHSA were the same with ITC titration between AHSA and PGDs. The mixtures of PGD and AHSA were prepared by mixing with 1.4 mL of PGD aqueous solution (concentration: PGD-G3; 0.1 mM, PGD-G4; 0.2 mM) and 250  $\mu$ L AHSA aqueous solution (concentration; 1 mM). Final concentration of AHSA was 0.2 mM. DLS data were analyzed by using a Zetasizer Software (Malvern Instruments Ltd.) with the provided DLS routines.

### 3. 3 Results and discussion

#### 3.3.1 Fluorescent measurements of AHSA in presence of various concentrations of PGDs

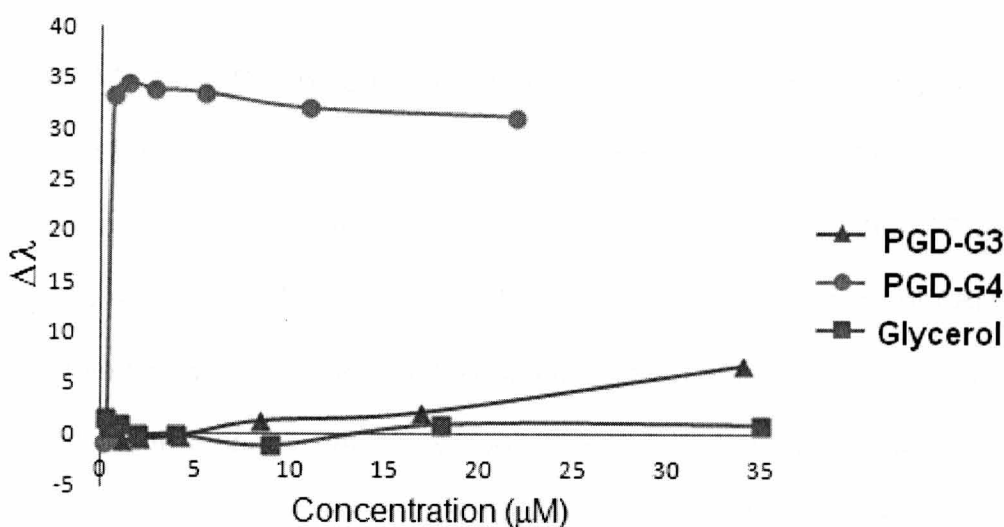


**Fig. 3. 2** Fluorescent spectral change for a solution of AHSA on the addition of PGDs (concentration of PGD-G3; 1.1, 2.1, 4.2, 8.5, 17 and 34  $\mu\text{M}$ , concentration of PGD-G4; 0.2, 0.4, 0.7, 1.4, 2.8, 5.5, 11 and 22  $\mu\text{M}$ , concentration of glycerol; 0.3, 0.5, 1.0, 4.0, 9.0, 18 and 35  $\mu\text{M}$ )

Fluorescent measurements of AHSA in the presence of PGD-G3, G4 and glycerol were performed (**Fig. 3.2**). A fluorescence of AHSA itself was observed at wavelength between 358 and 550 nm with a maximum intensity at 450 nm. The intensity at 450 nm of AHSA in presence of PGD-G3 was higher than in the presence of glycerol. In the presence of PGD-G4, the maximum intensity was sifted to low wavelength region, and the intensity increased slightly with increasing the concentration. In this case, hypsochromic shift was observed, whereas such an increase was not observed in the presence of any concentration of glycerol (**Fig. 3. 2**).

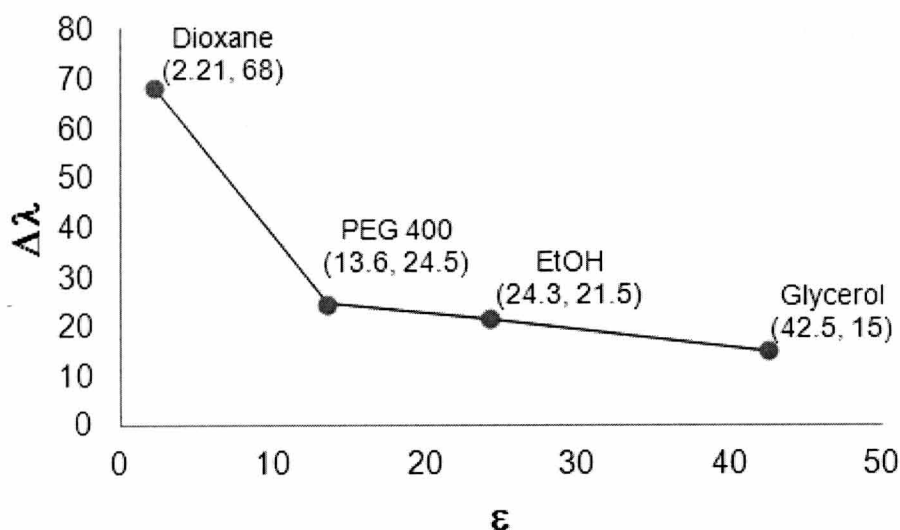
Concentration dependency of PGD-G3 against the intensity change was scarcely observed. However, fluorescent intensity with PGD-G3 was higher than with glycerol at the same concentration (**Fig. 3.2 (a) and (c)**). This means that the increased number of 2,3-dihydroxymethyl units in PGD-G3 provide an hydrophobic region capable of interaction with AHSA as well as the other solvatochromic fluorescent molecules. In the case of PGD-G4, the intensity of AHSA increased with the concentration of PGD-G4 (**Fig. 3.2 (b)**). The hypsochromic shift ( $\Delta\lambda$ ) of AHSA as seen in the case of PGD-G3 and G4 was calculated according to **Eq. 2-1** (see chapter 2, p. 50), and the concentration dependency of  $\Delta\lambda$  was summarized in **Fig. 3. 3**.

The  $\Delta\lambda$  of AHSA in presence of PGD-G3 increased slowly with increasing the concentration of PGD-G3. However,  $\Delta\lambda$  of AHSA in presence of PGD-G4 increased drastically, even at low concentration of PGD-G4. When the concentration of PGD-G4 was over 0.7 $\mu$ M,  $\Delta\lambda$  decreased moderately. These results suggest that AHSA in the presence of PGD-G4 located in much less polar microenvironment than in the presence of PGD-G3.



**Fig. 3. 3** Hypsochromic shift of AHSA with an increase in the concentration of PGD-G3, G4 and glycerol in the 10 mM acetate buffer (pH 5.0)

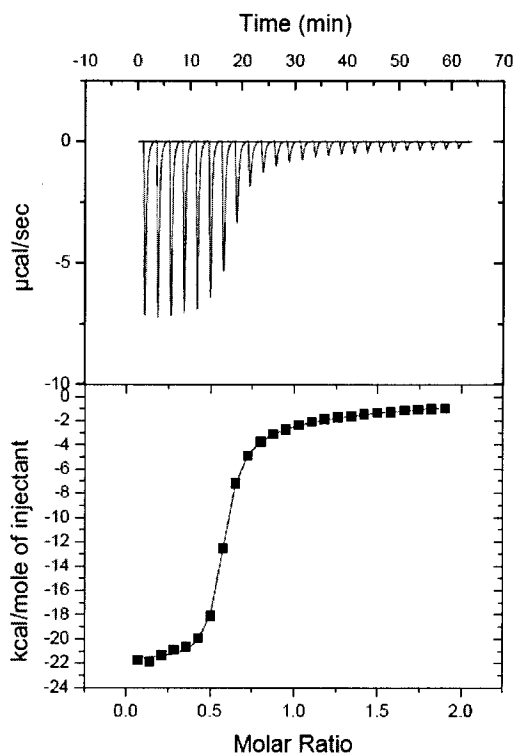
Considerable reason of the drastic hypsochromic shift of AHSA in presence of PGD-G4 is that the formation of intramolecular hydrogen bond between hydroxyl group and primary amine on AHSA molecule. When the hydrogen bond was formed, AHSA molecule becomes planar shape showing unstable energy state that is known to affect on hypsochromic shift <sup>1)</sup>. Another considerable reason is the decreased dielectric constant of the solution. It is known that the  $\Delta\lambda$  of fluorescent probe based on 2-naphthol like AHSA was changed by surrounded environmental polarity<sup>2)</sup>. This polarity is related to dielectric constant ( $\epsilon$ ). The  $\epsilon$  is the ratio of the permittivity of a substance to the permittivity of free space. The  $\epsilon$  of the solvent provides a rough measure of a solvent's polarity<sup>2)</sup>. It is known that the solvents with a  $\epsilon$  of less than 15 are suggested to be non-polar. To calculate the absolute  $\epsilon$  value of AHSA in presence of PGD-G3 or G4 solutions, fluorescent measurement of AHSA was carried out in various solvents bearing given  $\epsilon$  value.



**Fig. 3. 4** Dielectric constant and hypsochromic shift ( $\Delta\lambda$ ) of AHSA in various solvent

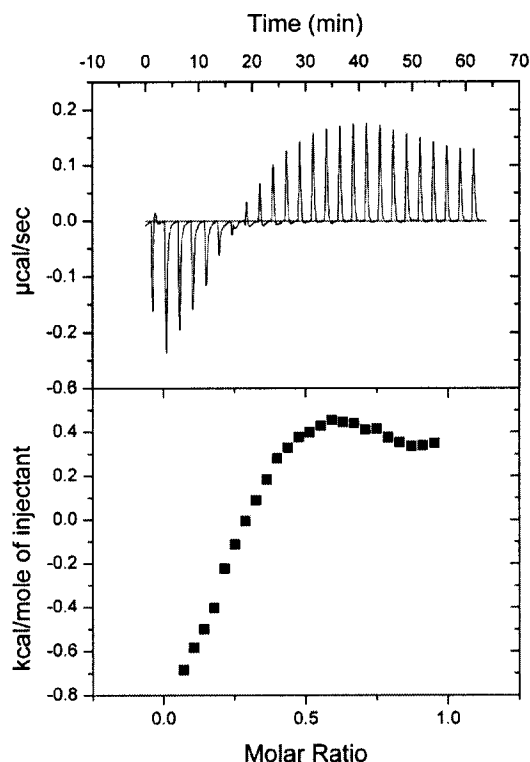
**Fig. 3.4** shows the relationship between the  $\Delta\lambda$  of AHSA in dioxane ( $\epsilon$ : 2.21), PEG 400 ( $\epsilon$ : 13.6), ethanol ( $\epsilon$ : 24.3) and glycerol ( $\epsilon$ : 42.5) and the corresponding  $\epsilon$  values. From the two results of **Fig. 3.3** and **Fig. 3.4**, the  $\epsilon$  of PGD-G3 or G4 solutions were calculated by using the calibration curve. In the case of PGD-G3 at the concentration of 34  $\mu\text{M}$ , the hypsochromic shift was too small to place on the graph (**Fig. 3. 4**), suggesting that the  $\epsilon$  of PGD-G3 in the concentration range from 1 – 34  $\mu\text{M}$  might be larger than 42.5. Meanwhile, the  $\epsilon$  of PGD-G4 at the concentration of 2  $\mu\text{M}$  was calculated to be 10.5. According to the calculated  $\epsilon$  values of PGD-G3, PGD-G3 might provide much polar environment than glycerol. On the other hand, the PGD-G4 solution was much less polar than glycerol, EtOH and PEG400. Thus, PGD-G4 solution might be act as a non-polar solvent, whereas PGD-G3 solution might behave like a polar protic solvents as well as EtOH.

### 3.3.2 ITC titration of AHSA in presence of various concentrations of PGD-G3 and G4



**Fig. 3. 5** ITC titration curves for PGD-G3 and AHSA in water. ITC measurements were performed to establish solution binding constants. In this experiment, a solution of PGD-G3 (0.1 mM) was titrated with a solution of AHSA (Total volume: 1 mM)

The result of a typical titration calorimetric measurement for PGD-G3 is shown in **Fig 3.5**. The results exhibit a monotonic decrease in the exothermic heat of binding with each successive injection until saturation is achieved. A non-linear least-squares fit of the ITC data to the identical site model described. As shown by the curve in **Fig 3.5**, the incremental heats per mole of added AHSA follows closely the injection number. The result of ITC measurements supported the interaction between AHSA and PGD-G3. The  $K_a$  value was calculated to be  $2.42 \times 10^6 \text{ (M}^{-1}\text{)}$  with a 1 : 2 stoichiometry of PGD-G3 and AHSA.  $\Delta H$  and  $\Delta S$  were calculated to be  $-2.17 \times 10^4 \text{ (kcal/mol)}$  and  $-43.6 \text{ (kcal/mol}\cdot\text{K)}$ , respectively.



**Fig. 3. 6** ITC titration curves for PGD-G4 and AHSA in water. ITC measurements were performed to establish solution binding constants. In this experiment, a solution of PGD-G4 (0.2 mM) was titrated with a solution of AHSA (Total volume: 1 mM)

The results of a typical titration calorimetric measurement for PGD-G4 were shown in **Fig 3.6**. The results exhibit two kinds of interaction mode. By adding of AHSA, endothermic interaction between PGD-G4 and AHSA decreased until 7<sup>th</sup> injection of AHSA. However, after 8<sup>th</sup> injection of AHSA, exothermic curve was observed. The titration curve between PGD-G4 and AHSA indicates that interaction between PGD-G4 and AHSA at initial stage is endothermic, and with increasing the concentration of AHSA, the interaction changes to exothermic interaction. The ITC titration curves for PGD-G4 and AHSA supported the interaction (from 1<sup>st</sup> injection to 7<sup>th</sup> injection) and dissociation (from 8<sup>th</sup> injection) between PGD-G4 and AHSA. Since the extent of the endothermic or exothermic heat was much smaller than that for

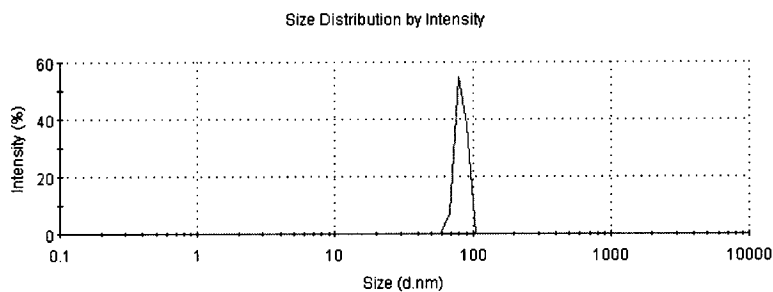
PGD-G3 titration, the strength of interaction between PGD-G4 and AHSA was obviously weaker than the interaction between PGD-G3 and AHSA. The considerable reasons might include; 1) weakly hydrophobic interaction accompanied by entropic gain of dissociation of water molecules from PGD-G4, and 2) dissociation of an intermolecularly assembled PGD-G4 by the increased addition of AHSA. Because PGD-G4 provided considerably less polar environment, hydrophobic interaction would be one of driving force to interact with AHSA.

### 3.3.3 DLS study of PGDs in presence of AHSA

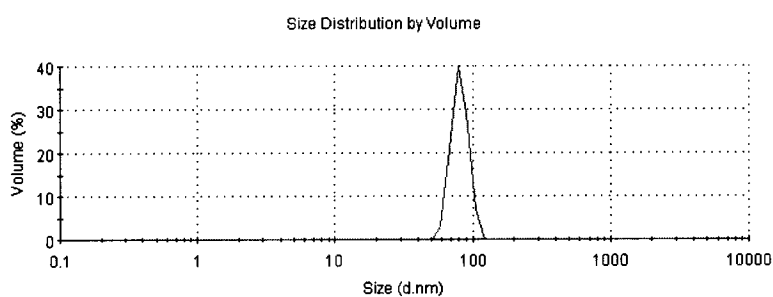
From the results of ITC, it is suggested that the interactions between PGD-G3 and AHSA were totally different from between PGD-G4 and AHSA. DLS measurements of the mixture of PGD-G3 or G4 and AHSA were performed to discuss how the solution states affect the molecular interaction.

**Figs. 3. 7 and 3. 8** show the size distribution by intensity and by mean volume of PGD-G3 in aqueous solution (concentration; 0.1 mM), respectively. The obtained results in **Fig. 3.7** suggest that PGD-G3 aggregates in aqueous solution with average diameter of 82.7 nm. Since the theoretical diameter of PGD-G3 calculated from a result of a molecular mechanics simulation was 2.47 nm, the observed diameter is likely to be caused by intermolecularly associated PGD-G3. In the presence of 0.2 mM of AHSA, the diameter of PGD-G3 became large to be 215 nm by intensity (**Fig. 3. 9**) and 216 nm by volume (**Fig. 3. 10**). These results suggest that AHSA molecules became incorporated into the assembly of PGD-G3.

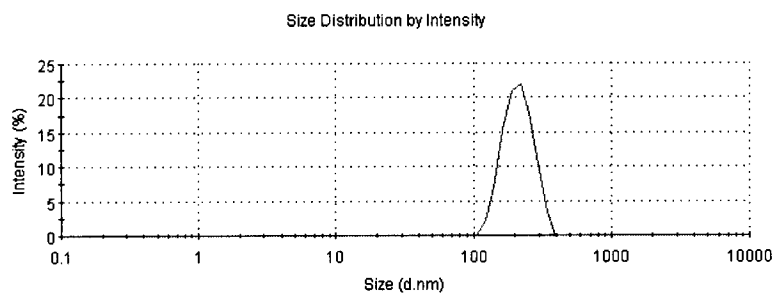




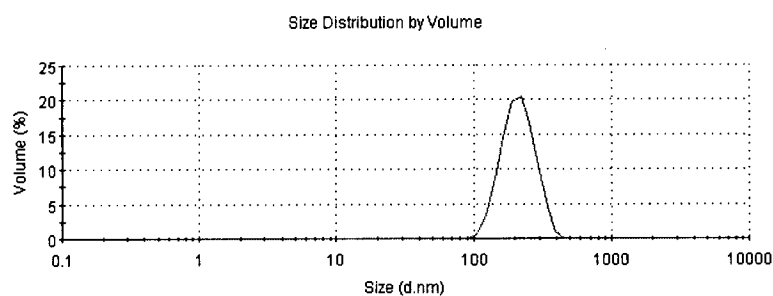
**Fig. 3. 7** Size distribution by intensity of PGD-G3 (concentration: 0.1 mM) aqueous solution by DLS



**Fig. 3. 8** Size distribution by volume of PGD-G3 (concentration: 0.1 mM) aqueous solution by DLS

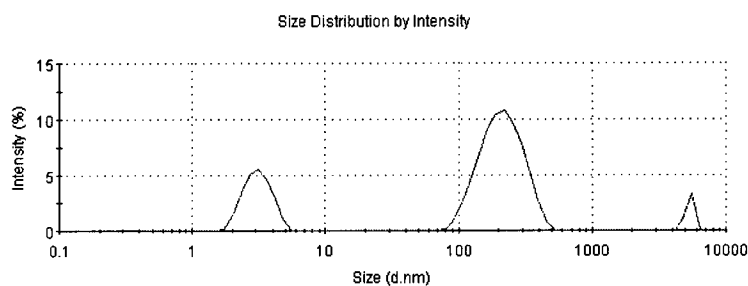


**Fig. 3. 9** Size distribution by intensity of PGD-G3 (concentration: 0.1 mM) aqueous solution in presence of AHSA (concentration: 0.2 mM) by DLS

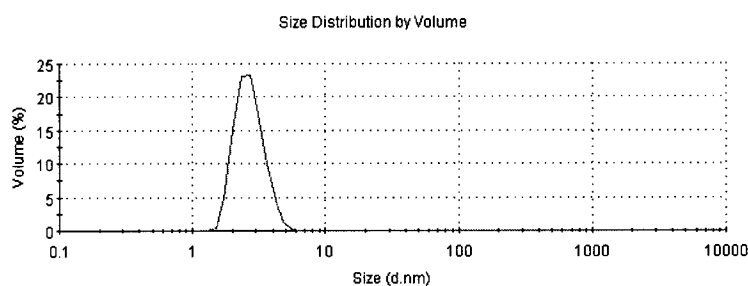


**Fig. 3. 10** Size distribution by volume of PGD-G3 (concentration: 0.1 mM) aqueous solution in presence of AHSA (concentration: 0.2 mM) by DLS

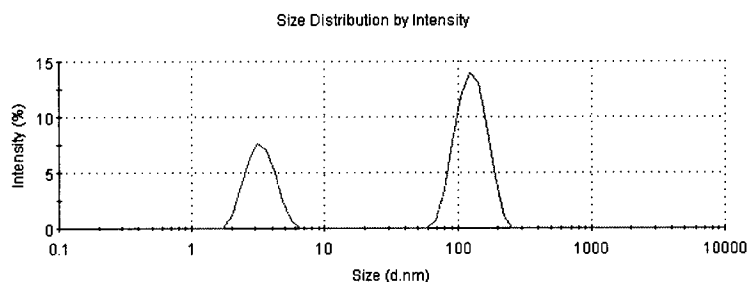
**Figs. 3. 11 and 3.12** show the size distribution of PGD-G4 by intensity in aqueous solution (concentration; 0.2 mM). The average diameter calculated from the histogram was 3.2, 221 and 5380 nm (dust) by intensity (**Fig. 3. 11**) and 2.7 nm by the volume (**Fig. 3.12**). Since the theoretical diameter of PGD-G4 calculated from a result of a molecular mechanics simulation was 3.40 nm, the observed diameter around 3.2 nm is likely to be the free PGD-G4 molecule. From the result of **Fig. 3.12**, the majority of PGD-G4 molecules in aqueous solution were the unimer of PGD-G4. The second histogram with mean diameter 221 nm is considered to be attributed to an associate of PGD-G4, since the diameter of PGD-G4 in solution was 1.9 nm calculated by DLS measurement <sup>3)</sup>. From these results, most of PGD-G4 molecules in aqueous solution hardly associate in water, presumably due to their highly densed terminal groups. In the presence of AHSA, the diameter by intensity attributed to the associate became small from 221 nm (**Fig. 3.11**) to 125 nm (**Fig. 3. 13**). The difference in DLS results of PGD-G4 between in the presence and absence of AHSA suggests that AHSA-induced dissociation of the associate of PGD-G4. The dissociation phenomena are possibly correlated with, the results of ITC with showing endothermic peaks (**Fig. 3.6**). Since the diameter of PGD-G4 by volume after adding AHSA was 0.78 nm that is attributed to the unimer of PGD-G4, the majority of PGD-G4 in presence of AHSA was considered the unimer (**Fig. 3. 14**). Even through the associated PGD-G4 molecules were not the majority of composition of PGD-G4 in aqueous solution, the decreased size of the association of PGD-G4 might be a dominant factor for the whole system of interaction between PGD-G4 and AHSA.



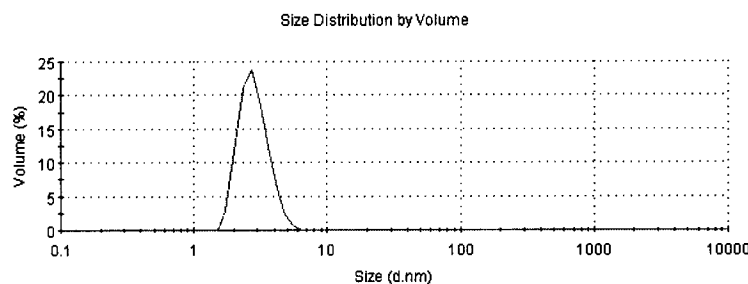
**Fig. 3. 11** Size distribution by intensity of PGD-G4 (concentration: 0.2 mM) aqueous solution by DLS



**Fig. 3. 12** Size distribution by volume of PGD-G4 (concentration: 0.2 mM) aqueous solution by DLS

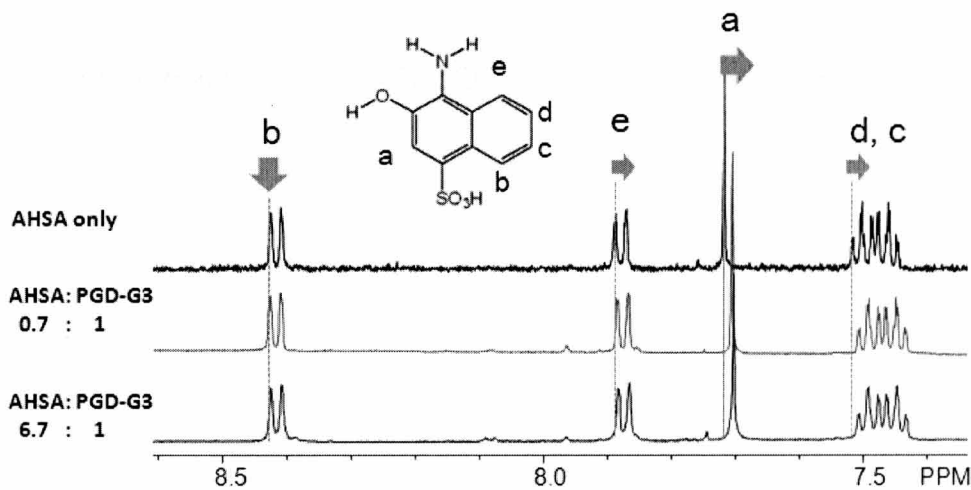


**Fig. 3. 13** Size distribution by intensity of PGD-G4 (concentration: 0.2 mM) aqueous solution in presence of AHSA (concentration: 0.2 mM) by DLS

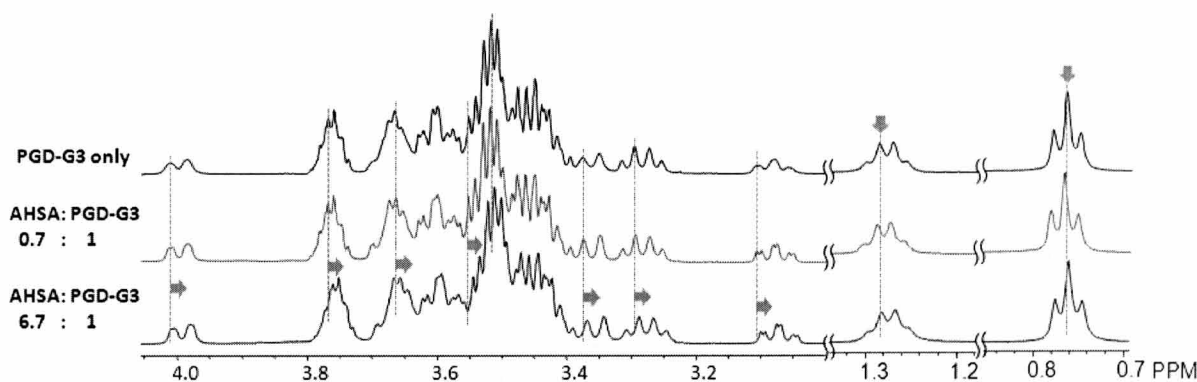


**Fig. 3. 14** Size distribution by volume of PGD-G4 (concentration: 0.2 mM) aqueous solution in presence of AHSA (concentration: 0.2 mM) by DLS

### 3.3.4 <sup>1</sup>H-NMR titration of AHSA in presence of various concentrations of PGDs



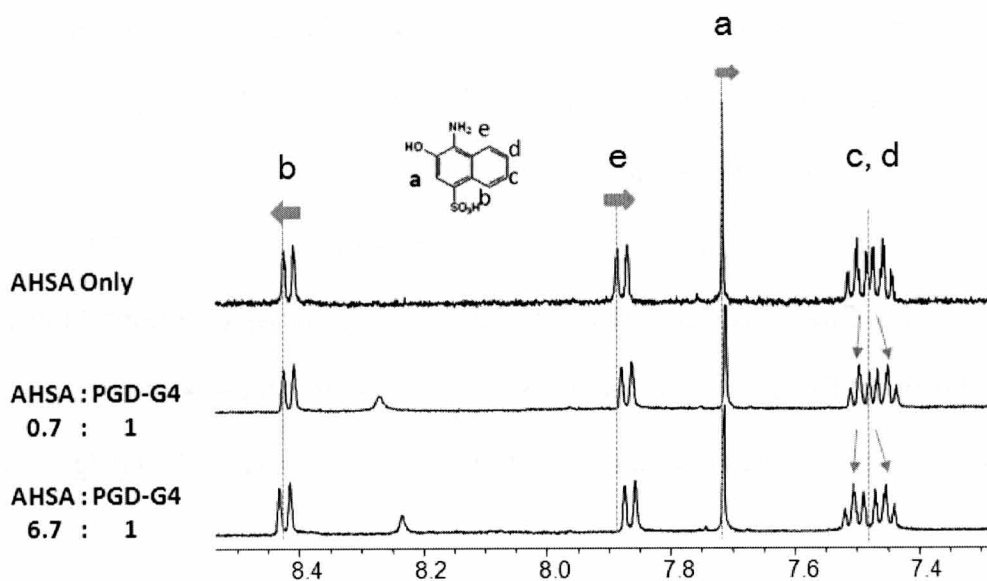
**Fig. 3. 15** <sup>1</sup>H-NMR spectra of the mixture of AHSA and PGD-G3



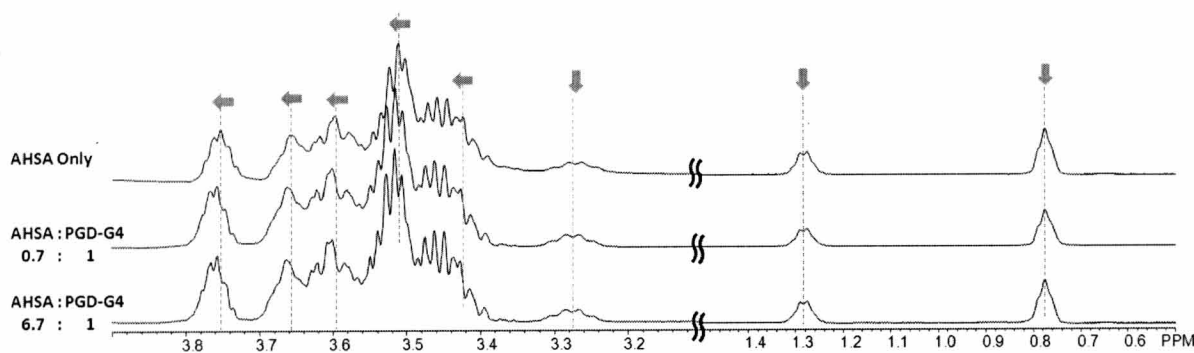
**Fig. 3. 16** <sup>1</sup>H-NMR spectra of the mixture of AHSA and PGD-G3

With increasing the molar ratio of AHSA to PGD-G3, the singlet peak for H<sub>a</sub> (7.7 ppm) was shifted towards upfield (**Fig. 3. 15**). A doublet peak for H<sub>e</sub> (7.9 ppm) and triplet peaks for H<sub>d</sub>, c (from 7.5 to 7.4 ppm) were slightly shifted toward upfield (**Fig. 3. 15**). Lastly, the doublet peak for H<sub>b</sub> (8.4 ppm) did not show any shift (**Fig. 3. 15**). In the <sup>1</sup>H-NMR titration of PGD-G3 with AHSA, most distinguishing point is that the state of AHSA was almost same with free AHSA (**Fig. 3. 15**, AHSA only). When the molar ratio

of AHSA to PGD-G3 increased, chemical shifts were slightly shielded except for the peak  $H_b$  in **Fig. 3.15**. The peaks of AHSA attributed to  $H_e$  (7.9 ppm),  $H_a$  (7.7 ppm) and  $H_{c, d}$  (from 7.5 to 7.4 ppm) were slightly shifted downfield (**Fig. 3. 15**). On the other hand, the doublet peak of  $H_b$  did not shift the chemical shift. It is noted that the peak of  $H_c$  and  $H_d$  did not show the peak separation. This result suggests that  $H_c$  and  $H_d$  protons kept the similar mobile motion with before mixing with PGD-G3, and AHSA molecule is considered to maintain a non-planar state that is supported by the moderate hypsochromic shift in presence of PGD-G3 (**Fig. 3.3**).



**Fig. 3. 17**  $^1\text{H}$ -NMR spectra of the mixture of AHSA and PGD-G4



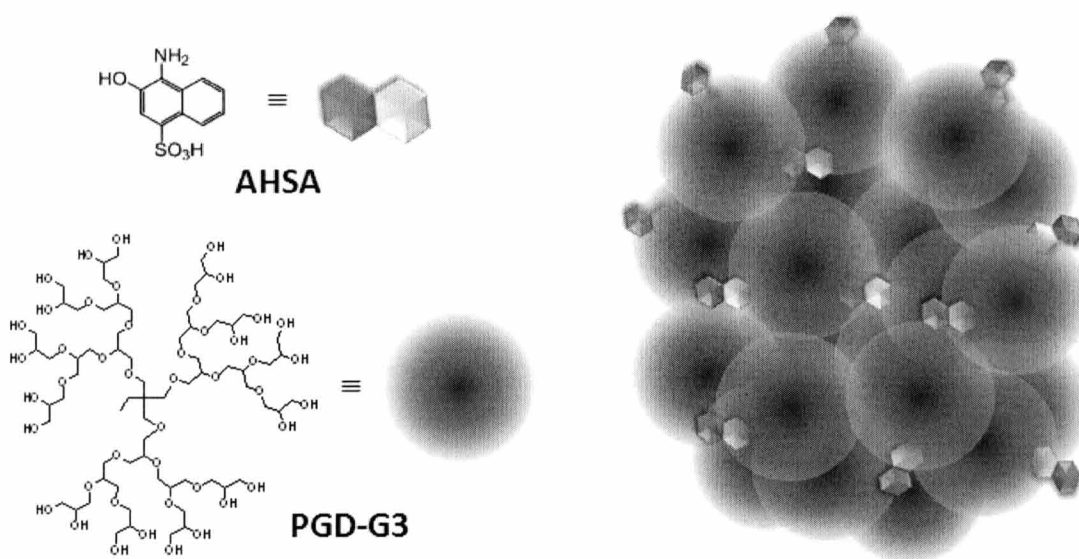
**Fig. 3. 18**  $^1\text{H}$ -NMR spectra of the mixture of AHSA and PGD-G4

$^1\text{H}$ -NMR titration between PGD-G4 and AHSA was also performed. When the molar ratio of AHSA to PGD-G4 increased, the doublet peak for  $\text{H}_b$  of naphthalene ring (8.4 ppm) noticeably shifted toward downfield, and the doublet peak of  $\text{H}_e$  of naphthalene ring (7.9 ppm) and the singlet peak for  $\text{H}_a$  (7.7 ppm) were shifted toward upfield (**Fig. 3.17**). With increasing the concentration of AHSA, the peaks attributed to the protons of branch part of PGD-G4 were found to move downfield, excluding the core part of PGD-G4 (**Fig. 3. 18**).

The spectra of  $^1\text{H}$ -NMR titration between PGD-G4 and AHSA were the almost same with the spectra of  $^1\text{H}$ -NMR titration between PGD-G2 and AHSA, excluding core part of PGDs (see chapter 2, p. 52) (**Fig. 3. 17** and **Fig. 3. 18**). These results support that the interaction mode between PGD-G4 and AHSA is almost same with the interaction between PGD-G2 and AHSA. Since the core parts of PGD-G4 did not show any shifts (**Fig. 3. 18**), the AHSA is not likely to permeate through highly densed hydroxyl group of PGD-G4. This is supported by the broad peak of core part (methyl and ethyl peak of PGD-G4) in relation to their slight solubility in  $\text{D}_2\text{O}$  (**Fig. 3. 18**).

### 3.3 Conclusion

In this chapter, molecular interactions between AHSA and PGD-G3 and G4 were analyzed by fluorescent measurements,  $^1\text{H}$ -NMR titration, ITC and DLS. AHSA was attractively interacted with PGD-G3 with a 1 : 2 stoichiometry, where AHSA might be incorporated into the associated PGD-G3 molecules (**Fig. 3. 19**). From the  $^1\text{H}$ -NMR spectra, non-polar part of naphthalene ring in the AHSA was located in the polar environment that might be formed in the associates PGD-G3 molecules. AHSA interacted moderately with periphery part of PGD-G4, the majority of which exists as a unimer.



**Fig. 3. 19** Image of aggregated PGD-G3 in presence of AHSA

## References

1. Molecular Fluorescence, Bernard Valeur, Wiley-VCH, 1st edition, 63
2. K. M. Solntsev, D. Huppert, N. Agmon, *J. Phys. Chem. A* **1998**, 102, 9599
3. T. Ooya, J. Lee, K. Park, *Bioconjugate Chem* 2004, 15, 1221



## **Chapter 4.**

# **NMR study of Host-Guest Interaction between Polyglycerol Dendrimers and an Anti-Cancer Drug**

## Chapter 4.

# NMR study of Host-Guest Interaction between Polyglycerol Dendrimers and an Anti-Cancer Drug

### 4.1 Introduction

Dendrimers have been focused on their controlling chemical and biochemical characteristics through fine control of their molecular architecture and molecular weight<sup>1)</sup>. One of the unique characteristics of dendrimers is molecular encapsulation of guest molecules, where the inside part of a dendrimer has the ability to act as a site of molecular recognition<sup>2)</sup>. For example, poly(amidoamine) (PAMAM) dendrimer and its derivatives could encapsulate drugs as a carrier<sup>3)</sup>. Since PAMAM dendrimers contain surface primary amine and internal tertiary amine groups, those groups can be protonated below those  $pK_a$  in aqueous conditions, which becomes driving force to form complexes with oppositely charged drug molecules including 5-fluorouracil (5-Fu)<sup>4)</sup>. However, PAMAM dendrimers express toxicity due to their high cationic charge density and this has limited their application *in vitro* and *in vivo*<sup>5)</sup>. Although chemical modification of the peripheral amine group using poly(ethyl glycol) (PEG) is thought to be a good approach to overcome the problem<sup>6)</sup>, it might be difficult to remove uncertainty toward the drawbacks unless nitrogen is included in dendrimers. Recently, glycerol-based materials, such as PGDs, have been received attention due to their biocompatibility.

Previous chapters (chapter 2 and 3), the interactions between different generation and various concentrations of PGDs and fluorescent probe were firstly suggested.

And the possibility of encapsulation of fluorescent probe within PGDs' interior was also implied. Taking this result into account, I tried to estimate the potential of PGDs with 5-Fu as a drug loader. This chapter deals with characterization of interaction between 5-Fu and PGDs. In this study, I focused the potential of encapsulation of 5-Fu within PGDs' interior to practical use. To estimate the potential of PGDs as a drug loader, the interaction between PGDs and 5-Fu was carried out by fluorescence measurement,  $^1\text{H}$ ,  $^{19}\text{F}$ -NMR titration and ITC. Based on these results, the potential as a nano-container was discussed.

## **4.2 Experimental**

### **4.2.1 Material**

5-Fu was purchased from Nacalai Tesque (Kyoto, Japan). Glycerol was purchased from Kanto Chemical Co., Inc. (Tokyo, Japan). PGD-G1, G2 and G3 were prepared according to the method of Haag et al.. Deutrium oxide and acetic acid- $d_4$  was purchased from Merch Chemicals (Darmstadt, Germany). Potassium fluoride was purchased from Wako Pure Chemical Industries (Osaka, Japan) and was used without further purification.

### **4.2.2 Fluorescent measurement of 5-Fu in presence of various concentrations of PGDs**

A stock solution of 5-Fu was prepared by dissolving 5-Fu in a 10 mM acetate buffer (pH 5) to be 12.5  $\mu$ M. Separately, PGD-G1, G2 and G3 (6, 12.5, 24, 50  $\mu$ mol) were dissolved in 800  $\mu$ L of the same buffer. The 5-Fu stock solution (200  $\mu$ L) was added to each PGD solution (final concentration; 5-Fu: 2.5  $\mu$ M, PGDs: 1.25, 2.5, 5, 10  $\mu$ L). The mixture of 5-Fu and PGDs was stood for 30 min at room temperature in a quartz cell, and then emission spectra of the solution were measured (excitation wavelength: 267 nm) at room temperature using a spectrofluorometer (F-2500, HITACHI, Ltd., Japan) under the conditions of 20 nm slit widths.

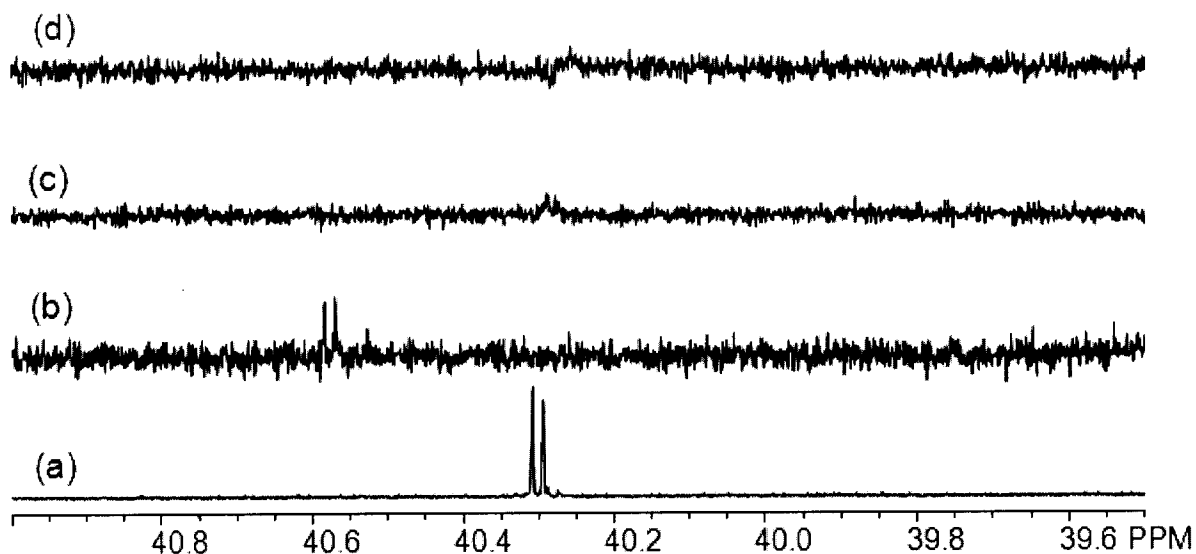
### **4.2.3 $^1\text{H}$ , $^{19}\text{F}$ -NMR titration of 5-Fu toward PGDs**

The 5-Fu was dissolved in a 10 mM acetate buffer prepared by  $\text{D}_2\text{O}$ , and the pD was adjusted to be 5.0 by adding NaOD and acetic acid- $d_4$  (concentration of 5-Fu:

12.5  $\mu\text{M}$ ). Each PGD (PGD-G1, G2 or G3) dissolved in the buffer were added to the 5-Fu solution to be (2.5, 5.0, 10.0  $\mu\text{M}$ ) (final concentration of 5-Fu: 2.5  $\mu\text{M}$ ).  $^1\text{H}$ -NMR and  $^{19}\text{F}$ -NMR spectra of each solution were measured using a 500 MHz FT-NMR apparatus (Bruker Advanced 500) and 400 MHz FT-NMR apparatus (Varian Unity Inova-400), respectively. In case of  $^{19}\text{F}$ -NMR, the shift is given relative to HF, a reference compound.

## 4. 3 Results and discussion

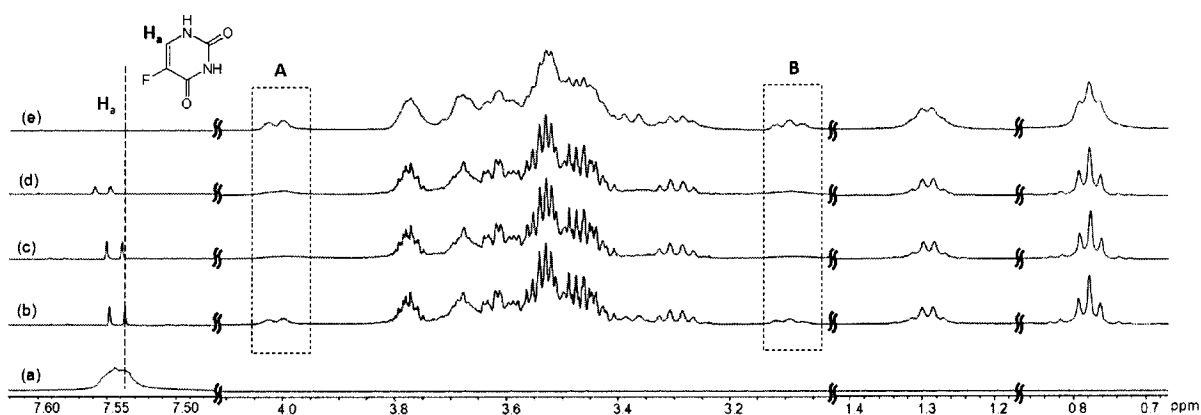
### 4.3.1 $^1\text{H}$ , $^{19}\text{F}$ -NMR titration of 5-Fu in presence of various concentrations of PGDs



**Fig. 4. 1**  $^{19}\text{F}$ -NMR titration of 5-Fu with PGD-G3; PGD-G3 : 5-Fu = (a) 0 : 1, (b) 1 : 1, (c) 2 : 1, and (d) 4 : 1. Solvent: 10 mM acetate buffer (pD 5.0)

Among the series of PGDs, I hypothesized that higher generation of PGDs have potential to incorporate inside into the interior part of PGDs<sup>1)</sup>. For the estimation of the interaction between 5-Fu and PGD-G3,  $^{19}\text{F}$ -NMR spectra of 5-Fu would give good information of the location in the presence of PGD-G3. **Fig. 4.1** shows the  $^{19}\text{F}$ -NMR spectra of 5-Fu titrated by PGD-G3. The chemical shift of  $^{19}\text{F}$  of 5-Fu itself was observed at 40.3 ppm, as a sharp doublet (**Fig. 4. 1**). When the concentration of PGD-G3 increased, the chemical shift of  $^{19}\text{F}$  was shifted toward down field (PGD-G3 : 5-Fu = 1 : 1, **Fig. 4.1(b)**) and difficult to find the peak (PGD-G3 : 5-Fu = 2 : 1 and 4 : 1, **Fig. 4.1 (c) and (d)**). Since the downfield shift of  $^{19}\text{F}$  peak is closely related with imino proton exchange caused by solute proton acceptor<sup>2)</sup>, it is suggested that the imino

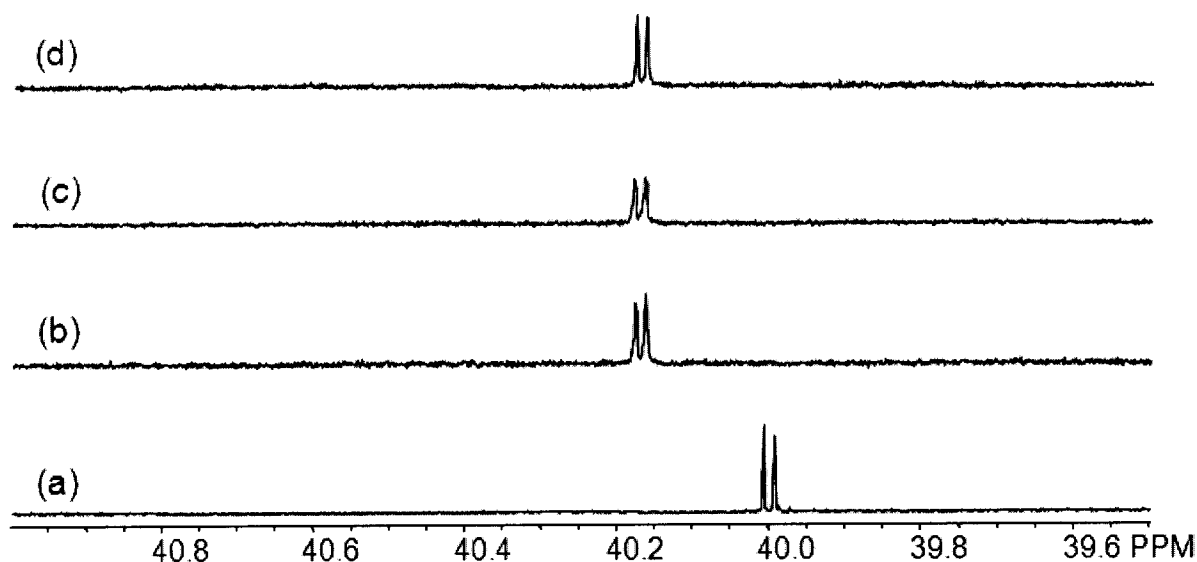
proton was attracted when the ratio of PGD-G3 and 5-Fu was 1 : 1. With increasing the ratio to 2 : 1 and 4 : 1, 5-Fu molecule is likely to be buried within the interior part of PGD-G3, because  $^{19}\text{F}$  signal was no longer detected as seen in the case of encapsulated drugs in polymeric micelles<sup>3)</sup>. These results clearly demonstrated that  $^{19}\text{F}$  moiety of 5-Fu in the presence of PGD-G3 showed much slower motions compared to that without PGD-G3.



**Fig. 4. 2**  $^1\text{H}$ -NMR titration of the mixture of 5-Fu and PGD-G3; (a) 5-Fu, (b) PGD-G3 : 5-Fu = 1 : 1, (c) PGD-G3 : 5-Fu = 2 : 1, (d) PGD-G3 : 5-Fu = 4 : 1 and (e) PGD-G3. Solvent: 10 mM acetate buffer (pD 5.0)

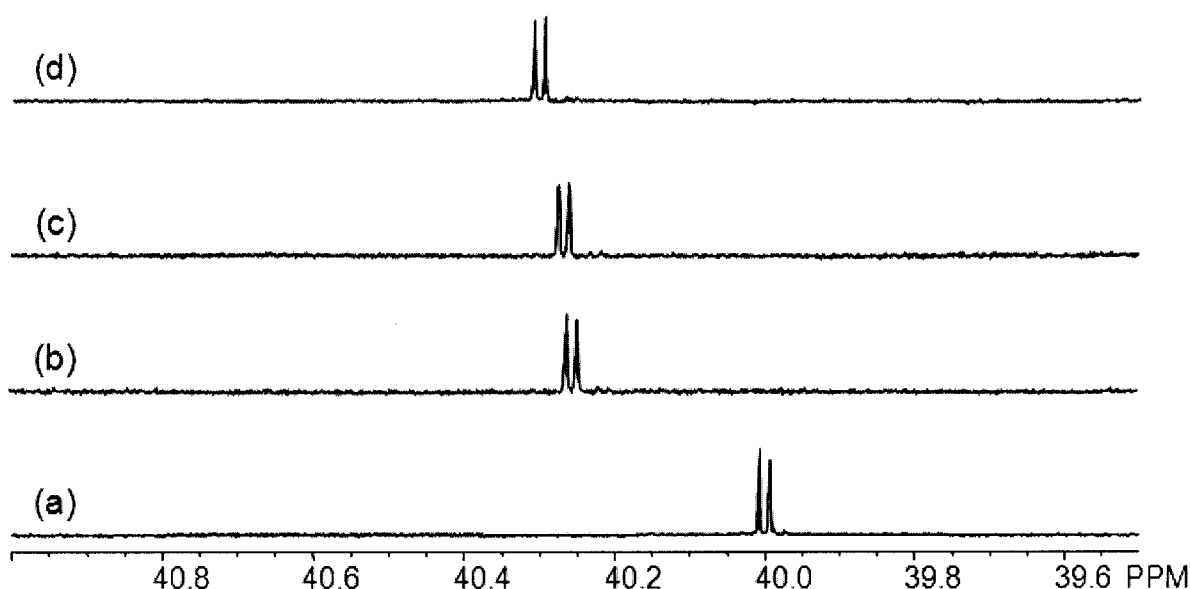
$^1\text{H}$ -NMR spectra were measured under the same condition of  $^{19}\text{F}$ -NMR measurements. The  $\text{H}_a$  peak of 5-Fu itself was appeared as a broad peak near 7.55 ppm, to slow mobility in relation to the poor solubility in water (10 mg/mL) (**Fig. 4. 2** (a)). At 1 : 1 molar ratio of PGD-G3 and 5-Fu, the peaks around 4.0 ppm (CH protons adjacent to terminal OH groups: (a) in **Fig. 4.2**) and 2.8 ppm (protons: B in **Fig. 4. 2**), which was the same as seen in the  $^1\text{H}$ -NMR spectrum of PGD-G3 itself. Here, it is noted that the most peaks attributed to PGD-G3 became sharp in comparison with the peaks of PGD-G3 without adding 5-Fu. This result suggests that molecular motion of PGD-G3 in the buffer was enhanced by the interaction with 5-Fu. Presumably, the

solubility of PGD-G3 in the buffer increased by elimination of intra- or intermolecular hydrogen bonds of hydroxyl groups due to the interaction with amide groups of 5-Fu<sup>4)</sup>. With increasing the molar ratio from 2 : 1 to 4 : 1, the chemical shift of H<sub>a</sub> in 5-Fu molecule was deshielded with signal boarding (**Fig. 4. 2 (e)**). In addition, the peaks attributed to the branch part of PGD-G3 (A and B in **Fig. 4. 2**) became broad. These phenomena suggest the interaction between 5-Fu and the branch part of PGD-G3. Taking the results of <sup>19</sup>F-NMR titration (**Fig. 4. 1**) into account 5-Fu molecule was encapsulated within the branched part of PGD-G3 at over two moles of PGD-G3 against one mole of 5-Fu.



**Fig. 4. 3** <sup>19</sup>F-NMR titration of the mixture of 5-Fu and PGD-G2: (a) 5-Fu, (b) PGD-G2 : 5-Fu = 1 : 1, (c) PGD-G2 : 5-Fu = 2 : 1 and (d) PGD-G2 : 5-Fu = 4 : 1. Solvent: 10 mM acetate buffer (pD 5.0)

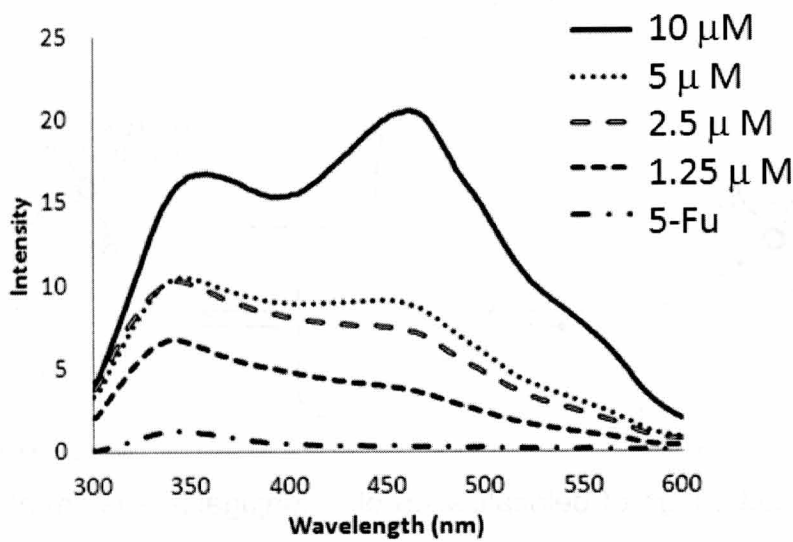




**Fig. 4. 4**  $^{19}\text{F}$ -NMR titration of the mixture of 5-Fu and PGD-G1: (a) 5-Fu, (b) PGD-G1 : 5-Fu = 1 : 1, (c) PGD-G1 : 5-Fu = 2 : 1 and (d) PGD-G1 : 5-Fu = 4 : 1. Solvent: 10 mM acetate buffer (pD 5.0)

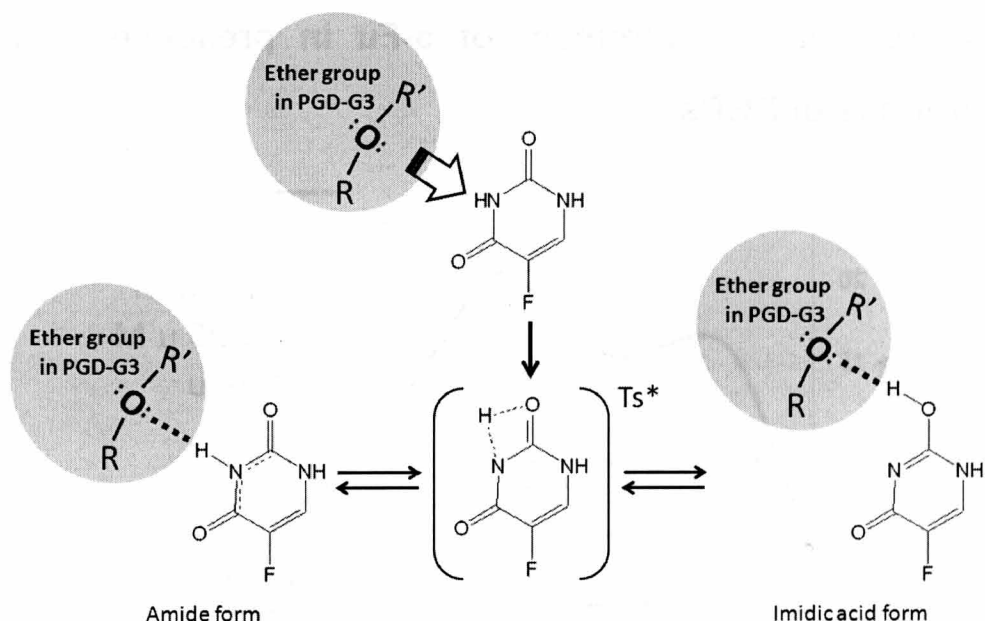
In a similar way as in the case of PGD-G3,  $^{19}\text{F}$ -NMR titration of 5-Fu against PGD-G2 and PGD-G1 were performed under the same conditions. With increasing the concentration of PGD-G2 and G1,  $^{19}\text{F}$  signal of 5-Fu were shifted to downfield, and signal broadening as seen in the case of PGD-G3 (**Fig. 4. 1**) was not observed even when the molar ratio of PGDs and 5-Fu was over 2 : 1 (**Fig. 4. 3** (b)-(d), **Fig. 4. 4** (b)-(d)). These results suggest that 5-Fu was actually interacted with PGD-G2 and G1, but not fully incorporated into the interior part of PGD-G2 and G1.

4.3.2 Fluorescent measurement of 5-Fu in presence of various concentrations of PGDs



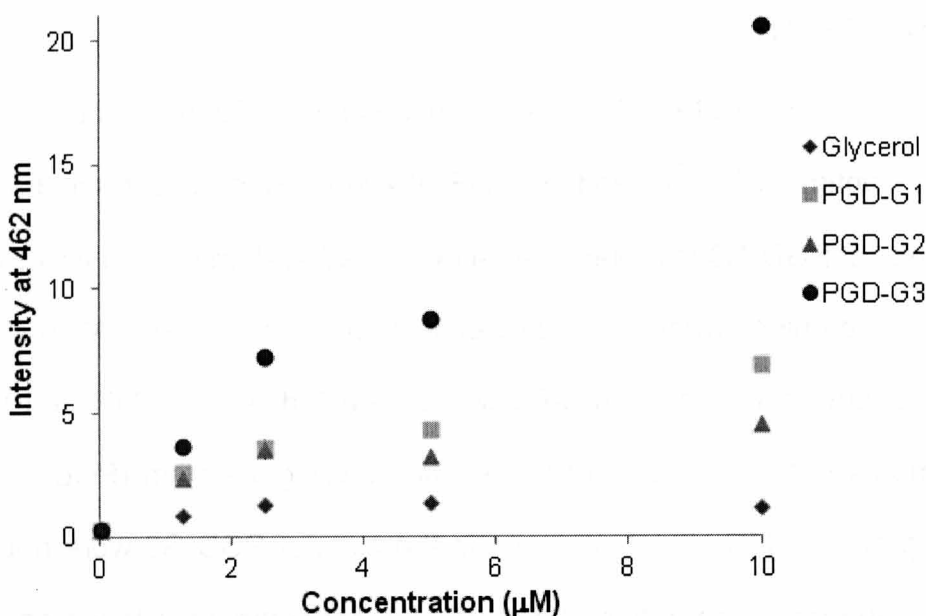
**Fig. 4. 5** Fluorescent spectral change (Ex: 267 nm) of 5-Fu (2.5 mM) on the addition of PGD-G3 in 10 mM acetate buffer (pH 5.0) at room temperature. PGD-G3 concentration = 1.25, 2.5, 5.0, 10.0 mM

In order to understand the encapsulation of 5-Fu within the interior part of PGD-G3, fluorescent spectra were measured under. It is known that 5-Fu has been previously studied as a photosensitizer capable of fluorescent change via tautomeric formation; the amide form and imidic acid form<sup>5</sup>). Since I obtained both the <sup>19</sup>F and <sup>1</sup>H-NMR signal changes in the presence of PGD-G3, I hypothesized that fluorescent spectra would also give some information of the location of 5-Fu within the interior part of PGD-G3 in relation to the formation of 5-Fu tautomers. A fluorescence spectrum of 5-Fu excited at 267 nm, exhibited bands in the range between 300 and 500 nm (**Fig. 4. 5**). With increasing the concentration of PGD-G3, the intensity around 462 nm remarkably increased, especially, when the concentration of PGD-G3 was 10.0 mM.



**Fig. 4. 6** Proposed image of delocalization of  $\pi$ -conjugated system attracted by the ether oxygen of PGD-G3

The increased intensity at low energy band region (462 nm) means that the  $\pi$ -conjugated system of 5-Fu is extended. Since 5-Fu exhibits the amide and imidic acid forms, this result strongly suggests the imidic acid form of 5-Fu increased with the concentration of PGD-G3. Therefore, when 5-Fu was encapsulated within the interior part of PGD-G3, the imine proton is possibility attracted by ether oxygen of PGD-G3, resulting in changing a kind of reduction product of 5-Fu with delocalization of  $\pi$ -conjugation (**Fig. 4. 6**). Thus, the increase intensity near 462 nm suggests encapsulation of 5-Fu within interior part of PGD-G3.



**Fig. 4. 7** Fluorescent intensity change of 5-Fu at 462 nm (Ex: 267 nm) with increasing the concentration of PGD-G1, G2, G3 and glycerol in the acetate buffer (pH 5)

Generation dependency of PGDs for the encapsulation of 5-Fu was demonstrated by the fluorescent change. **Fig. 4. 7** shows fluorescent intensity change of 5-Fu at 462 nm (Ex: 267 nm) with increasing the concentration of PGD-G1, G2, G3 and glycerol in the acetate buffer (pH 5.0). The intensity increase of PGD-G1, G2 and glycerol with increasing those concentrations were significantly small as compared with PGD-G3, indicating that the ability of attaching the imine proton within the interior of PGDs with low generation might be poor.

### 4.3 Conclusion

The dendritic interior of PGD-G3 could encapsulate 5-Fu in an aqueous condition, which was confirmed by  $^{19}\text{F}$ - and  $^1\text{H}$ -NMR titrations. Fluorescent spectra of 5-Fu in the presence of PGD-G3 revealed that  $\pi$ -conjugated system of 5-Fu was extended by attraction of the imine proton of 5-Fu by ether oxygen of PGD-G3. Although such the attraction of the imine proton in 5-Fu was suggested by  $^{19}\text{F}$ -NMR and fluorescent measurements in the presence of PGDs with lower generation (PGD-G1 and G2), broadening of  $^{19}\text{F}$ -NMR signals as seen in the case of PGD-G3 were not observed. Therefore, the higher generation of dendritic interior contributed to the encapsulation of 5-Fu, where ether oxygen plays an important role for the attraction of the imine proton of 5-Fu. The encapsulation of 5-Fu in aqueous solution using the biocompatible PGDs is expected to develop as nano-sized drug carriers with showing well-defined size and structure, which is believed to be a key factor for drug targeting *in vivo*.

## References

1. H. LEE, T. Ooya, *Chem. Commun.* **2012**, Advance Article, DOI: 10.1039/C1CC15949F
2. J. B. Parker and J. T. Stivers, *Biochemistry* **2011**, 50, 612-617
3. T. Chandran, U. Katragadda, Q. Teng, C. Tan, *Int. J. Pharm* **2010**, 392, 170-177  
Y. I. Jeong, J. W. Nah, H. C. Lee, S. H. Kim, C. S. Cho, *Int. J. Pharm* **1999**, 188, 49-58
4. T. Ooya, J. Lee, K. Park, *Bioconjugate Chem.* **2004**, 15(6), 1221-1229
5. M. L. Pascu, M. Brezeanu, L. Voicu, A. Staicu, B. Carstocea, R. A. Pascu, *In vivo* **2005**, 19, 215-220
6. N. Markova, V. Enchev, G. Ivanova, *J. Phys. Chem. A* **2010**, 114, 13154-13162

# **Chapter 5.**

## **Exploratory Study of Guest Molecules toward Polyglycerol Dendrimers by Isothermal Titration Calorimetry.**

### **5.1 Introduction**

The results in chapter 4 suggest that the host-guest system using PGDs has a potential for pharmaceutical applications. To expand the application of PGDs as a host molecule, the exploratory study was performed. Since the internal interior of PGDs was found to be contributed to the encapsulation of 5-Fu, where ether oxygen plays an important role for the attraction of the imine proton of 5-Fu. In order to obtain the information of guest molecules capable of amino acids, which have various  $pK_a$  side chains, were employed as candidates of the guest molecules. This chapter describes a preliminary study of the host-guest interaction between amino acids and PGD-G3.

## 5.2 Experimental

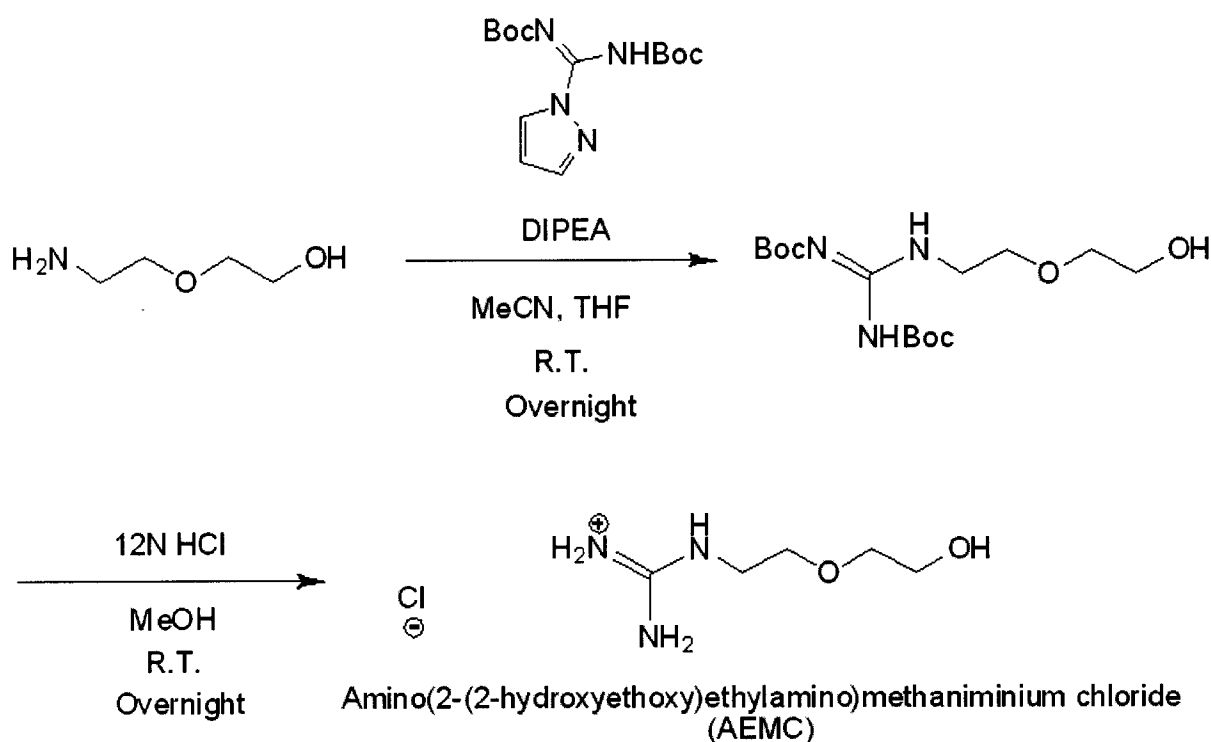
### 5.2.1 Material

Acetonitrile ( $\text{CH}_3\text{CN}$ ) and tetrahydrofuran (THF) were purchased from Wako Pure Chemical Industries (Osaka, Japan) and were used without further purification. Sodium chloride ( $\text{NaCl}$ ), ethyl acetate ( $\text{AcOEt}$ ), sodium sulfate ( $\text{Na}_2\text{SO}_4$ ), L-arginine, L-histidine, L-lysine and glutamic acid were reagent grade and purchased from Nacalai Tesque (Kyoto, Japan). 2-(2-aminoethoxy ethanol), 4-aminobutyric acid (GABA) and *N, N*-Diisopropylethylamine (DIPEA) were purchased from Tokyo Chemical Industry Co. (Tokyo, Japan). *N, N'*-Di-Boc-1H-pyrazole-a-carboxyamidine was purchased from Sigma-Aldrich Co. (St. Louis. USA) and used without further purification.

### 5.2.2 Preparation of amino(2-(2-hydroxyethoxy)ethylamino)methaniminium chloride (AEMC)

To  $\text{CH}_3\text{CN}$ /THF (30 mL, v/v = 2/1) solution of 2-(2-aminoethoxy ethanol) (2.93 mmol, 0.41 mL) were successively added DIPEA (1.6 mL) and *N, N'*-di-Boc-1H-pyrazole-a-carboxyamidine (3.22 mmol, 1 g). After being stirred overnight at room temperature, the reaction mixture was evaporated to dryness, and the residue was dissolved in  $\text{AcOEt}$  (160 mL), and washed with brine (160 mL). The organic extract was dried over  $\text{Na}_2\text{SO}_4$ , evaporated to dryness. Clear oil (**1**) was obtained (58%). To a MeOH (94.5 mL) solution of **1** (1.14 mmol, 0.38 g) was added 12N HCl (3.15 mL), and the mixture was stirred overnight at room temperature. Then, the reaction mixture was evaporated to dryness to give AEMC white oil in 70% yield.





**Scheme 4. 1** Preparation of AEMC

1 : Yield: 58 %

$^1\text{H-NMR}$  ( $\text{CDCl}_3$ , 300 MHz):  $\delta$  = 3.84 (t, 2H,  $-\text{NHCH}_2\text{CH}_2\text{O}-$ ), 3.6 (t, 2H,  $-\text{OCH}_2\text{CH}_2\text{O}-$ ), 3.45 (t, 2H,  $\text{HOCH}_2\text{CH}-$ ), 2.8 (m, 2H,  $-\text{NHCH}_2\text{CH}_2-$ ), 1.5 (s, 18H,  $-\text{OCCH}_3$ )

AEMC: Yield: 70 %

$^1\text{H-NMR}$  ( $\text{CDCl}_3$ , 300 MHz):  $\delta$  = 3.84 (m, 2H,  $-\text{NHCH}_2\text{CH}_2\text{O}-$ ), 3.6 (m, 2H,  $-\text{OCH}_2\text{CH}_2\text{O}-$ ), 3.45 (t, 2H,  $\text{HOCH}_2\text{CH}-$ ), 2.8 (m, 2H,  $-\text{NHCH}_2\text{CH}_2-$ )

### 5.2.3 ITC study of amino acids and AEMC against PGD-G3

ITC titrations were carried out using a VP-ITC microcalorimeter (MicroCal LLC, GE Healthcare). PGD-G3 was dissolved in distilled water. And amino acids (glutamic acid, histidine, lysine and arginine) or AEMC were also prepared in the same way (concentration: 0.5 mM or 1 mM or 10 mM). The PGD-G3 solutions were placed in the calorimeter cell. The titration syringe was loaded with amino acid or AEMC solution at

a 5 ~ 100 times higher concentration than in the cell. The titrations were carried out with 25 injections of 10  $\mu$ L each with time intervals of 20 second. The solution was stirred at 300 rpm as suggested by the manufacturer. Titrations were carried out at a cell temperature of 25 °C and with a reference power of 10  $\mu$ cal $s^{-1}$ . ITC data analyses were carried out in Origin 7 SR 2 (OriginLab Corp.) with the provided microcal ITC routines.

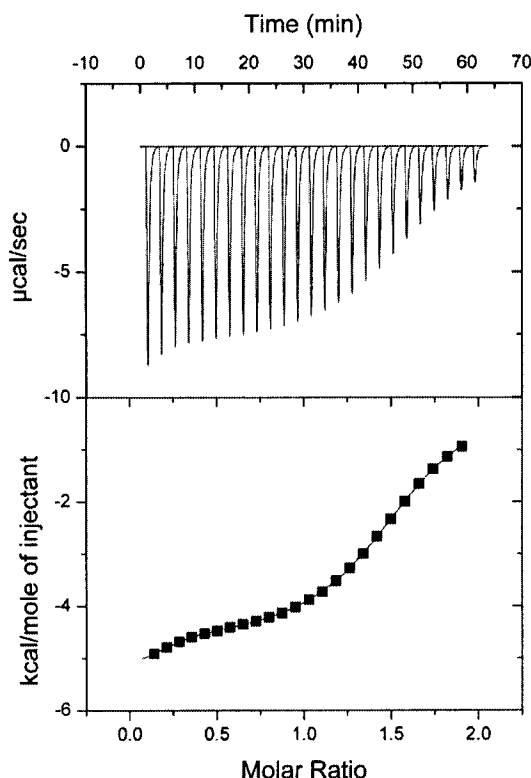
#### **5.2.4 $^1\text{H}$ -NMR and 2D $^1\text{H}$ - $^1\text{H}$ NOESY NMR of L-arginine or L-lysine against PGD-G3**

PGD-G3 was dissolved in  $\text{D}_2\text{O}$ . L-arginine or L-lysine dissolved in  $\text{D}_2\text{O}$  was added to the PGD-G3 dissolved solution to be 0.5 mM. (final concentration of L-arginine or L-lysine: 5 mM).  $^1\text{H}$ -NMR spectra of each solution were measured using 500 MHz FT-NMR apparatus (Bruker Advanced 500).

Using the same solution with  $^1\text{H}$ -NMR, NOESY experiments were obtained and acquired at 500 MHz, using 300 ms mixing time. The data were processed XWINPLOT and zero filling in both dimensions to display on a 1024 x 1024 2D matrix.

## 5.3 Results and discussion

### 5.3.1 ITC study of amino acids and AEMC against PGD-G3

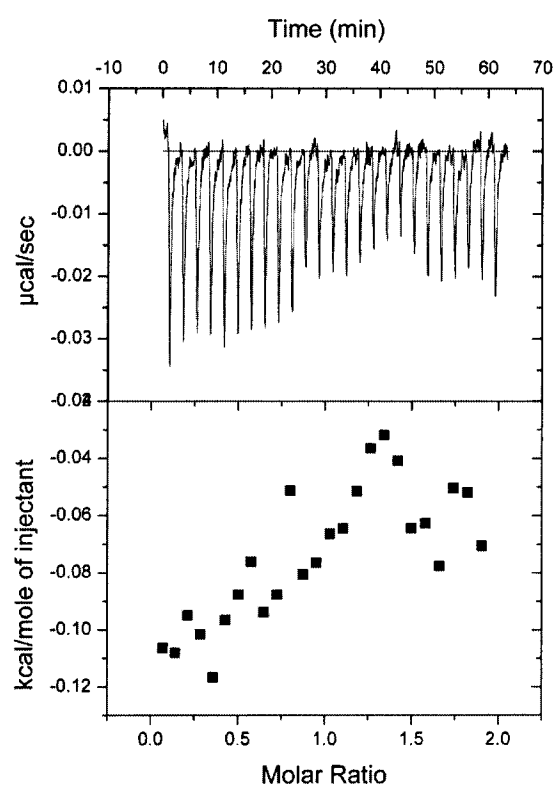


**Fig. 5. 1** ITC titration curves for PGD-G3 and L-arginine in water. ITC measurements were performed to establish solution binding constants. In this experiment, a solution of PGD-G3 (0.5 mM) was titrated with a solution of L-arginine (5 mM)

The result of a typical titration calorimetric measurement of PGD-G3 with L-arginine is shown in **Fig 5.1**. The titration curves between PGD-G3 and L-arginine exhibit a two site model which decrease in the exothermic heat of binding with each injection. This ITC titration curves support the interaction between PGD-G3 and L-arginine. The stoichiometries of each binding site were PGD-G3 : L-arginine = 1 : 5 and 1 : 0.7, respectively. The  $K_{a1}$  value was calculated to be  $1.12 \times 10^6 \text{ (M}^{-1}\text{)}$ .  $\Delta H_1$  and  $\Delta S_1$  were calculated to be  $-5.19 \times 10^3 \text{ (M}^{-1}\text{)}$  and  $10.3 \text{ (M}^{-1}\text{)}$ . The  $K_{a2}$  value was calculated to be

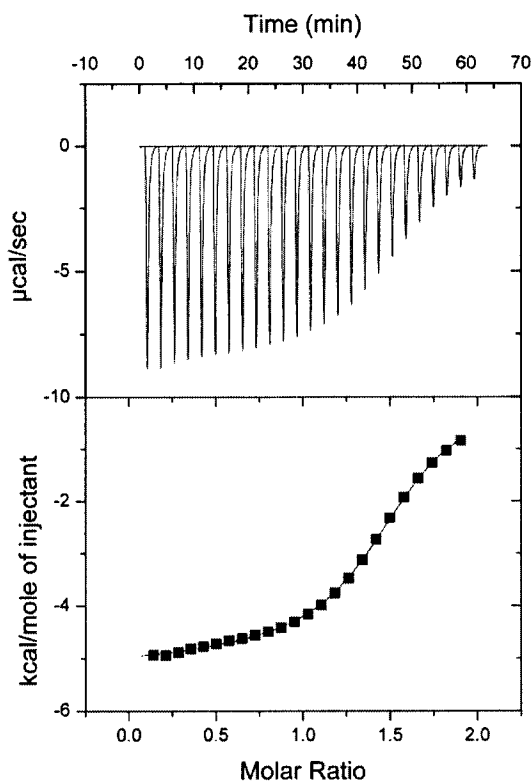
$4.19 \times 10^4 \text{ (M}^{-1}\text{)}$ .  $\Delta H_2$  and  $\Delta S_2$  were calculated to be  $-4.68 \times 10^3 \text{ (M}^{-1}\text{)}$  and  $5.46 \text{ (M}^{-1}\text{)}$ . Comparing the binding constant of first and second binding site, the first binding was much stronger than second binding.

From ITC study between PGD-G3 and L-arginine, the interaction between PGD-G3 and L-arginine was suggested. For this reason, I hypothesized that the guanidine group on arginine is the dominant factor on the interaction between PGD-G3 and L-arginine. According to the hypothesis, synthesized AEMC which has guanidine function group was prepared. The result of a typical titration calorimetric measurement for PGD-G3 with AEMC is shown in **Fig 5.2**.



**Fig. 5. 2** ITC titration curves for PGD-G3 and AEMC in water. ITC measurements were performed to establish solution binding constants. In this experiment, a solution of PGD-G3 (0.1 mM) was titrated with a solution of AEMC (1 mM)

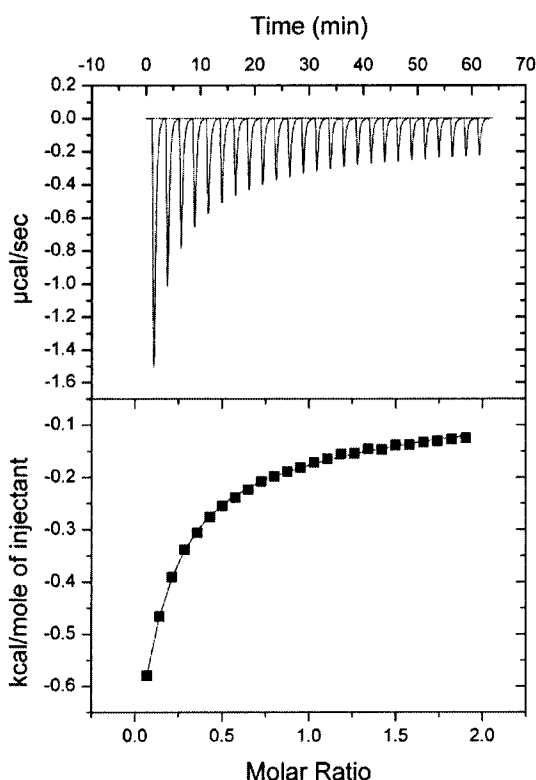
The result shows endothermic heat which is inadequate to recognize the interaction between PGD-G3 and AEMC (**Fig. 5. 2**). This ITC titration of PGD-G3 with AEMC supports that the guanidine group on L-arginine is not the dominant factor of interaction between PGD-G3 and L-arginine. Therefore, I amended the hypothesis. In case of L-arginine, the  $pK_a$  of side group is 12.48 indicating the high  $pK_a$  value in amino acids. Focused on  $pK_a$  of L-arginine, other amino acids, such as L-lysine ( $pK_a$ : 10.79), L-histidine ( $pK_a$ : 6.04), and glutamic acid ( $pK_a$ : 4.25), were employed.



**Fig. 5. 3** ITC titration curves for PGD-G3 and L-lysine in water. ITC measurements were performed to establish solution binding constants. In this experiment, a solution of PGD-G3 (0.5 mM) was titrated with a solution of L-lysine (5 mM)

**Fig. 5. 3** shows the result of ITC titration of PGD-G3 with L-lysine in water. The titration curves between PGD-G3 and L-lysine also exhibit a two site model This ITC

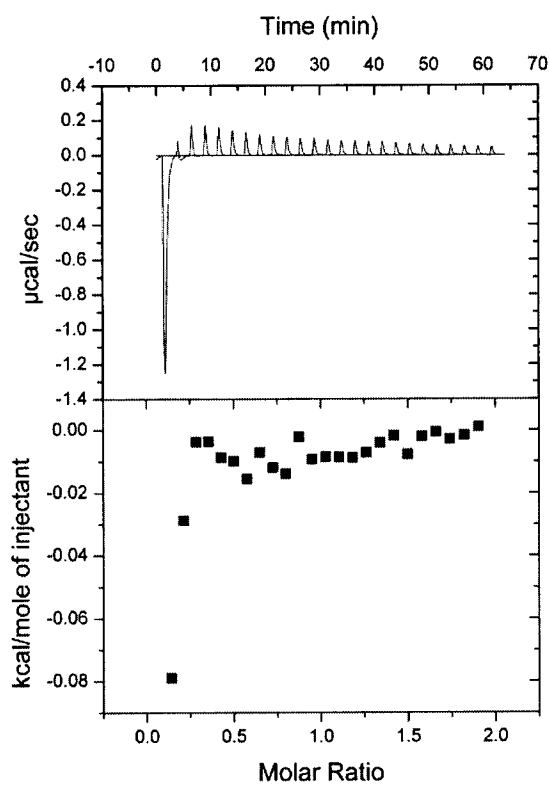
titration curves support the interaction between PGD-G3 and L-lysine, similarly to the ITC titration curves of PGD-G3 with L-arginine. The stoichiometries of each binding site were PGD-G3 : L-lysine = 1: 2 and 1 : 1, respectively. The  $K_{a1}$  value was calculated to be  $9.64 \times 10^4 \text{ (M}^{-1}\text{)}$ .  $\Delta H_1$  and  $\Delta S_1$  were calculated to be  $-5.44 \times 10^3 \text{ (M}^{-1}\text{)}$  and  $4.56 \text{ (M}^{-1}\text{)}$ . The  $K_{a2}$  value was calculated to be  $4.97 \times 10^4 \text{ (M}^{-1}\text{)}$ .  $\Delta H_2$  and  $\Delta S_2$  were calculated to be  $-4.60 \times 10^3 \text{ (M}^{-1}\text{)}$  and  $6.08 \text{ (M}^{-1}\text{)}$ .



**Fig. 5. 4** ITC titration curves for PGD-G3 and L-histidine in water. ITC measurements were performed to establish solution binding constants. In this experiment, a solution of PGD-G3 (0.5 mM) was titrated with a solution of L-histidine (5 mM)

The result of ITC titration of PGD-G3 with L-histidine is shown in **Fig. 5. 4**. Like previous ITC titration of PGD-G3 with L-arginine or lysine, the ITC titration curves of PGD-G3 with L-histidine also showed two site model. However, the endothermic heat

of each injection was remarkably decreased, compared with endothermic heat of PGD-G3 with L-arginine or L-lysine. The  $K_{a1}$  value was calculated to be  $8.17 \times 10^4$  ( $M^{-1}$ ).  $\Delta H_1$  and  $\Delta S_1$  were calculated to be  $-2.51 \times 10^3$  ( $M^{-1}$ ) and  $9.50$  ( $M^{-1}$ ). The  $K_{a2}$  value was calculated to be  $2.27 \times 10^2$  ( $M^{-1}$ ).  $\Delta H_2$  and  $\Delta S_2$  were calculated to be  $-3.50 \times 10^3$  ( $M^{-1}$ ) and  $-1.00$  ( $M^{-1}$ ).

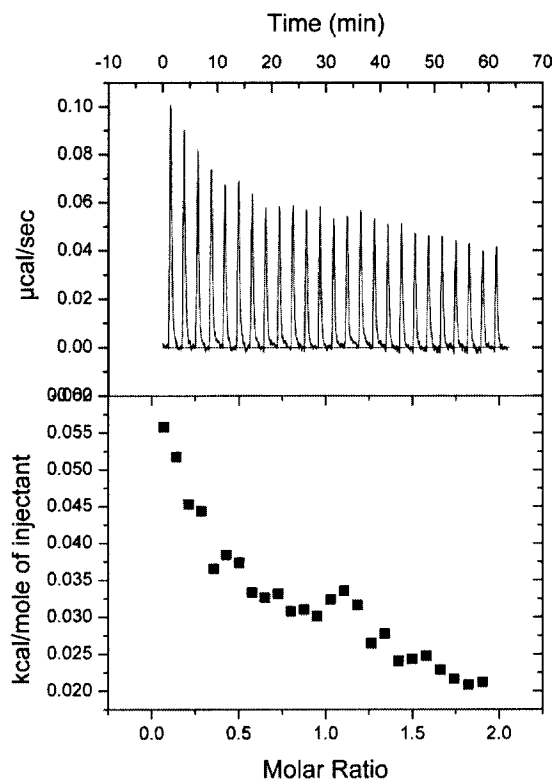


**Fig. 5. 5** ITC titration curves for PGD-G3 and glutamic acid in water. ITC measurements were performed to establish solution binding constants. In this experiment, a solution of PGD-G3 (0.5 mM) was titrated with a solution of glutamic acid (5 mM)

**Fig. 5. 5** shows the ITC titration for PGD-G3 and glutamic acid in water. Generally, the ITC titration result showed exothermic process during the injection of glutamic acid into PGD-G3 solution. The amount of exothermic heat was few compared with previous ITC titration results, such as L-lysine. Therefore, it was difficult to find the

interaction between PGD-G3 and glutamic acid. Considerable reason of exothermic heat is the separation of glutamic acid dimer. Glutamic acid has carboxylic acid (as an electron donor) on side chain and amine (as an electron acceptor). Therefore, it is easy to form the dimer of glutamic acid. With injection of glytamic acid into PGD-G3, the dimer of glutamic acid might begin to be separated.

To understand the ineration between PGD-G3 and amino acids, PGD-G3 ITC titration with L-arginine or L-lysine or L-histidine or glutamic acid was carried out. Each ITC titration curves suggests that the amino acids interacted with two binding site within PGD-G3. The series of side chain  $pK_a$  showed that the main driving force for interaction between PGD-G3 and amino acid is basicity of side chain on amino acid. While, the role of  $\alpha$ -amino on the interaction between PGD-G3 and amino acid is still veiled. Therefore, GABA, which does not bear  $\alpha$ -amino, was employed.



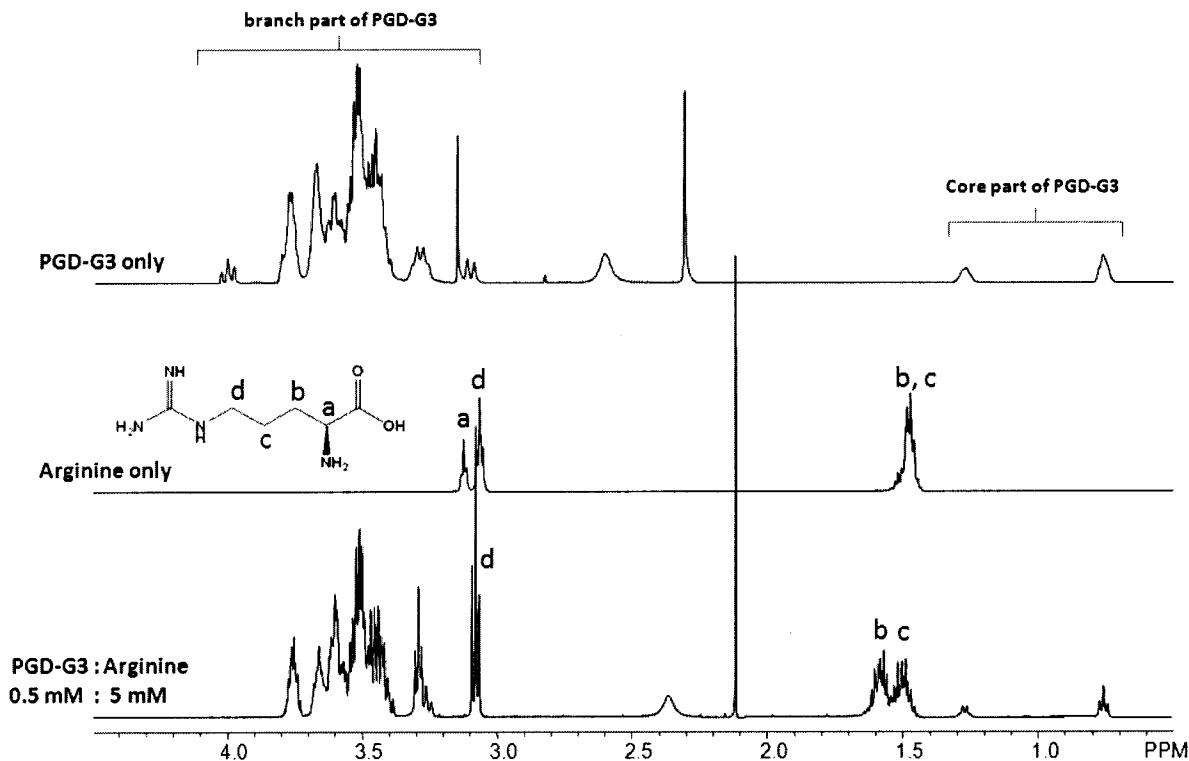
**Fig. 5. 6** ITC titration curves for PGD-G3 and GABA in water. ITC measurements were performed to establish solution binding constants. In this experiment, a solution



of PGD-G3 (0.5 mM) was titrated with a solution of 4-aminobutyric acid (5 mM)

**Fig. 5. 6** shows the ITC titration curves for PGD-G3 and GABA. During injection of GABA into PGD-G3 solution, exothermic heat was observed. And the amount of heat was less than the ITC titration of PGD-G3 with glutamic acid. This exothermic phenomenon is also considered the separation heat of GABA dimer. This result supports that the  $\alpha$ -amino of amino acid is also involved in the interaction between PGD-G3 and amino acids.

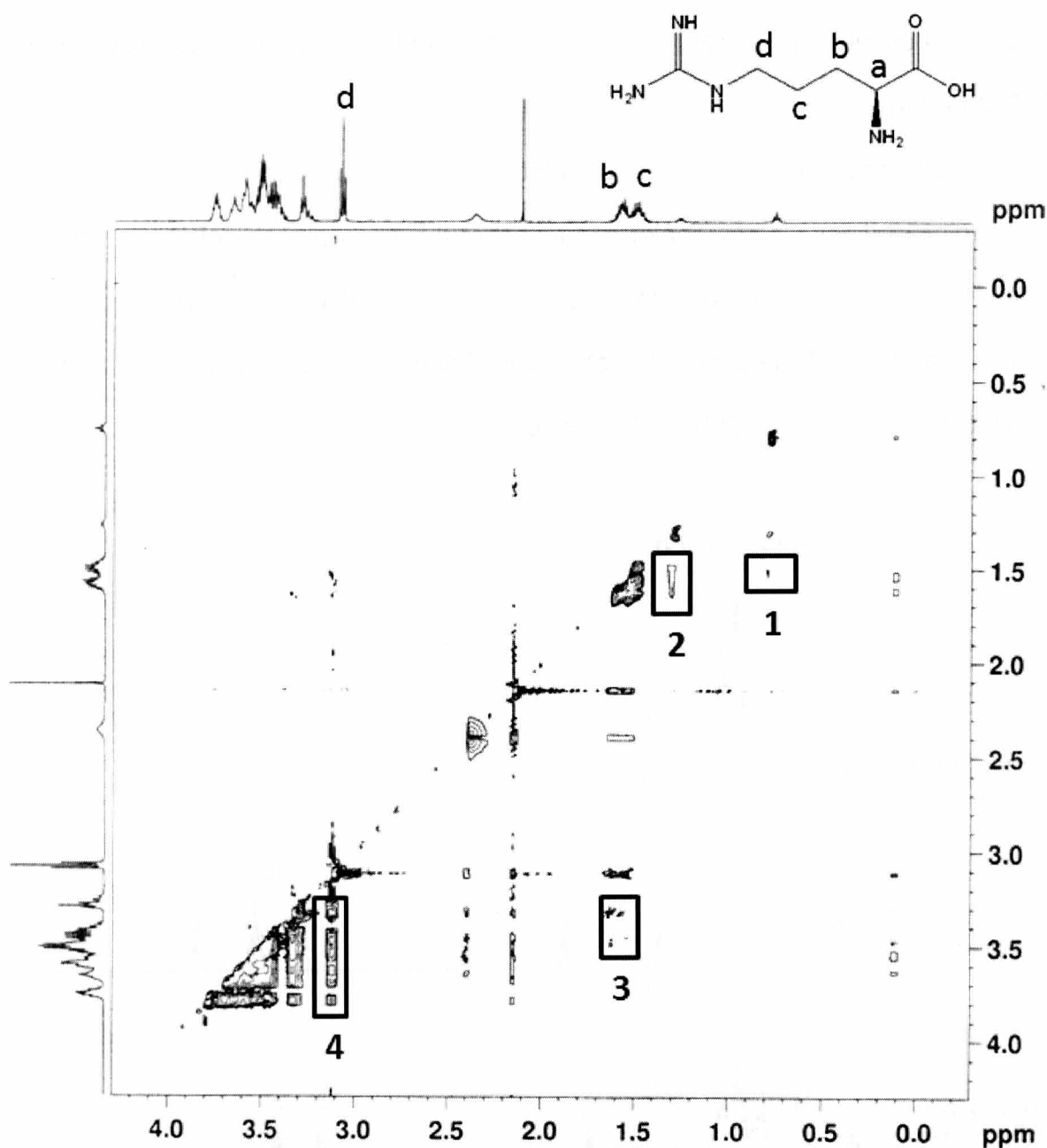
**5.3.2  $^1\text{H}$ -NMR and 2D  $^1\text{H}$ - $^1\text{H}$  NOESY NMR of L-arginine or L-lysine against PGD-G3**



**Fig. 5. 7**  $^1\text{H}$ -NMR spectra of PGD-G3, L-arginine and mixture of PGD-G3 and L-arginine

When the L-arginine was mixed with PGD-G3, the multiplet for  $\text{H}_{\text{b, c}}$  (1.5 ppm) were

separated and deshielded toward upfield. The triplet for  $H_d$  (3.1 ppm) was also deshielded toward upfield. The triplet for  $H_a$  might be overlapped branch part of PGD-G3. In case of PGD-G3, the chemical shift such as shielding or deshielding, was not observed. However, the triplet peak for branch part of PGD-G3 (4.0 ppm) was disappeared. And whole peaks attributed to PGD-G3 became to be sharp. This phenomenon means that the solubility of PGD-G3 in  $D_2O$  increased, because of the interaction between PGD-G3 and L-arginine. The peak separation of  $H_b$  and  $H_c$  means that the electronic condition was nonequivalent. These results support the interaction between PGD-G3 and L-arginine in aqueous solution. However, the interaction site within PGD-G3 was still unknown. Therefore, NOESY between PGD-G3 and L-arginine was carried out.

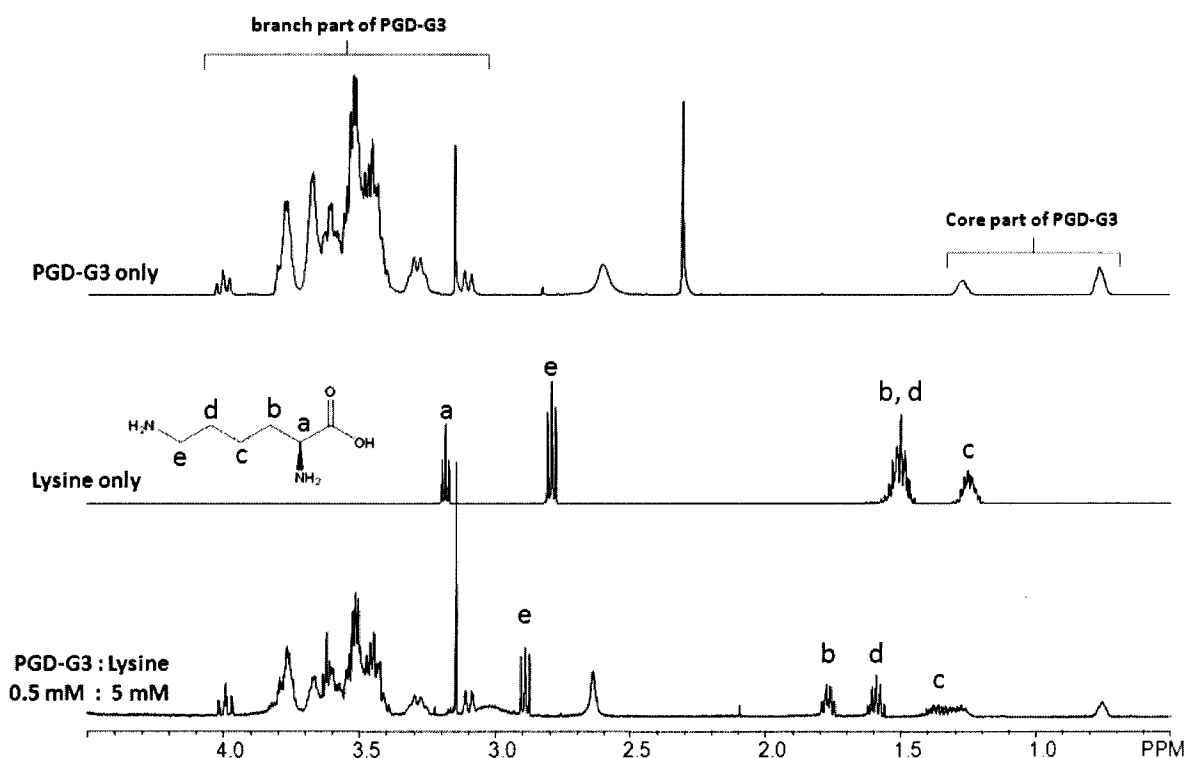


**Fig. 5. 8** 2D  $^1\text{H}$ - $^1\text{H}$  NOESY spectra of the PGD-G3 and L-arginine in  $\text{D}_2\text{O}$

2D homonuclear  $^1\text{H}$ - $^1\text{H}$  NOESY spectra of the PGD-G3 and L-arginine are shown in **Fig. 5. 8**. NOESY analysis is capable of revealing the distance of two nuclei in a single molecule or a complex. Nuclei within a spatial distance of 5 Å give NOE cross-peaks while distant nuclei show much weaker NOE interactions because the NOE signal intensity decays with distance<sup>1)</sup>. As shown in **Fig. 5. 8**, cross-peaks are

observed between protons H<sub>b</sub>, H<sub>c</sub> and H<sub>d</sub> in the dendritic interior of PGD-G3 (**Fig. 5. 6 1, 2, 3 and 4**).

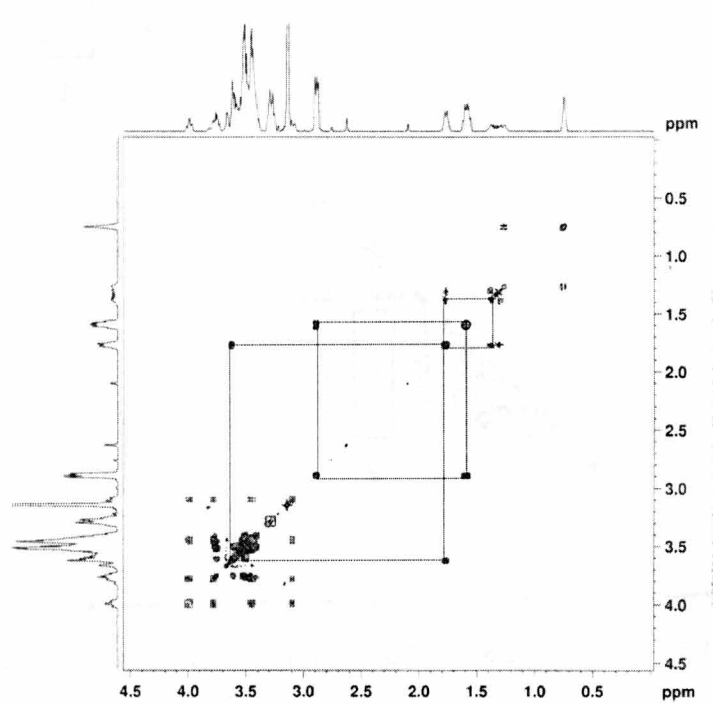
The cross-peak of **1** and **2** were observed between core part of PGD-G3 and H<sub>b</sub>, <sub>c</sub> of L-arginine. These corss-peaks suggest that the H<sub>b</sub>, <sub>c</sub> protons of L-arginine were located within 5 Å with core of PGD-G3. The cross-peaks **4** between branch part of PGD-G3 and H<sub>d</sub> of L-arginine were observed. These cross peaks suggest that the H<sub>d</sub> was located within 5 Å with branch of PGD-G3.



**Fig. 5. 9** <sup>1</sup>H-NMR spectra of PGD-G3, L-lysine and mixture of PGD-G3 and L-lysine

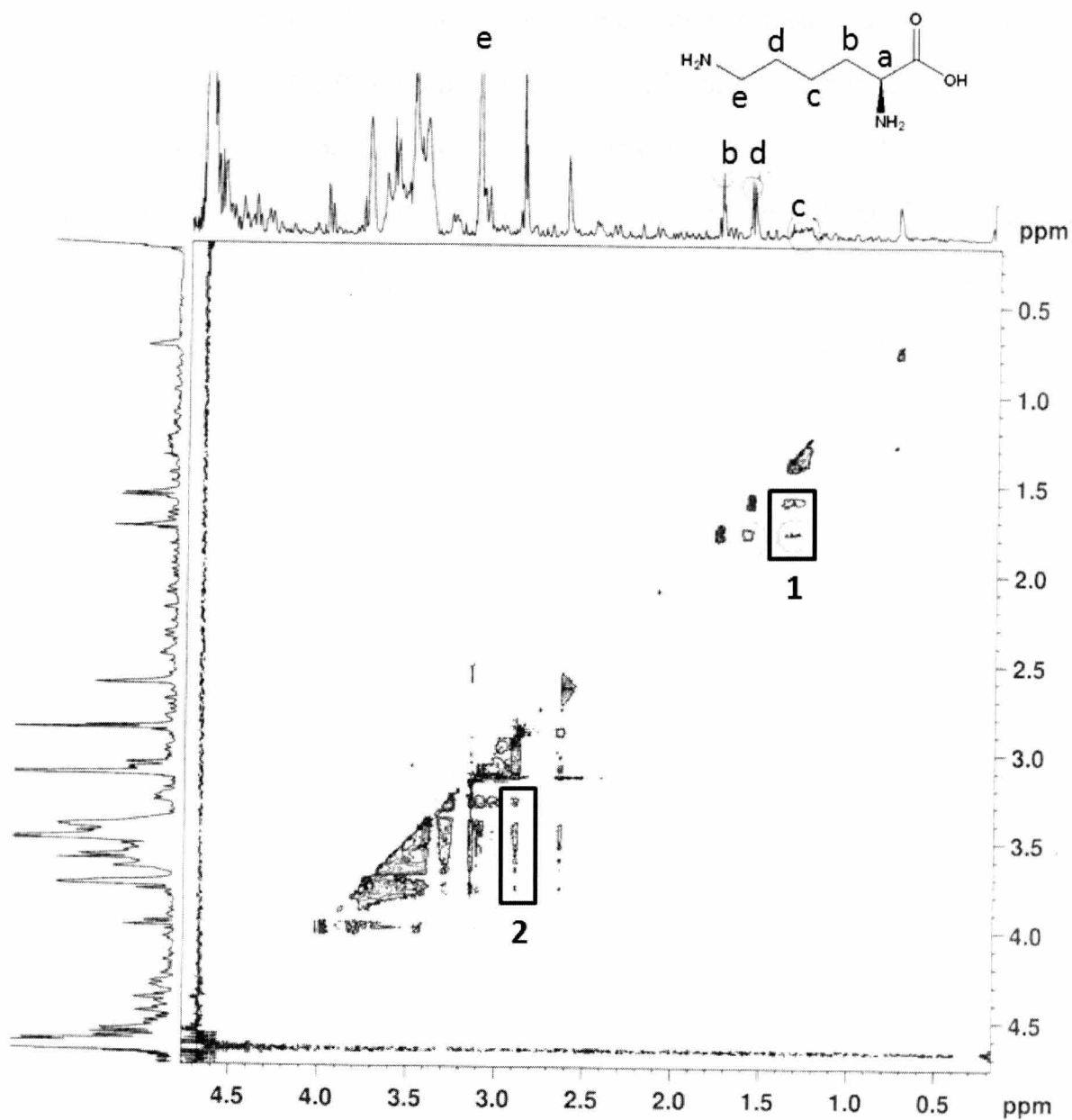
When the L-lysine was mixed with PGD-G3, the multiplet for H<sub>b</sub>, <sub>d</sub> (1.5 ppm) were separated and deshielded toward upfield. The triplet for H<sub>e</sub> (2.8 ppm) was also deshielded toward upfield. The triplet for H<sub>a</sub> might be overlapped branch part of PGD-G3. To find triplet for H<sub>a</sub> in branch part of PGD-G3, COSY was employed. At 3.6 ppm on COSY, the cross peak of L-lysine was observed (**Fig. 5. 9**). The whole peaks

attirubed PGD-G3 did not show any change, like  $^1\text{H}$ -NMR spectra of mixture of PGD-G3 and L-arginine. And whole peaks attributed to PGD-G3 also became to be sharp. Due to the interaction between PGD-G3 and L-lysine, the solubility of PGD-G3 was increased in  $\text{D}_2\text{O}$  and the peak separation between  $\text{H}_b$  and  $\text{H}_d$  was observed. These results support the interaction between PGD-G3 and L-lysine in aqueous solution. To understand the interaction site between PGD-G3 and L-lysine, NOESY was carried out.



**Fig. 5. 10** 2D  $^1\text{H}$ - $^1\text{H}$  COSY spectra of the PGD-G3 and L-lysine in  $\text{D}_2\text{O}$

The cross-peak of **1** was observed between core part of PGD-G3 and  $\text{H}_c$  of L-lysine. This corss-peak suggests that the  $\text{H}_d$ ,  $c$  protons of lysine were located within 5 Å with core of PGD-G3. The cross-peaks of **2** were observed between core part of PGD-G3 and  $\text{H}_e$  of L-lysine. These corss-peaks suggest that the  $\text{H}_e$  proton of L-lysine were located within 5 Å with branch of PGD-G3.



**Fig. 5. 11** 2D  $^1\text{H}$ - $^1\text{H}$  NOESY spectra of the PGD-G3 and L-lysine in  $\text{D}_2\text{O}$

## 5.4 Conclusion

The dendritic interior of PGD-G3 could interact with amino acids, such as L-arginine or L-lysine or L-histidine, in an aqueous condition, which was confirmed by ITC,  $^1\text{H}$ -NMR and 2D  $^1\text{H}$ - $^1\text{H}$  NOESY NMR. The ITC results revealed that L-arginine and L-lysine were found to interact with PGD-G3, as “two site model”. With increasing the  $\text{pK}_a$  value of amino acids, the binding constant was increased (L-arginine > L-lysine > L-histidine). The ITC titration of PGD-G3 with GABA suggests that two basic groups like L-arginine and L-lysine in one molecule is necessary for the binding toward PGD-G3. The results of 2D  $^1\text{H}$ - $^1\text{H}$  NOESY NMR measurements supported the localization of the side chain groups at approximate position of the interior parts of PGD-G3. Therefore, it is suggested that ether oxygen atom in PGD-G3 attract the protonated basic chain groups, the  $\text{pK}_a$  of which is a dominant factor for the molecular interaction. In addition,  $\alpha$ -amino groups of the basic amino acids play an essential role for the interaction.

## References

1. M. H. chai, A. K. Holley, M. Kruskamp, *Chem Commun.* **2007**, 168  
M. H. chai, T. H. Niu, W. J. Youngs, P. L. Rinaldi, *J. Am. Chem. Soc.*, **2001**, 123, 4670



## **Chapter 6.**

### **General conclusion**

## Chapter 6.

### General conclusion

This dissertation described the host-guest complexation using polyglycerol dendrimers (PGDs) as host molecules, focusing on dendritic interior constructed by glycerol unit.

In **chapter 2**, the host-guest interactions between fluorescent molecule (AHSA) and polyglycerol dendrimer of generation 1 (PGD-G1) and generation 2 (PGD-G2) were analyzed by fluorescent measurements,  $^1\text{H}$ -NMR titration and ITC. The core, interior and peripheral hydroxyl group of PGD-G2 interacted attractively with AHSA. A less polar and hydrophobic environment was found to be formed by the addition of PGD-G2 in aqueous solution, which enhanced uptake of AHSA into the dendritic interior of PGD-G2 with a 1 : 1 stoichiometry. The core part of PGD-G1 did not interact with AHSA, whereas the peripheral part of PGD-G1 interacted with AHSA. From this study, PGD-G1 and G2, which should be bio-inert molecules, have hydrophobic dendritic interior and donated the space for host-guest complexation.

In **chapter 3**, the host-guest interaction between AHSA and PGD-G3 and PGD-G4 was described. The molecular interaction between AHSA and PGDs were analyzed by the similar analytical methods described in chapter 2. PGD-G3 was found to be associated at 0.1 mM. After adding AHSA into PGD-G3 aqueous solution at the same concentration, AHSA and PGD-G3 were interacted with 2 : 1 stoichiometry, which was clarified by ITC measurements. Some of PGD-G4 molecules were also found to be associated at 0.2 mM, and most of PGD-G4 molecules existed as unimer

state. ITC data reflect the PGD-G4 and AHSA interaction, the driving force of which includes hydrophobic interaction. Probably, AHSA was embedded in highly dense hydroxyl group layer located on PGD-G4 periphery. In conclusion of this part, AHSA was located in the associated molecules of PGD-G3, where polarity was higher than glycerol. On the other hand, AHSA was stuck in the dense surface of PGD-G4 unimer, where the solution environment was less polar than glycerol, EtOH and PEG400.

In **chapter 4**, based on the possibility of host-guest interaction (from Chapters 2 and 3), the host-guest interaction between PGDs and 5-fluorouracil (5-Fu) as a model drug was investigated to estimate the system for the application of PGDs as host molecules. 5-Fu is known as a photosensitizer capable of fluorescent change via tautomeric formation. The interaction between PGDs and 5-Fu in an acetate buffer (pH 5.0) was proved by  $^1\text{H}$ - and  $^{19}\text{F}$ -NMR titrations. Downfield shift of  $^{19}\text{F}$  peak with increasing concentration of PGD-G3 against 5-Fu might suggest the buried 5-Fu within dendritic interior of PGD-G3. It is suggested that the ether oxygen of 2,3-dihydroxy-propoxymethyl unit acted as an electron donor, and thus, the interaction between PGDs and 5-Fu was probably based on an electron donor-acceptor relationship. Therefore, the driving force of the interaction in the interior part of PGD-G3 should provide new insight into the host-guest interaction, which should be different from hydrophobic interaction-based driving force observed in encapsulation of guest molecules into micelles.

In **chapter 5**, the exploratory study of guest molecules toward PGD-G3 by ITC was described. In order to obtain the information of guest molecules capable of interacting

with ether oxygen in the interior part, amino acids, which have various  $pK_a$  side chains, were employed as candidates of the guest molecules. Most of interaction mode between PGD-G3 and amino acids was fitted to the two binding model. With increasing of side chain  $pK_a$ , the binding constant of interaction between PGD-G3 and amino acids was increased; L-arginine ( $pK_a$ ; 12.48,  $K_{a1}$ ;  $1.12 \times 10^6$  ( $M^{-1}$ ),  $K_{a2}$ ;  $4.19 \times 10^4$  ( $M^{-1}$ )), L-lysine ( $pK_a$ ; 10.79,  $K_a$ ;  $1.12 \times 10^6$  ( $M^{-1}$ ),  $K_{a2}$ ;  $4.97 \times 10^4$  ( $M^{-1}$ )) and L-histidine ( $pK_a$ ; 6.04,  $K_a$ ;  $8.17 \times 10^4$  ( $M^{-1}$ ),  $K_{a2}$ ;  $2.27 \times 10^2$  ( $M^{-1}$ )). Glutamic acid ( $pK_a$ ; 4.25) did not interact with PGD-G3. To understand the role of  $\alpha$ -amino group of amino acids, 4-aminobutyric acid (GABA) was employed. The ITC curves of PGD-G3 with GABA suggest that the  $\alpha$ -amino group was essential for the interaction with PGD-G3. From these results, the PGD-G3 cooperatively interacts with both the basic side chain and  $\alpha$ -amino group. The bivalent interaction was proved by 2D  $^1H$ - $^1H$  NOESY NMR measurements, which supported the localization of the side chain groups at approximate position of the interior parts of PGD-G3. Therefore, the  $pK_a$  value of side chain was the key factor of the strength of the binding because the binding constant increased with the  $pK_a$  values (L-arginine > L-lysine > L-histidine). It was concluded that two basic groups of  $\alpha$ -amino groups or side chain in one molecule is necessary for the binding toward PGD-G3. Probably, ether oxygen atom in PGD-G3 attracted the protonated basic chain groups.

There are two ways for application of PGDs; Surface modification and host-guest complexation within the dendritic interior. The surface modification of hydroxyl group on surface is the dominant research on the application of PGDs. However, this type of research is based on the recognition which PGDs are considered as a building block for molecular design. On the other hand, the application of dendritic interior is still insufficient because polyglycerols' interior is obscure. I believe that these

fundamental studies of PGD interior contribute to establish the foundation of PGD research.